Information transmission by the synchronous activity of neuronal populations

D I S S E R T A T I O N

zur Erlangung des akademischen Grades

doctor rerum naturalium
(Dr. Rer. Nat.)
im Fach Physik
Spezialisierung: Theoretische Physik
eingereicht an der
Mathematisch-Naturwissenschaftlichen Fakultät
Humboldt-Universität zu Berlin

von
Dipl. Phys. Alexandra Kruscha

Präsidentin der Humboldt-Universität zu Berlin:
Prof. Dr.-Ing. Dr. Sabine Kunst

Dekan der Mathematisch-Naturwissenschaftlichen Fakultät:
Prof. Dr. Elmar Kulke

Gutachter:
1. Prof. Dr. Benjamin Lindner (HU Berlin)
2. Prof. Dr. Martin Nawrot (Universität zu Köln)
3. Prof. Dr. Leonard Maler (University of Ottawa)

Tag der mündlichen Prüfung: 22. Mai 2017

Zusammenfassung

Sensorische Nervenzellen kodieren Informationen über die Umwelt oder Zustände des Körperinneren mittels elektrischer Impulse, sogenannte Aktionspotentiale oder Spikes. Diese werden weitergeleitet zu postsynaptischen Neuronen im zentralen Nervensystem, welche unterschiedliche Auslesestrategien verwenden. Integratorzellen summieren alle ankommenden Aktionspotentiale auf, wodurch sie die Gesamtaktivität einer präsynaptischen Population messen. Koinzidenzdetektoren hingegen, werden nur durch das synchrone Feuern der zuführenden Neuronenpopulation aktiviert.

Die grundlegende Frage dieser Dissertation lautet: Welche Information eines zeitabhängigen Signals kodieren die synchronen Spikes einer Neuronenpopulation im Vergleich zu der Summe all ihrer Aktionspotentiale? Hierbei verwenden wir die Theorie stochastischer Prozesse: wir berechnen Spektralmaße, die es ermöglichen Aussagen darüber zu treffen welche Frequenzkomponenten eines Signals vorwiegend transmittiert werden. Im Gegensatz zu früheren Studien, verstehen wir unter einem synchronen Ereignis nicht zwangsläufig, dass die gesamte Population simultan feuert, sondern, dass ein minimaler Anteil („Synchronizitätsschranke") gleichzeitig aktiv ist. Diese Definition von Synchronizität ist realistischer, da sie berücksichtigt, dass Koinzidenzdetektoren eine festgelegte Aktivierungsschranke aufweisen.

Unsere Analyse zeigt, dass die synchrone Populationsaktivität als ein Bandpass-Informationsfilter agieren kann: die synchronen Spikes kodieren hauptsächlich schnelle Signalanteile. Diesen Effekt bezeichnen wir als 'Synchrony Code'. Damit stellt die Selektion simultaner Neuronenaktivität ein potentielles Mittel dar um gleichzeitig anwesende, konkurrierende Signale voneinander zu trennen. Dabei hängen die genauen Charakteristika der Informationsfilterung ausschlaggebend von der Synchronizitätsschwelle ab. Insbesondere zeigt sich, dass eine Symmetrie in der Schwelle vorliegt, die die Äquivalenz der Kodierungseigenschaften von synchronem Feuern und synchronem Schweigen offenlegt. Wir führen ein einfaches Qualitätsmaß des Synchrony Codes ein, welches die Abschätzung einer optimalen Synchronizitätsschwelle ermöglicht. Unsere analytischen Ergebnisse, welche nicht an ein bestimmtes Neuronenmodell gebunden sind, testen wir mittels numerischer Simulationen vom Leaky Integrate-and-Fire Modell.

Die afferenten Neuronen der Elektrorezeptoren von schwach elektrischen Fischen stellen ein biologisches Modellsystem für unsere Fragestellung dar. Auswertungen von in-vivo-Versuchen an diesem Organismus belegen, dass unsere theoretischen Vorhersagen qualitativ auch für reale Nervenzellen gültig sind. Die Güte der Informationsübertragung der synchronen Aktivität hängt jedoch wesentlich von den physiologischen Eigenschaften der sensorischen Zellen ab. Anhand theoretischer Untersuchungen zeigen wir, dass eine minimale Leck-Leitfähigkeit der Zellmembran (Durchlässigkeit für Ionen im Ruhezustand der Zelle) eine notwendige Bedingung für einen Synchrony Code darstellt. Im schwach elektrischen Fisch findet man zwei Arten von sensorischen Neuronen mit sehr unterschiedlichen Kodierungseigenschaften vor: *P-Units* weisen einen ausgeprägten Synchrony Code auf, wohingegen die synchronen Spikes von *Ampullärzellen* kaum Information über einen Stimulus beinhalten. Unsere theoretischen Resultate legen demnach nahe, dass P-Units effektiv eine viel höhere Leck-Leitfähigkeit aufweisen als Ampullärzellen.

Abstract

Populations of sensory neurons encode information about the environment into electrical pulses, so called action potentials or spikes. Neurons in the brain process these pulses further by using different readout strategies. Integrator cells sum up all incoming action potentials and are thus sensitive to the overall activity of a presynaptic population. Coincidence detectors, on the other hand, are activated by the synchronous firing of the afferent population.

The main question of this thesis is: What information about a common time-dependent stimulus is encoded in the synchronous spikes of a neuronal population in comparison to the sum of all spikes? We approach this question within the framework of spectral analysis of stochastic processes, which allows to assess which frequency components of a signal are predominantly encoded. Here, in contrast to earlier studies, a synchronous event does not necessarily mean that all neurons of the population fire simultaneously, but that at least a prescribed fraction ('synchrony threshold') needs to be active within a small time interval. This more realistic form of synchrony takes into account that a coincidence detector has a certain activation threshold. We derive analytical expressions of the correlation statistics and test them against numerical simulations of the leaky integrate-and-fire neuron model.

We show that the information transmission of the synchronous output depends highly on the synchrony threshold. We uncover a symmetry in the synchrony threshold, unveiling the similarity in the encoding capability of the common firing and the common silence of a population. Our results demonstrate that the synchronous output can act as a band-pass filter of information, i.e. it extracts predominantly fast components of a stimulus, which can be considered as a 'synchrony code'. If signals in different frequency regimes are concurrently present, the selection of synchronous firing events can thus be a tool to separate these signals. Introducing a simple measure of the quality of the band-pass filtering effect allows us to make predictions about an optimal synchrony threshold.

The electroreceptor afferents of the weakly electric fish constitute a biological model system for our problem. In vivo recordings from this organism show that our theoretical predictions are qualitatively found in real neurons. The potential coding efficiency of the synchronous output is, however, determined by physiological properties of the sensory cells: we deduce from theoretical considerations that a minimal leak conductance of the membrane (permeability for ions in the cell's resting state) is necessary to obtain a synchrony code in terms of information filtering. In the weakly electric fish one finds two types of sensory neurons: *P-units* show a pronounced synchrony code, whereas the synchronous spikes of *ampullary cells* hardly carry any information about the stimulus. Our theoretical results thus suggest that P-units have a much higher leak conductance than ampullary cells do.

Contents

Chapter 1.

Introduction

Sensory neurons transfer information about the environment (like light, sound, skin pressure, scent, etc.) to other elements of the nervous system via the language of action potentials (spikes). One of the key challenges of neuroscience is to understand how information about the outer world is encoded in this activity of sensory neurons, i.e. to comprehend the 'neuronal code'. The brain has to recover analogue, dynamic signals (input) from a digital sequence of spikes (output). This reconstruction problem needs to be addressed by a probabilistic approach because neurons are not deterministic systems: when repeatedly exposed to an identical stimulus, a neuron's response differs at each trial. Information theory, pioneered by Claude Shannon, provides a theoretical framework that is able to quantify neuronal signal transmission in a probabilistic and model-free way. Information-theoretical measures, such as the mutual information or the related coherence function, do not tell us how, but how much information about a stimulus is transferred by a spike train. This allows to make statements about the efficiency of a neuronal system to encode a certain stimulus. This way one can test which stimuli or stimulus aspects are transmitted best and thus learn more about the neuronal code.

Usually, a signal is encoded not by a single cell, but by an ensemble of sensory neurons that convey their spikes to postsynaptic cells in a feed-forward, converging manner. One finds different readout strategies by the postsynaptic neuron: integrators sum up all incoming spikes, whereas coincidence detectors are activated only if the population fires synchronously. The aim of this thesis is to investigate and to compare the encoding properties of both population outputs: the summed and the synchronous population activity. Novel in this work is that we keep the requirement for synchrony as a free parameter, i.e. not the entire population but a minimal fraction of it ('synchrony threshold') needs to fire simultaneously. We call the time series of these synchronous events the *partially synchronous output* (PSO).

1.1. Thesis outline

The thesis is organized as follows: in the remainder of this chapter we give a brief overview about basic neurophysiological mechanisms and concepts (generation of action potentials, types of postsynaptic cells, sources of neuronal noise). Then, we introduce the mathematical and statistical description of neuronal activity and discuss the model that we use in this thesis. Furthermore, we introduce the weakly electric fish as

an important model organism to study sensory information transmission. We expound that they possess two types of electroreceptor afferents that feature very different coding properties. Finally, we review earlier findings about the mathematical mechanism behind a synchrony code for the simple case of pairs of neurons.

In Chapter 2 we show in theoretical terms that the distinct coding behaviors of the electrosensory afferents in weakly electric fish are much likely linked to different levels of the leak conductance.

In Chapter 3 we investigate the distribution of the summed activity of a neuronal population driven by common noise. We show that under weak stimulation the summed output of a large population can be approximated by a Gaussian process.

In Chapter 4 we investigate the statistical properties of the partially synchronous output. We derive analytical approximations of the mean of the PSO, its power spectrum and its cross-spectrum with a weak common stimulus. We employ two different approaches and test the results against numerical simulations of leaky integrate-and-fire neurons. From the analytical results we can deduce general properties of the PSO, in particular we unveil a symmetry in the synchrony threshold around the mean population activity.

Finally, in Chapter 5, we put together all previous results to examine the spectral coherence function of the PSO. We show that in contrast to the broadband coding of the summed population output, the PSO can act as a band-pass filter of information. We discuss under which circumstances one can expect a pronounced 'synchrony code'. We show that these predictions are in line with simulation results of leaky integrate-and-fire neurons and hold qualitatively true for recordings from the weakly electric fish.

Some of the results in this thesis have been published in three papers. Plots from recordings of the weakly electric fish that occur in the introduction and parts of Chap. 2 were published in (Grewe et al., 2017). The results in Chap. 3 have been published in (Kruscha and Lindner, 2015) and the main part of Chap. 4 was published in (Kruscha and Lindner, 2016).

1.2. Biological properties of neuronal activity

In this section we briefly introduce basic properties of neuronal activity. A detailed introduction to neurophysiology and neuroanatomy can be found, for example, in Kandel et al. (2000).

A neuron is said to get 'activated' if its electrical membrane potential crosses an individually defined threshold value, which leads to the opening of ion channels, such that the voltage potential rapidly rises and falls again (within 1-2 ms). This event is called action potential or spike (the neuron 'fires') and it is believed that all important information is encoded in the times or rate at which action potentials occur. The time series of consecutive action potentials is called spike train.

Sensory neurons, also called receptor afferents, are nerve cells that transmit sensory information about the environment to other elements of the nervous system. A stimulus generates action potentials in the sensory neuron that travel along the axon to the

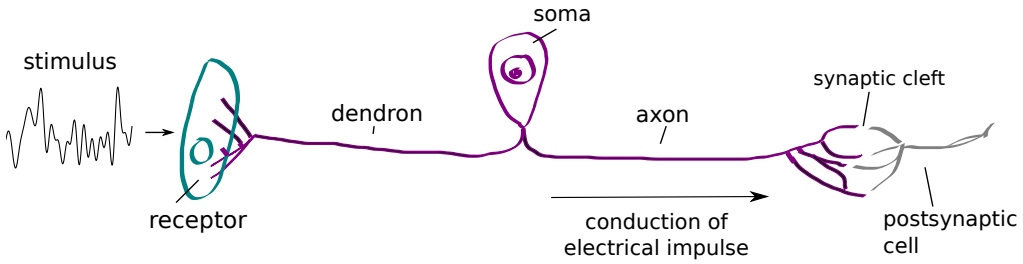

Figure 1.1.: **Sketch of a sensory neuron.** Sensory neurons [purple] transmit the stimulus-induced activation of receptors [cyan] into electrical impulses that travel along the axon towards the central nervous system. The activated sensory neuron releases neurotransmitters in the synaptic cleft, which may activate a postsynaptic cell [grey].

central nervous system, where it may activate a postsynaptic neuron by releasing neurotransmitters into the synaptic cleft between the two cells (see Fig. 1.1 for illustration).

The receptive field of a sensory neuron is the particular region of the sensory space (e.g., the body surface, the visual field, or a location in space) in which a stimulus will modify the firing of that neuron. Typically, the receptive fields from adjacent sensory neurons overlap. This means that a stimulus is usually encoded by a population of neurons that project their electrical impulses to postsynaptic cells ('projection neurons') in a convergent manner (see Fig. 1.2 for illustration).

1.2.1. Rate coding vs coincidence coding

There are different readout strategies how a postsynaptic neuron extracts information from a presynaptic population. *Integrator cells* have a small leakage current, such that they are able to sum up incoming action potentials over a comparatively long time window. For these cells, it is rather the firing rate that is important instead of the exact timing of the presynaptic spikes ('rate coding'). On the other hand, there are *coincidence detectors* that only get activated if a certain number of action potentials arrives within a very short time window, i.e. when the presynaptic neurons fire simultaneously ('synchrony coding'). This would imply that the precise timing of a spike matters, such that coincidence detection is a form of temporal coding (see Fig. 1.2 for illustration).

The main goal of this thesis is the investigation of the coding properties of these distinct readout mechanisms. Do integrators and coincidence detectors extract different information about a weak sensory stimulus? Put differently, what information is encoded in the synchronous spikes in comparison to the summed spikes of a neuronal population? We will in particular focus on the case of uncoupled sensory neurons (which do not interact with each other), such as can be found, for example, in the olfactory (in Drosophila) and the auditory system. In the following, we introduce these two sensory systems in order to underline the relevance of our model. The electroreceptor affer-

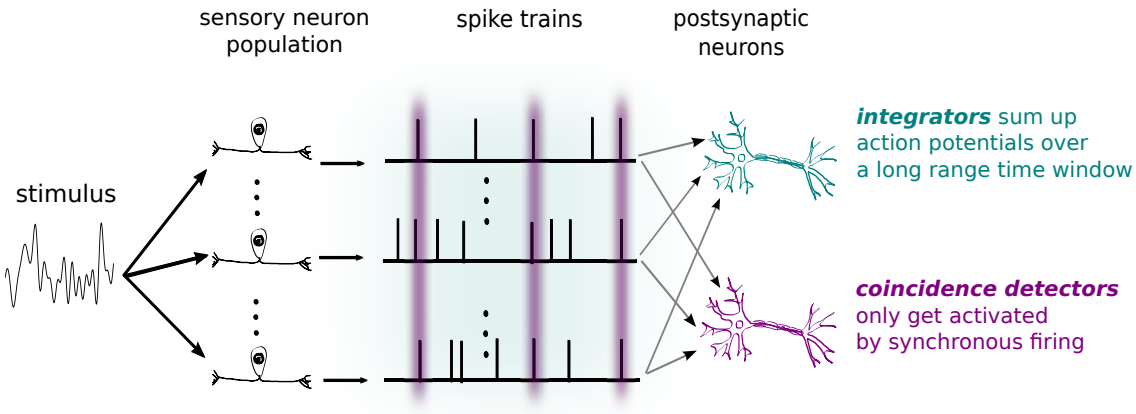

Figure 1.2.: **Illustration of sensory information encoding.** A population of sensory neurons receives a common stimulus as an input, due to overlapping receptive fields. These neurons project their output to postsynaptic cells, which either sum up all incoming spikes (integrators) or which select only synchronous firing events (coincidence detectors).

ents of weakly electric fish are another example of uncoupled sensory neurons that are specialized to encode weak stimuli. We introduce them in more detail in the end of the introduction, because they will serve as the main biological application of our theoretical considerations.

Olfactory system

In most mammals and insects, the olfactory receptor neurons (ORNs) that are activated by a distinct odor converge onto projection neurons (PN) in the same glomerulus (Vosshall et al., 2000). The convergence ratio is high, on the order of 50 ORNs per PN in Drosophila and 5000 ORNs per PN in rodents (Wilson and Mainen, 2006). The high convergence ratios are believed to allow for the integration and amplification of weak signals (Su et al., 2009). In fact, the PNs are most sensitive to low firing rates of the ORNs, indicating that they are specialized in detecting weak stimuli (Olsen et al., 2010). In the third stage of sensory processing pyramidal cells receive synapses from multiple glomeruli and thus multiple odor receptor types. The pyramidal neurons are known to act as coincidence detectors. This form of processing is believed to enhance the capacity of the system to discriminate structurally similar odorants (Poo and Isaacson, 2009).

Auditory system

Sounds induce vibrations of the basilar membrane in the cochlea, which are transduced into electrical signals by the cochlear hair cells. There are around 16,000 of these receptor cells in each ear of a mammal. The hair cells are spatially arranged in a tonotopic manner:

every hair cell is most sensitive to stimulation at a specific frequency. Hair cells trigger action potentials in the spiral ganglion neurons, which do not interact with each other and whose axons project to the brain via the auditory nerve. The auditory nerve fibres (axons of the spiral ganglion neurons) synapse onto diverse target cells in the cochlear nucleus. There are at least six classes of projecting neurons, each of which exhibits a different topology of dendrites and of activation patterns.

Stellate cells, for example, have dendrites that lie parallel to the auditory nerve fibres. They are narrowly tuned, fire very regular with a rate that depends on the strength of the auditory input (Young et al., 1992). They thus encode the frequencies present in an auditory stimulus. On the contrary, the dendrites of *octopus cells* extend perpendicular to the paths of the auditory nerve fibres (Osen, 1969) and thus get input from ganglion cells representing a broad range of frequencies. Accordingly, octopus cells exhibit broad tuning curves and are effectively driven by transient broadband stimuli such as clicks (Godfrey et al., 1975; Bal and Oertel, 2000). At least 50 ganglion cells converge to an octupus cell (Golding et al., 1995). Because each input contributes only a small submillivolt depolarization to the postsynaptic response, the initiation of an action potential requires strong synchronous presynaptic activity. Hence, octopus cells detect the coincident activity of a large population of auditory nerve fibres encoding a broad range of frequencies (Golding et al., 1995). These two types of projecting neurons demonstrate that very different readout strategies are used to extract information about auditory input from the activity of receptor afferents.

1.2.2. Noise in neuronal activity: sources and benefits

Neurons are not deterministic systems. When a neuron is subject to a fixed stimulus, its output varies over repeated trials (see Fig. 1.3 for an example recording). Even if no stimulus is present, the spontaneous firing activity of a neuron displays degrees of randomness. This variability is called *neuronal noise* and is believed to have the following major sources: first of all, there is so called 'channel noise', which accounts for the fact that the ion channels in the neuron's membrane open and close stochastically and solely the probability with which they do so changes with the membrane voltage or the concentration of neurotransmitter. This leads to fluctuations in the total membrane conductance (White et al., 2000).

The main cause of the noise experienced by a neuron at later processing stages originates in its synaptic input. The amount of neurotransmitters that are released into the synaptic cleft as well as the exact timing of their release are governed by probabilities that depend on the history of both the pre- and the postsynaptic neuron (Allen and Stevens, 1994; Koch, 1999). Furthermore, a neuron in the central nervous system usually has a myriad of synapses made by other cells onto it. The irregularity of the arrival time of each presynaptic action potential in addition to the synaptic release noise leads in summation to postsynaptic voltage fluctuations. This 'synapse bombardment', also called 'synaptic noise' is the dominant source of the firing variability in cortical neurons (Destexhe and Rudolph-Lilith, 2012). The term 'synaptic noise' can be misleading though, because the irregularly arriving spikes from presynaptic cells may contain important in-

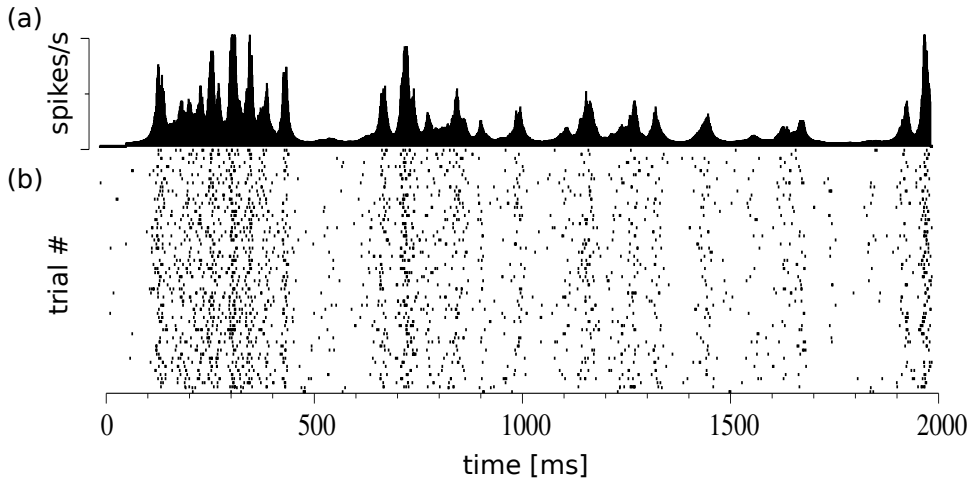

Figure 1.3.: **Neuronal response is variable.** Response of a neuron in the visual cortex of a macaque to repeated trials of the same moving visual stimulus. The spike times for different trials are marked as dots in (b), the rate of their spiking in short time bins is shown in (a). Adapted from Bair and Koch (1996). ©1996, Massachusetts Institute of Technology.

formation and only appear in their sum and complex nature random to us. The term synaptic noise does not mean that the entire input to postsynaptic cells is random in its nature, but that it can be described with statistical tools.

In this thesis we are mainly concerned with peripheral sensory neurons, i.e. neurons at the first stage of signal processing. These cells often receive no synaptic input from other neurons, but they are affected by the precision and reliability of the receptors (Berg and Purcell, 1977; Bialek and Setayeshgar, 2005). In addition, external sensory stimuli may first be converted into a chemical signal (e.g., through photon absorption by photoreceptors or ligand-binding of odour molecules by olfactory receptors) or into a mechanical signal (such as the vibration of hair cells in the cochlea). The subsequent transduction process amplifies the sensory signal and converts it into an electrical one, which may lead to additional noise ['transducer noise' (Lillywhite and Laughlin, 1979)].

Neuronal noise can be advantageous

Noise limits the accuracy of a neuron's response to a signal or stimulus and thus interferes with the encoding of a signal. This limited information transmission is quantified by the signal-to-noise ratio, which is the ratio of signal power to noise power (Rieke et al., 1996).

However, noise is not necessarily detrimental for signal encoding. For instance, for weak signals that by themselves are not able to excite the neuron, noise can help to amplify the signal such that the latter can be encoded in the firing pattern. This concept of noise making it possible for a weak stimulus to pass a threshold in a nonlinear system is called *stochastic resonance* (Gammaitoni et al., 1998). The term 'resonance' refers to the

fact that there is an optimal non-zero amount of noise that maximises the signal-to-noise ratio.

Another case where noise is beneficial occurs when a signal is encoded by a homogeneous population of neurons [1]. Without noise, every neuron would respond to the signal in the same way, such that the population would act as a single threshold unit. However, when each neuron is subject to independent noise, the firing thresholds become effectively variable and vary over the population, such that more features of the signal can be encoded by the neuron ensemble. This concept is called *suprathreshold stochastic resonance* (SSR) (Stocks, 2000; Stocks and Mannella, 2001) [2]. In conclusion, variability in neural firing can be beneficial for signal encoding.

1.3. Important statistics of stochastic processes

As discussed above, single neurons are noisy encoders, i.e. their output can be regarded as a stochastic process. As a consequence, also the summed or synchronous output of a neuronal population are stochastic. In this section, we introduce the notation and definition of important statistical measures which allow us to classify a stochastic process and the correlation between two different processes. The introduced measures and detailed theory about stochastic processes can be found, for example, in Gardiner (1985).

Let $X(t)$ and $Z(t)$ be two stationary, real valued stochastic processes, where the term stationary indicates that the statistics does not change over time.

Mean Value and Variance

By $\langle X \rangle$ we denote the average value of process X. If one knows the probability density p_X of X, then for any function $g : \mathbb{R} \mapsto \mathbb{R}$ holds

$$\langle g(X) \rangle = \int_{-\infty}^{\infty} p_X(x) g(x) dx \, .$$

The variance σ_X^2 quantifies how strongly the process X fluctuates around its mean value

$$\sigma_X^2 := \langle X^2 \rangle - \langle X \rangle^2 \, .$$

Autocorrelation

The *autocovariance* tells us how a process is correlated with its own history. It reads

$$C_{X,X}(\tau) := \langle X(0) X(\tau) \rangle - \langle X \rangle^2 \, . \tag{1.1}$$

By $\overline{C}_{X,X}(\tau) := \langle X(0) X(\tau) \rangle$ we denote the *autocorrelation function* of X.

[1] Here, the term 'homogeneous' means that all neurons have the same firing threshold and that the deterministic part of the single dynamics has the same nonlinearity.

[2] The term 'suprathreshold' in SSR came up in order to distinguish the effect from the occurrence of stochastic resonance in a single threshold system, which only occurs if the signal is subthreshold.

Noise intensity

Noise is characterized by a zero mean and the intensity of a noise process X is defined via an integral of the autocorrelation function

$$D := \int_0^\infty \overline{C}_{X,X}(\tau) d\tau \,. \tag{1.2}$$

Cross-correlation

The *cross-covariance* between two processes X and Z tells us how much a process X is correlated with Y at different points in time

$$C_{X,Z}(\tau) := \langle X(0)Z(\tau)\rangle - \langle X\rangle\langle Z\rangle \,. \tag{1.3}$$

The two processes X and Z are *independent* of each other, if $C_{X,Z}(\tau) = 0$ for all $\tau \geq 0$. The *cross-correlation function* is defined by the first term of Eq. (1.3).

Power spectrum and cross-spectrum

The power spectrum of a stochastic process describes the distribution of power (variance) of frequency components of the process. The cross-spectrum is a measure of frequency-resolved cross-correlation between two processes. In numerical simulations we calculate the power spectrum of X and the cross-spectrum between two stationary stochastic processes X and Z by

$$\begin{aligned} S_X(f) &= \frac{\langle \tilde{X}_T(f)\tilde{X}_T^*(f)\rangle}{T} \quad \text{and} \\ S_{X,Z}(f) &= \frac{\langle \tilde{X}_T(f)\tilde{Z}_T^*(f)\rangle}{T} \,, \end{aligned} \tag{1.4}$$

where the brackets $\langle\ \rangle$ denote averaging over repeated trials and the $T \gg 1$ is the recording time. The asterisk stands for the complex conjugate and $\tilde{X}_T$ is finite-time-window Fourier transform

$$\tilde{X}_T(f) = \int_{-T/2}^{T/2} dt\ X(t) e^{i2\pi f t},$$

where the measurement time window is centered around $t = 0$. The integral of the power spectrum gives the variance of a process:

$$\sigma_X^2 = \int_{-\infty}^{\infty} S_X(f) \,. \tag{1.5}$$

In the analytical calculations we make use of the Wiener-Khinchin-Theorem and derive the power spectrum by the Fourier transform of the autocovariance and the cross-

spectrum via the Fourier transform of the cross-covariance:

$$S_{X,Z} = \tilde{C}_{ZX} \,, \tag{1.6}$$

$$S_X = \tilde{C}_{XX} \,. \tag{1.7}$$

The tilde indicates the formal Fourier transform (FT)

$$\tilde{X}(f) = \mathrm{FT}(X) := \int_{-\infty}^{\infty} dt\; X(t) e^{i2\pi f t}.$$

Note that we define the spectra without the DC-peak (The mean values are subtracted in Eq. (1.1) and Eq. (1.3) such that the spectra do not have a δ-peak at zero frequency). If we want to include the DC-peak, we indicate this by a bar:

$$\overline{S}_X := S_X + \langle X \rangle^2 \delta(f) \,.$$

Coherence function

The spectral *coherence function* between two stochastic processes X and Z is the absolute square of the cross-spectrum between these processes, normalized by the respective power spectra:

$$\mathcal{C}_{X,Z}(f) := \frac{|S_{X,Z}(f)|^2}{S_X(f) S_Z(f)} \,. \tag{1.8}$$

The coherence function is the squared linear correlation coefficient between two stochastic processes in the frequency domain and satisfies $0 \leq \mathcal{C}_{X,Z} \leq 1$. It takes the value one, if X is a noiseless linear transformation of Z or vice versa.

1.4. Information transmission by neuronal activity

Of special interest is the coherence between a stimulus $s(t)$ and a neuronal output $x(t)$, such as the spike train of a single neuron or the summed or the synchronous activity of a neuronal population. The stimulus-response coherence is related to the mean square error, ϵ^2, of the best linear reconstruction of the stimulus by the response (Wessel et al., 1996):

$$\epsilon^2 = \int_0^{\infty} df\; S_s(f)[1 - \mathcal{C}_{x,s}(f)] \;. \tag{1.9}$$

Hence, if the coherence equals one at a certain frequency, the stimulus component belonging to this frequency can be perfectly reconstructed from the output. The coherence is smaller than one if the output is a non-linear transformation of the signal or because correlation is lost due to noise. The spike train of a neuron is a highly non-linear encoder due to the firing threshold. In addition, neurons are generally noisy. The coherence between the output of a single neuron and a stimulus will thus always be smaller than one.

If the stimulus is a Gaussian process, the coherence provides a lower bound, R_{info}, on the Shannon mutual information rate (Shannon, 1948) between stimulus and output (Bialek et al., 1993; Gabbiani, 1996):

$$R_{\text{info}} = -\int_0^\infty df \log_2[1 - \mathcal{C}_{x,s}(f)] \,. \tag{1.10}$$

Eq. (1.10) has been used in many studies to quantify information transmission in the neural context (Bialek et al., 1993; Gabbiani, 1996; Rieke et al., 1995; Borst and Theunissen, 1999). This approximation of the mutual information is very convenient because it requires only second-order statistics, such that fewer data is needed in comparison to the direct definition of mutual information (Strong et al., 1998). Another advantage compared to the Shannon information (which is only a single number of bits per second) is that the coherence function is a frequency-resolved measure of information transmission (Stein et al., 1972; Chacron et al., 2003; Oswald et al., 2004; Krahe et al., 2008a; Massot et al., 2011). It is therefore an indicator of whether a neuron preferentially encodes information about slow, intermediate, or fast components of a stimulus. This gives rise to the concept of *information filtering*. According to the frequency band where the coherence amplitude is maximal, one can characterize a neural system as a low-pass, band-pass or high-pass filter of information (see Fig. 1.4). An overview about different neuronal mechanisms that lead to information filtering is presented in (Lindner, 2016).

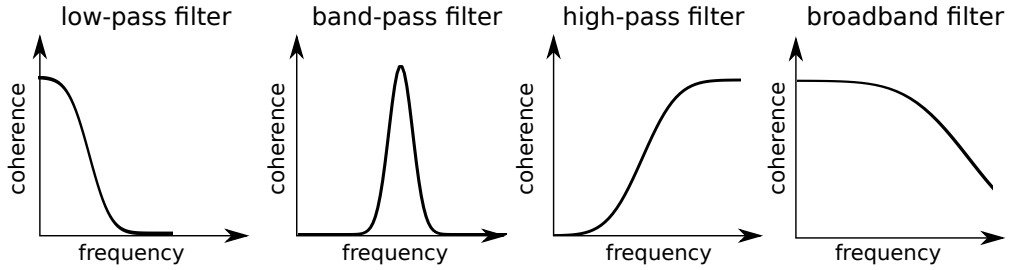

Figure 1.4.: **The coherence function reveals spectral information filtering properties.** Sketch of different shapes of the coherence function between an input and output process. According to the frequency where the coherence amplitude is maximal, one can characterize the output as a low-pass (coherence is maximal at low frequencies), band-pass (coherence is maximal at intermediate frequencies), high-pass (coherence is maximal at high frequencies) or broadband (coherence is high for a broad range of frequencies) filter of information.

In order for the coherence to really make a statement about the information filtering properties of the encoder, the stimulus should contain all frequencies with equal power and different frequency components of the stimulus should be independent of each other. Gaussian white noise fulfils these demands and is therefore used as a stimulus in theoretical calculations or experiments (as appropriate with a cutoff frequency) to obtain the coherence function.

In the following we will occasionally denote the cross-spectrum or spectral coherence

function between a neuronal output $x(t)$ and a stimulus simply as the 'cross-spectrum/ coherence of x', if it is clear what kind of stimulus process is used.

Limitations of the coherence function

When using the coherence function one needs to be aware that it is blind to nonlinear correlations between input and output. Frequency components that are suppressed according to the coherence may be encoded in higher-order correlations between the stimulus and the neuronal response. This issue was thoroughly addressed by Bernardi and Lindner (2015), where the coherence was compared to a frequency-resolved Shannon information measure. Bernardi et al. showed that for weak stimuli, the lower bound formula Eq. (1.10) equals indeed the Shannon mutual information rate for single Poisson and LIF neurons. However, qualitative differences were disclosed for the synchronous output of pairs of LIF neurons in certain parameter regimes.

1.5. Models of single neuron activity

In this section, we introduce theoretical concepts that allow us to describe, classify and model neural activity. Detailed introductions to concepts and methods used in computational neuroscience can be found in the text books by e.g. Rieke et al. (1996); Dayan and Abbott (2001) and Gerstner et al. (2014).

Mathematical representation of a neuron's output

The spike train $x(t)$ of a neuron can be formally written as a sum of δ-peaks,

$$x(t) = \sum_i \delta(t - t_i) \,, \tag{1.11}$$

$\{t_i\}$ being the times of the action potentials. This somehow artificial representation has the advantage that the firing rate of the neuron can be written as an ensemble average (average over all noise sources) over the spike train:

$$r_0 = \langle x(t) \rangle \,. \tag{1.12}$$

The number of spikes occuring within a time window $[a, b]$ is [using Eq. (1.11)] given by $\int_a^b x(t')dt'$. The instantaneous firing rate $r(t)$ is the average number of spikes that occur within an infinitesimal time interval $[t - dt/2, t + dt/2]$ divided by the with of the interval, i.e.

$$r(t) = \lim_{dt\to 0} \left\langle \int_{t-dt/2}^{t+dt/2} x(t')dt' \right\rangle / dt = \lim_{dt\to 0} \langle x(t)dt \rangle / dt = \langle x(t) \rangle \,.$$

If the average is the same for all times (stationarity), we denote the constant mean firing rate by r_0.

If the neuron is subject to a time dependent stimulus, the trial average of the spike train (keeping the stimulus realization s fixed) leads to the time-dependent *instantaneous firing*

rate which captures the mean response of the neuron to a fixed stimulus:

$$r(t)[s] = \langle x(t) \rangle \, . \tag{1.13}$$

The distribution of the times between two consecutive spikes, $\{t_{i+1} - t_i\}_i$, the so-called interspike intervals (ISI), is often used to study the variability (the 'noisiness') of the output of a neuron. A popular meassure of the neurons variability is the *coefficient of variation* (CV), which is the ratio between the standard deviation of the ISI and its mean value $\langle ISI \rangle = 1/r_0$,

$$CV := \frac{\sigma_{ISI}}{\langle ISI \rangle} \, . \tag{1.14}$$

We will also consider a filtered version of Eq. (1.11), which we call the *box train*, $b(t)$. It is defined by convolving the spike train with the boxcar function $\mathcal{B}(t) = \theta(t) - \theta(t - \Delta)$ (where θ is the Heaviside funtion):

$$b(t) := \mathcal{B} * x(t) = \int_{t-\Delta}^{t} x(t') \, dt' \, , \tag{1.15}$$

i.e. each spike at time t_i is replaced by a box of height one, going from t_i to $t_i + \Delta$. Hence, if Δ is much smaller than the mean ISI, $b(t) = 1$, if the neuron spiked within $[t - \Delta, t]$, otherwise it is zero (see Fig. 1.5 for illustration). The (stationary) mean value of the box train is then the probability that a neuron spikes within a time bin of width Δ:

$$\langle b(t) \rangle = \int_{t-\Delta}^{t} r_0 \, dt' = r_0 \Delta := R_0 \, . \tag{1.16}$$

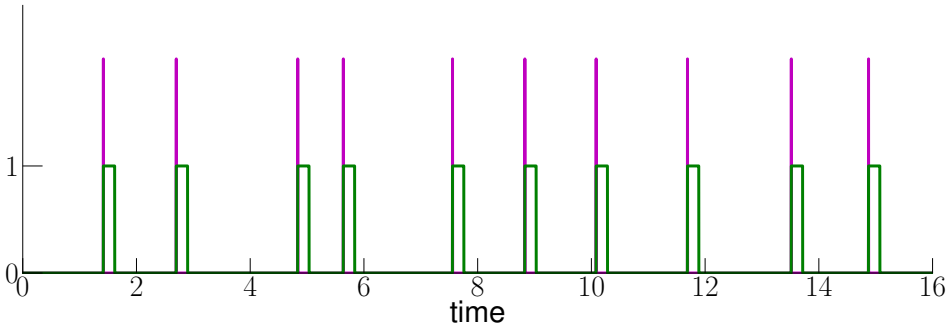

Figure 1.5.: **Spike train vs box train.** Example of a spike train, where the stripes indicate δ-peaks [magenta]. The corresponding 'box train', Eq. (1.15), [green] is obtained by convolving the spike train with a box of height one and width Δ. In this example, $r_0\Delta = 0.33$.

Integrate-and-fire neuron model

In this thesis we will use the *leaky integrate-and-fire* (LIF) neuron model (Stein, 1965; Knight, 1972). In this model the entire neuron is characterized by the membrane voltage potential $v(t)$, which is assumed to have the same value along the entire neuron. Its one-dimensional subthreshold dynamics is determined by

$$C\dot{v}(t) = -g_L v(t) + I(t) \,, \tag{1.17}$$

where C is the capacitance of the neuron, g_L is the effective leak conductance and $I(t)$ is the effective current that flows into the neuron. The creation of action potentials is added artificially through a fire- and-reset rule: whenever the voltage crosses the threshold voltage v_T, a spike is registered and the voltage is then reset to a value v_R where it is clamped for an absolute refractory period τ_{ref} before the sub-threshold dynamics continues. In all our simulations we use the parameter values $v_R = 0, v_T = 1$ and $\tau_{ref} = 0$.

The term 'leaky' refers to the fact, that the neuron is not a perfect insulator, such that ions diffuse through open ion channels in the membrane when some equilibrium (the effective leak potential, which we set to zero) is not reached in the cell. For this reason, the input current has to exceed the threshold $I_T = g_L v_T$ in order to cause the cell to fire, else the current will simply leak out of the cell. This can be seen from the solution of Eq. (1.17) for a constant net current $I(t) = I_0$, which reads

$$v(t) = \frac{I_0}{g_L}\left[1 - \exp\left(-\frac{t}{\tau_m}\right)\right] \,, \tag{1.18}$$

where $\tau_m = C/g_L$ is the effective membrane time constant, which determines how quickly the subthreshold voltage increases towards the threshold value.

If the mean net current is very large in comparison to the leak conductance, the leak term can be neglected, which leads to the dynamics of the perfect-integrate-and-fire (PIF) model

$$C\dot{v}(t) = I(t) \,. \tag{1.19}$$

As mentioned above, neurons are noisy systems. The intrinsic noise can be explicitly introduced by specifying the current as a sum of a mean base current μ and Gaussian white noise

$$\dot{v}(t) = -v(t) + \mu + \sqrt{2D}\xi(t) \,, \tag{1.20}$$

where D is the intensity of the additive intrinsic noise and $\langle \xi(t)\xi(t') \rangle = \delta(t - t')$. In Eq. (1.20), time is measured in multiples of the effective membrane time constant τ_m. Depending on the value of μ one can distinguish two firing regimes:
If $\mu < (v_T - v_R) = 1$, the base current by itself is not strong enough to excite the neuron (*subthreshold regime*). However, the voltage can be pushed above the firing threshold by the intrinsic noise. That is why this regime is also called 'fluctuation driven regime'. If $\mu \geq (v_T - v_R)$ (*suprathreshold regime*), the base current alone is sufficient to induce firing,

which is why this case is called 'mean driven regime'. Examples of realizations of the LIF model are shown in Fig. 1.6.

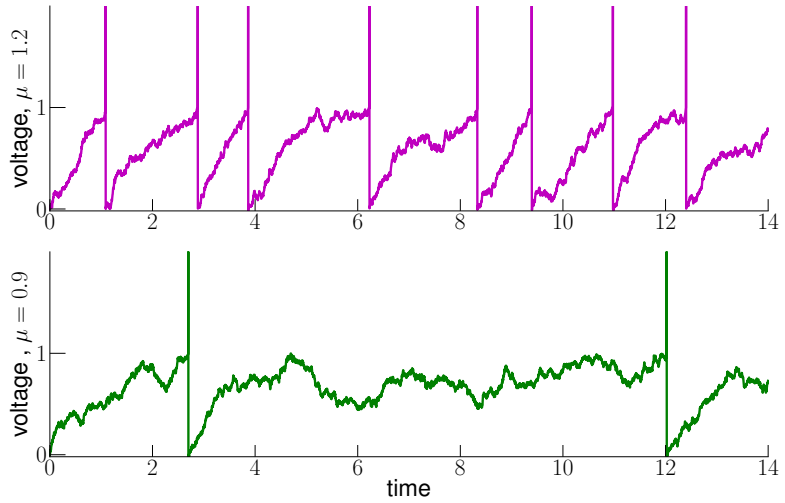

Figure 1.6.: Membrane voltage traces of the LIF neuron model, Eq. (1.20), in the suprathreshold firing regime ($\mu = 1.2$; magenta) and in the subthreshold regime ($\mu = 0.9$; green). Spikes at threshold crossings at $v_T = 1$ are added for the purpose of illustration. Intrinsic noise intensity $D = 0.02$.

1.6. Linear response theory

Linear response of a single neuron to a weak stimulus

If we consider a stimulus $s(t)$ to be weak, one can make the ansatz that the instantaneous, time dependent firing rate of the neuron is modulated only linearly by the stimulus (Fourcaud and Brunel, 2002; Gerstner and Kistler, 2002):

$$r(t) = \langle x(t) \rangle_\xi \approx r_0 + K * s(t) =: \hat{r}(t) \,, \tag{1.21}$$

where ξ denotes the intrinsic noise of the neuron, r_0 is the mean firing rate, and $K(t)$ is the linear response function. The asterisk in Eq. (1.21) stands for the convolution; $K * s\,(t) = \int_{-\infty}^{\infty} K(t-t')s(t')\,dt'$. Whenever we use the linear response ansatz, Eq. (1.21), to approximate a quantity, we mark the variable name of that quantity with a hat.

Usually one does not measure or compute the linear response function but its Fourier transform $\chi = \tilde{K}$ which is called *susceptibility*. One can derive the susceptibility, for example, by measuring the cross-spectrum between the spike train and a stimulus noise

process via the relation

$$\chi(f) = \frac{S_{x,s}(f)}{S_s(f)} \,. \tag{1.22}$$

To get acquainted with calculation methods used in this thesis we show how relation Eq. (1.22) can be derived. The cross-covariance between x and s reads

$$C_{s,x}(\tau) = \langle s(0)x(\tau)\rangle_{\xi,s} = \langle s(0)\langle x(\tau)\rangle_{\xi}\rangle_s \,, \tag{1.23}$$

where we used that the signal s and the intrinsic noise ξ are independent of each other and that $\langle s(t)\rangle_s = 0$ for all t. Using the linear response ansatz Eq. (1.21), we can approximate the cross-covariance by

$$\begin{aligned}
\hat{C}_{s,x}(\tau) &= \left\langle s(0)\left(r_0 + \int_{-\infty}^{\infty} K(\tau - t')s(t')\,dt'\right)\right\rangle_s && (1.24)\\
&= \int_{-\infty}^{\infty} K(\tau - t')\langle s(0)s(\tau)\rangle_s\,dt' && (1.25)\\
&= [K * C_{s,s}](\tau) \,. && (1.26)
\end{aligned}$$

By taking the Fourier transform of both sides and applying the convolution theorem ($\mathrm{FT}[g_1 * g_2] = \tilde{g}_1 \cdot \tilde{g}_2$) we obtain the desired relation between cross-spectrum and susceptibility

$$\hat{S}_{x,s}(f) = \chi(f)S_s(f) \,. \tag{1.27}$$

For the PIF and the LIF model there are analytical expressions for the susceptibility for an additive Gaussian white noise stimulus (Fourcaud and Brunel, 2002; Lindner and Schimansky-Geier, 2001; Brunel et al., 2001) [3]. The formula for the LIF model is stated in appendix Sec. A.1.

From Eq. (1.21) one can deduce a linear response approximation of the mean box train value, i.e. for the instantaneous windowed firing rate $R(t) = \int_{t-\Delta}^{t} r(t')\,dt'$:

$$\begin{aligned}
\langle b(t)\rangle_{\xi} = \langle \mathcal{B} * x(t)\rangle_{\xi} &= \int_{t-\Delta}^{t} r(t')\,dt' \\
&\approx r_0\Delta + \mathcal{B} * K * s(t) \\
&=: R_0 + \hat{s}(t) = \hat{R}(t) \,. && (1.28)
\end{aligned}$$

In this approximation, the probability that a neuron fires within the interval $[t-\Delta, t]$ is modulated by the *effective stimulus*

$$\hat{s}(t) := \mathcal{B} * K * s\ (t) \,. \tag{1.29}$$

Its Fourier transform reads

$$\tilde{\hat{s}}(f) = \tilde{\mathcal{B}}(f)\chi(f)\tilde{s}(f) \,. \tag{1.30}$$

The stochastic process $\hat{s}(t)$ is a linear functional of the Gaussian process s and therefore Gaussian as well. Like $s(t)$, the effective stimulus is centered around zero ($\langle\hat{s}\rangle = 0$), and

[3] Richardson (2007) presented a numerical scheme for deriving the susceptibility of an arbitrary integrate-and-fire neuron.

its power spectrum is by Eqs. (1.4) and (1.30) given by

$$S_{\hat{s}}(f) = |\tilde{\mathcal{B}}(f)\chi(f)|^2 S_s(f) \,. \tag{1.31}$$

The variance of the effective stimulus reads (by Eq. (1.5))

$$\begin{aligned} \langle \hat{s}^2 \rangle &= \int_{-\infty}^{\infty} S_{\hat{s}}(f)\, df \\ &= \Delta^2 \int_{-\infty}^{\infty} \mathrm{sinc}^2(\Delta\pi f) |\chi(f)|^2 S_s(f)\, df \,, \end{aligned} \tag{1.32}$$

where the sinc function, $\mathrm{sinc}(x) = \sin(x)/x$, emerges from the Fourier transform of the box filter:

$$|\tilde{\mathcal{B}}(f)| = \Delta\, \mathrm{sinc}(\Delta\pi f) \,. \tag{1.33}$$

1.7. Main model considered in this thesis

Motivated by the topology of sensory neurons, which we discussed in section 1.2, we study the following model. We consider a homogeneous population of N uncoupled spiking neurons, each of which has intrinsic, independent Gaussian white noise sources $\xi_k(t)$, $k \in \{1, \ldots, N\}$ with $\langle \xi_k(t)\xi_{k'}(t')\rangle = \delta_{k,k'}\delta(t-t')$. By homogeneous we mean that every neuron is defined by the same stochastic dynamical system receiving an identical mean input and therefore exhibiting the same average firing rate r_0. In addition, every neuron is stimulated by the same realization of a zero-mean Gaussian noise process $s(t)$, which we will refer to as the *common stimulus*. This common noise has a prescribed power spectrum $S_s(f)$ and an intensity of cD ($c \in [0,1], D \geq 0$), i.e.

$$\int_0^{\infty} \langle s(0)s(\tau)\rangle\, d\tau = cD \,. \tag{1.34}$$

When applying our theory to particular models, we will mostly consider white noise as a stimulus having a constant power spectrum of $S_s(f) = 2cD$ with an optional cutoff frequency f_c , i.e. $S_s(f) = 0$ for $|f| > f_c$. This choice is useful to see how the system reacts to an arbitrary frequency component of an input. However, white noise is certainly not a very natural stimulus. That is why we will also consider stimuli with a temporal correlation ('colored noise').

The constant D is the noise intensity of the total noise (common plus intrinsic noise) the single neuron is subject to, i.e. the total noise input of each neuron reads

$$\mathcal{N}_k(t) = s(t) + \sqrt{(1-c)2D}\, \xi_k(t) \,. \tag{1.35}$$

The noise intensity of Eq. (1.35) is given by

$$\int_0^\infty \langle \mathcal{N}_k(0)\mathcal{N}_k(\tau)\rangle \, d\tau = \int_0^\infty \langle s(0)s(\tau)\rangle \, d\tau + (1-c)2D \int_0^\infty \langle \xi_k(0)\xi_k(\tau)\rangle \, d\tau$$
$$= cD + (1-c)2D \int_0^\infty \delta(\tau) \, d\tau = D \,,$$

where we used Eq. (1.34) and that $\xi_k(t)$ is a Gaussian white noise process.

The parameter c quantifies the fraction of the total noise which is identical for each neuron. It is the correlation coefficient of the inputs of two different neurons and determines how large the common external stimulus is in comparison to the independent intrinsic fluctuations.

The correlation coefficient between the inputs of two different neurons ($k \neq k'$) is determined by

$$\frac{\int_0^\infty \langle \mathcal{N}_k(0)\mathcal{N}_{k'}(\tau)\rangle \, d\tau}{\sqrt{\int_0^\infty \langle \mathcal{N}_k(0)\mathcal{N}_k(\tau)\rangle \, d\tau}\sqrt{\int_0^\infty \langle \mathcal{N}_{k'}(0)\mathcal{N}_{k'}(\tau)\rangle \, d\tau}} = \frac{\int_0^\infty \langle s(0)s(\tau)\rangle \, d\tau}{D} = \frac{cD}{D} = c \,,$$

where we used the independence of the processes s, ξ_k and $\xi_{k'}$, Eq. (1.34) and the last auxiliary calculation.

If $c = 0$ there is no common stimulus and all neurons are completely independent. For $c = 1$, the independent fluctuations vanish such that every neuron in the population receives exactly the same input and thus behaves asymptotically (in the long-time limit) just the same way. In the analytical calculations we focus on the case of a weak common stimulus, being small in comparison to the other inputs of the neuron ($c \ll 1$).

Our theoretical considerations are general and do not assume a specific spiking neuron model. To compare our analytical results to numerical simulations we apply our theory to a population of LIF neurons, each of which follows the voltage dynamics

$$\dot{v}_k = -v_k + \mu + s(t) + \sqrt{(1-c)2D}\, \xi_k(t) \,; \qquad k = 1, ..., N \tag{1.36}$$

complemented by the fire-and-reset rule ($v_R = 0, v_T = 1$).

1.7.1. Summed vs synchronous population output

Motivated by the different readout mechanisms of postsynaptic cells we will consider two population outputs of the model described above: the summed population activity and the synchronous activity (see Fig. 1.7 for a schematic illustration) [4]. The sum of all N spike trains is the accessible input of a postsynaptic integrator. By the *summed activity* of a population we mean the sum of all presynaptic spike trains convolved with a boxcar function. This continuous time series can be also interpreted as the firing rate of an integrator cell.

A postsynaptic coincidence detector is only activated by synchronously arriving impulses, such that the synchronous presynaptic population output can be regarded as

[4] The explicit mathematical representations of the summed and synchronous activity will be introduced in chapter 3 and 4, respectively.

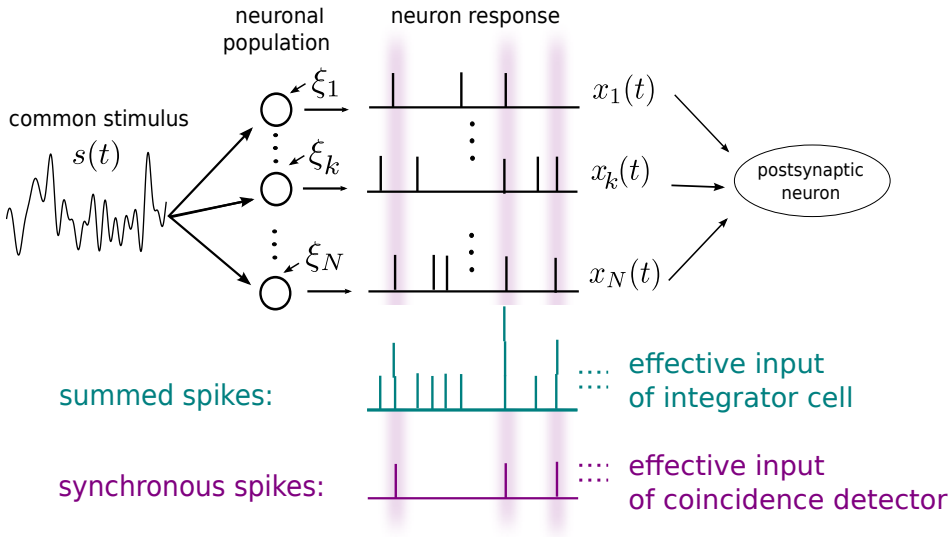

Figure 1.7.: **Schematic illustration of the model.** A population of N uncoupled neurons is subject to a common stimulus $s(t)$ and independent noise sources $\xi_k(t)$, leading to variable single neuron output spike trains $x_k(t)$. The sum of all spike trains ('all-spikes') [cyan] can be interpreted as the accessible input of an integrator cell. The partially synchronous output measures the times where at least a fixed fraction γ of the population has spiked within a short time window of width Δ [shaded stripes]. This time series [purple spike train] can be interpreted as the effective input of a postsynaptic coincidence detector, but also as its output.

the accessible or effective input of a coincidence detector. The activation threshold of the coincidence detector determines the minimal fraction of the population that needs to fire simultaneously. We will therefore consider the *partially synchronous output* of the presynaptic population, which we define as the time series that is one if *at least* a certain fraction γ of the population fired in synchrony within a short time interval of width Δ ('synchrony precision'), otherwise it is zero. Such a time series can be interpreted as the effective input, but also as the output of a coincidence detector, which needs $\gamma \cdot N$ simultaneously arriving action potentials in order to fire.

For a population of only two neurons (which we consider in the next chapter), only $\gamma = 1$ is meaningful, i.e. a synchronous event is recorded if both neurons fire simultaneously. However, for large populations, a lower value of γ will be biologically relevant because then it is very unlikely that all neurons fire at the same time if the common stimulus is weak.

The main goal of this thesis is to compare the coding properties of the summed to the synchronous population output. Do they extract different information about the common stimulus? Hence, in contrast to many other recent studies we are not primarily interested in measuring how much a population (or network) is synchronized, but rather we want to investigate the encoding capacity of the time series of synchronous events.

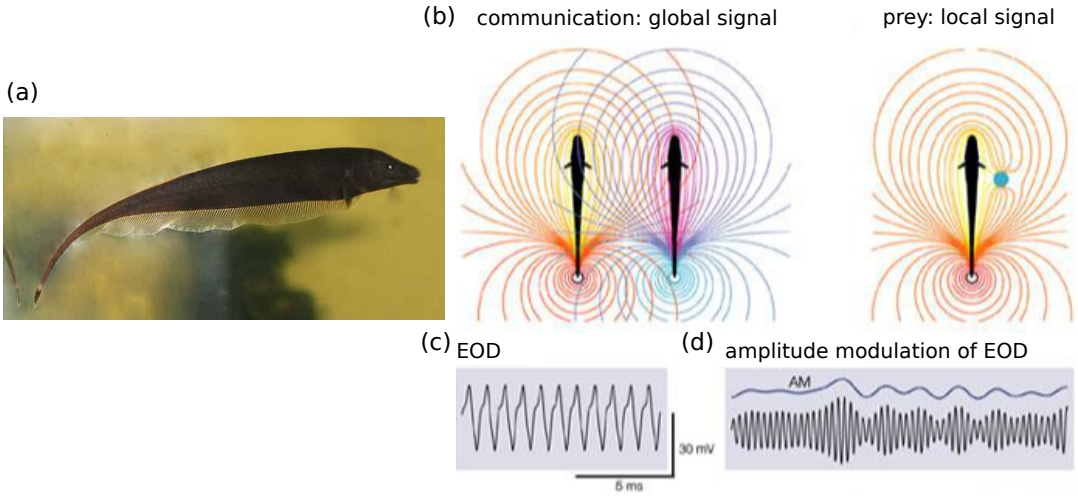

Figure 1.8.: **Weakly electric fish communicate and sense their environment by using electromagnetic fields.** Weakly electric fish, such as Apteronotus leptorhynchus [a], emit an electric field, called EOD, around their body. Electroreceptors in the skin of the fish sense perturbations like amplitude modulations [d] of the field caused by nearby objects or conspecifics. Communication signals lead to a global modulation of the EOD field [b, left], whereas perturbations caused by small prey animals effect only a localized, limited part of the sensory receptors [b, right]. Adapted from (Krahe and Gabbiani, 2004). ©2004, Nature Publishing Group.

In particular, we will examine the role of the synchrony threshold γ on the information transmission of the partially synchronous output.

1.8. Weakly electric fish: a model organism for studying neuronal information transmission

A popular model organism to study sensory information transfer is the weakly electric fish. This animal has developed an electro sense that enables it to communicate with conspecifics, to navigate, and to detect objects, such as prey. There are two classes of electroreceptors: passive and active ones. The passive or ampullary receptors are most sensitive to low-frequency (below 20 Hz) and spatially localized signals like those emitted by muscle activity of prey (Kalmijn, 1974; Engelmann et al., 2010). Weakly electric fish are, however, also able to actively generate an electromagnetic field around their body by discharging an electric organ in their tail (Bullock and Heiligenberg, 1986; Benda et al., 2013; Krahe and Maler, 2014). This regularly oscillating high-frequency field is called EOD ('electric organ discharge'). For the species *Apteronotus leptorhynchus*, EOD frequencies range from 600 to 800 Hz for females and from 800 to 1100 Hz for males (Meyer et al., 1987). The active tuberous organs detect distortions of the fish's own EOD

and those of conspecifics. The most prominent type of these active electroreceptors are P-units, which mainly encode amplitude modulations of the EOD (Scheich et al., 1973; Bastian, 1981; Kreiman et al., 2000) [see Fig. 1.8 for illustration]. Compared to ampullary cells, P-units code for a much wider frequency range up to about 400 Hz (Stamper et al., 2010; Walz et al., 2014; Henninger, 2015).

The electroreceptor afferents project onto postsynaptic cells in a feedforward- convergent manner and do not influence each other. In this model system the relevance of weak stimulation becomes evident, because weakly electric fish communicate at the limit of sensation (Henninger, 2015). They need to detect rivals and to communicate with conspecifics at large distances, leading to extremely low field intensities. Even if the distance between communication partners is small, a mismatch between signal frequency and P-unit tuning can lead to a weak activation of the receptors (Henninger, 2015; Walz et al., 2014; Stamper et al., 2010). Hence, the missing lateral connection between sensory receptors and their ability of encoding weak stimuli makes the weakly electric fish a suitable biological counterpart to our model setup presented in section 1.7.

Synchronous spikes of P-units code for high frequencies - ampullary cells do not show a synchrony code

A recent study by Grewe et al. (2017) investigated and compared the baseline (spontaneous) firing statistics and response properties of P-units to the ones of ampullary cells in the weakly electric fish *Apteronotus leptorhynchus*. Without stimulation, P-units fire very irregularly, having a high coefficient of variation of 0.5 on average. On the contrary, ampullary cells stand out by their regular spiking activity (mean CV of 0.1). This suggests that P-units are subject to much more intrinsic noise than ampullary cells are. The study revealed two main findings concerning the response of the receptors to a broadband white noise stimulus:

i) The synchronous output of pairs of P-units carries more information about a common stimulus than the synchronous output of ampulary cells does: the magnitude of the coherence of the synchronous spikes, which we abbreviate by 'synchro coherence', is higher for P-units than for ampulary cells (compare dashed lines in Fig. 1.9 C and F and see Fig. 1.10 A), even though the opposite holds true for the coherence of the summed output (compare solid lines in Fig. 1.9 C and F). Hence, ampullary cells encode stimuli more reliably (when taking all spikes into account), but there is hardly information encoded in their synchronous spikes, although the occurrence of synchronous events is comparable to the one of P-units if the synchrony precision Δ is fixed (see Fig. 1.10 C).

ii) Confirming the results from Middleton et al. (2009), the synchronous output of P-units acts as a band-pass filter of information in the case of weak stimulation. Compared to the coherence of the summed spike trains, the synchronous spikes discard low-frequency information and encode predominantly higher frequencies matching the ones of communication signals (see Fig. 1.9C). In contrast, the synchronous spikes of ampullary cells do not filter out special information about a stimulus. The synchro coher-

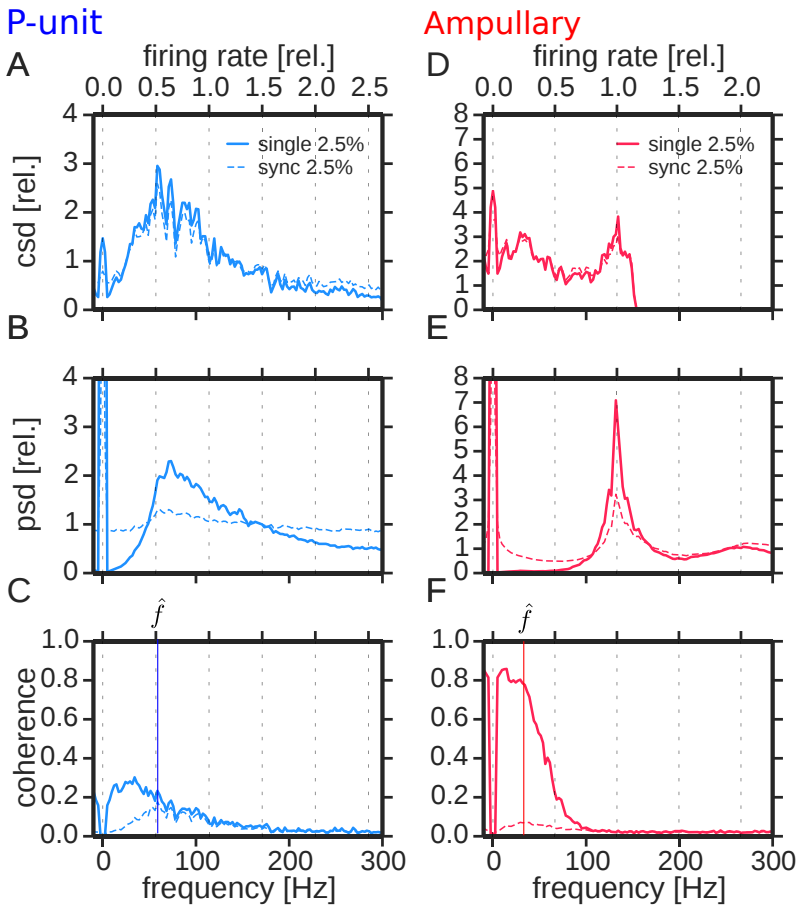

Figure 1.9.: **Comparison of stimulus-response spectra of P-unit and ampullary afferents.** [A–C] Cross-, power and coherence spectra of an example P-unit. Stimulus standard deviation was calibrated to 2.5 % of the EOD amplitude ('weak stimulus'). Cross- and powerspectrum are normalized by their average value. Solid lines show the single-neuron response and dashed lines the response of the synchronounous output of pairs of trials (synchrony precision: Δ =1ms). Vertical colored line in C marks the peak position of the coherence of the synchronous output $\hat{f}$. [D-F] Same analysis for an example ampullary cell. Adapted from (Grewe et al., 2017). ©2017, National Academy of Sciences.

ence of ampullary cells is strongly reduced in all frequency bands compared to the one of the single neuron (see Fig. 1.9F).

The band-pass filtering effect was quantified by measuring the peak position of the synchro coherence relative to the mean baseline firing rate. The all-spikes coherence has its maximum at a low frequency for both cell types. Hence, a synchro-coherence peak position close to the firing rate was regarded as an indicator for a synchrony code. In Fig. 1.10 B one sees that for weak stimulation (small response modulation) the peak of the synchro-coherence of P-units is closer to the baseline firing rate than it is the case for

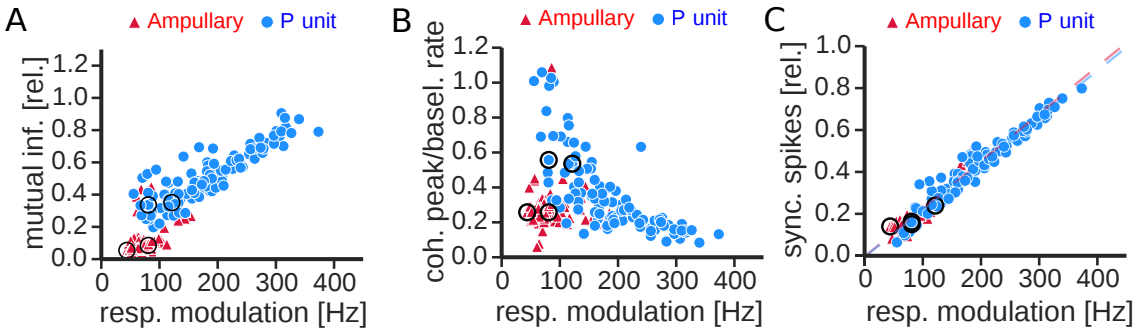

Figure 1.10.: **Coding efficiency and information filtering of the synchronous output of P-units and ampullary receptors.** Scatter plots compare properties of the spectral coherence of the synchronous spikes of ampullary afferents [red triangles] and P-units [blue dots] as a function of response modulation (effective stimulus strength). Black circles mark the example cells shown in Fig. 1.9. [A] Lower bound of the mutual information, Eq. (1.10), between stimulus and synchronous output relative to the mutual information of the summed response. [B] Position of the maximum of the coherence of synchronous spikes relative to the respective baseline firing rate. [C] Firing rate of the synchronous spikes relative to the average firing rate during stimulation. Dashed lines are linear regressions for the two types of electroreceptor afferents. Synchrony precision: $\Delta = 1$ms. Adapted from (Grewe et al., 2017). ©2017, National Academy of Sciences.

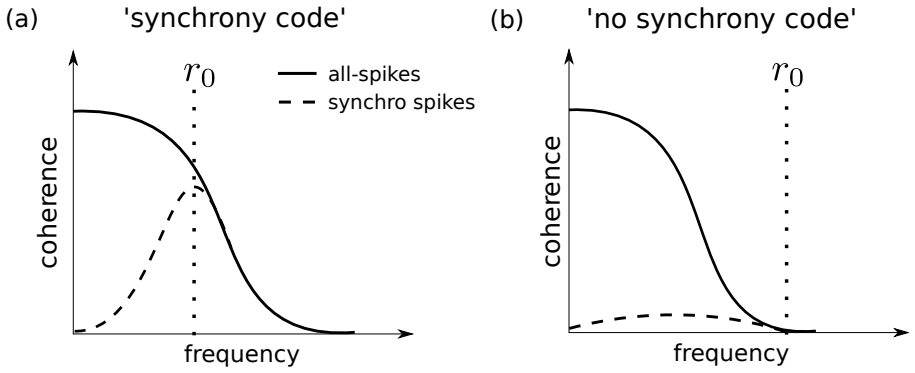

Figure 1.11.: **Illustration of the term 'synchrony code'.** [a] A population is to be regarded to carry a frequency resolved 'synchrony code', if the coherence of the synchronous spikes [dashed line] is strongly reduced at low frequencies, but close to the coherence of all-spikes [solid line] for high frequencies. A synchro coherence maximium around the single neuron firing rate r_0 is an indicator of such an information filtering behavior. [b] A population carries no synchrony code if the coherence of the synchronous output is strongly diminished at all frequencies. A synchro coherence maximum at much lower values than the firing rate is an indicator of such a behavior.

ampullary cells.

Put differently, i) and ii) suggest that there is a synchrony code in P-units but none in ampullary cells (see Fig. 1.11 for a schematic illustration of a 'synchrony code'). This disparity seems biologically very plausible. Ampullary receptors need to encode low-frequency signals as reliable as possible (Nelson and MacIver, 1999; Wilkens and Hofmann, 2005; Neiman and Russell, 2011). However, there is no need for ampullary afferents to encode or to extract high frequencies from a stimulus. P-units, on the other hand, encode signals with a much wider frequency range. It has been shown that during foraging and navigation low-frequency signals dominate (Nelson and MacIver, 1999; Fotowat et al., 2013; Krahe and Maler, 2014; Clarke et al., 2015), whereas high frequencies up to 400 Hz are relevant in the context of communication (Stamper et al., 2010; Walz et al., 2014; Henninger, 2015). Hence, a filtering mechanism that is able to extract certain frequency bands, such that these two types of signals can be distinguished, seems to be desirable for P-units. The synchronous output could be a candidate for such a filter.

What are the physiological properties that determine whether a sensory neuron is capable of a synchrony code? Is it solely the different intrinsic noise levels of the P-units and ampullary cells that lead to the distinct coding properties or do other characteristics like the leak conductance play a role as well? We address this question in detail in chapter 2.

1.9. The mechanism behind a synchrony code of pairs of neurons

The theoretical mechanism behind a synchrony code, as described in the last section, was uncovered in Sharafi et al. (2013). In their paper, analytical expressions were derived for the spectral statistics of the total synchronous output (SO) of a population of arbitrary size. 'Total' means that a synchronous event is recorded when *all* neurons of the population fire simultaneously within a certain time precision.

In the following, we want to recapitulate their results for the case of a pair of neurons. In Sharafi et al. (2013) the SO was measured by first convolving each individual spike train with a fixed Gaussian filter and then multiplying the convolved spike trains with each other [5]. In this thesis, we choose a different filter, namely the causal boxcar filter $\mathcal{B}(t) = \theta(t) - \theta(t - \Delta)$. The synchronous output of a pair of spike trains $x_1(t)$ and $x_2(t)$ is then given by the product of the respective box trains $b_k = \mathcal{B} * x_k$:

$$Y_{SO} = b_1 \cdot b_2 \,. \tag{1.37}$$

Choosing the box filter has the advantage of having a discrete synchrony condition: $Y_{SO}(t)$ measures whether both neurons spiked within the interval $[t - \Delta, t]$.

If a neuron spiked at time t_i, the corresponding box train equals one for $t \in [t_i, t_i + \Delta]$. If both neurons spiked within $[t - \Delta, t]$, both box trains have consequently the value one at time t, such that their product, Y_{SO}, equals one as well. If however one neuron has not spiked within this interval, the corresponding box train is zero at time t, such that Y_{SO} is zero as well. Hence, Y_{SO} measures indeed the synchronous spiking of the two neurons.

[5] A similar measure was used in (Schreiber et al., 2003) in order to assess the spike timing reliability.

We define the summed output for a pair of neurons by

$$A = \frac{1}{2}(b_1 + b_2) \,. \tag{1.38}$$

Cross-spectrum of the total synchronous output has the same shape as the cross-spectrum of the single and summed output

Sharafi et al. (2013) showed that the cross-spectrum between the total synchronous output and a weak common stimulus has approximately the same relative shape as the cross-spectrum of the single neuron or the summed output [6] , i.e.

$$S_{Y_{SO},s}(f) \propto S_{b,s}(f) = S_{A,s}(f) \,. \tag{1.39}$$

Here, we demonstrate this result for the synchronous output of a pair of neurons. The cross-covariance between the synchronous output, Eq. (1.37), and the common stimulus reads

$$\langle Y_{SO}(0)\, s(\tau)\rangle = \langle b_1(0) b_2(0)\, s(\tau)\rangle = \langle \langle b_1(0)\rangle_{\xi_1} \langle b_2(0)\rangle_{\xi_2}\, s(\tau)\rangle_s \,, \tag{1.40}$$

where we used that the intrinsic noise processes ξ_1 and ξ_2 are independent of each other and of $s(t)$. Using the linear response ansatz Eq. (1.28), $\langle b(t)\rangle_\xi \approx R_0 + \hat{s}(t)$, we can approximate the cross-correlation by

$$\begin{aligned} \langle Y_{SO}(0)\, s(\tau)\rangle &\approx \langle (R_0 + \hat{s}(0))^2\, s(\tau)\rangle_s \\ &= 2R_0 \langle \hat{s}(0)\, s(\tau)\rangle \,, \end{aligned} \tag{1.41}$$

where we used that the stimulus s and the effective stimulus $\hat{s}$ are both Gaussian processes with zero mean value, such that $\langle \hat{s}^2(0) s(\tau)\rangle = 0$.

The cross-covariance between the summed output, $A = (b_1 + b_2)/2$, and the stimulus equals the one of the single box train b_i and reads in linear response

$$\begin{aligned} \langle A(0)\, s(\tau)\rangle = \langle b(0)\, s(\tau)\rangle &= \langle \langle b(0)\rangle_\xi\, s(\tau)\rangle_s \approx \langle (R_0 + \hat{s}(0)) s(\tau)\rangle_s \\ &= \langle \hat{s}(0)\, s(\tau)\rangle \,. \end{aligned} \tag{1.42}$$

Combining Eq. (1.41) and Eq. (1.42), and applying the Wiener-Khinchin-Theorem, we derive the desired relation

$$S_{Y_{SO},s}(f) = 2R_0\, S_{b,s}(f) = 2R_0\, S_{A,s}(f) \,. \tag{1.43}$$

Because of Eq. (1.39), a change in the shape of the synchro coherence function, $C_{Y_{SO},s} = |S_{Y_{SO},s}|^2/(S_{Y_{SO}} \cdot S_s)$, in comparison to the one of the single neuron or summed output, must originate in an altered shape of the synchro power spectrum.

Synchro power spectrum is determined by self-convolutions of the single neuron power spectrum

Sharafi et al. showed that the power spectrum of the SO can be expressed by convolutions of the single neuron's power spectrum with itself. At this point, we want to

[6] We show in chapter 4 that this proportionality holds true for the more general partially synchronous output as well.

recapitulate this finding for the simple case of an independent pair of neurons (without stimulation).

The autocorrelation of process Eq. (1.37) reads

$$\begin{aligned}\langle Y_{SO}(0)Y_{SO}(\tau)\rangle &= \langle b_1(0)b_2(0)b_1(\tau)b_2(\tau)\rangle \\ &\overset{s=0}{=} \langle b_1(0)b_1(\tau)\rangle\langle b_2(0)b_2(\tau)\rangle \,,\end{aligned}$$

where we used in the last line that b_1 and b_2 are independent of each other if no common stimulus is present. By taking the Fourier transform and applying the convolution theorem, we obtain the power spectrum of the spontaneous synchronous output, reading

$$\bar{S}_{Y_{SO}}(f) = \bar{S}_b * \bar{S}_b(f) \,, \tag{1.44}$$

where we used that both spike trains are identically distributed. The bars in Eq. (1.44) indicate that the DC peaks are taken into account ($\bar{S}_b(f) = S_b(f) + \langle b\rangle^2\delta(f)$). The power spectrum of the synchronous output is therefore the single box train power spectrum convolved with itself ('self convolution'). Because usually, the single neuron power spectrum features a major nonzero-width peak around the firing rate, the self convolution results in an additional peak at zero frequency.

For the sake of completeness, we demonstrate the occurence of the additional peak, replicating the calculations in Sharafi et al. (2013). Lets consider the function

$$S(f) := T_-g(f) + T_+g(f) + R_0^2\,\delta(f) \,, \tag{1.45}$$

where $g(f)$ is a function with some nonzero-width peak at $f = 0$ and $T_\pm$ are shift operators that shift a function by the value $\hat{f}$. The last term is the DC-peak of a box train. Hence, Eq. (1.45) is a prototype of the power spectrum, $\bar{S}_b$, of a single box filtered spike train, having a firing rate around $\hat{f}$. Using the translation invariance of the convolution, i.e. $(T_\pm g) * (T_\pm g)(f) = T_\pm^2(g*g)(f)$, the convolution of $S(f)$ with itself brings

$$\begin{aligned}S * S(f) &= [T_-g(f) + T_+g(f) + R_0^2\delta(f)] * [T_-g(f) + T_+g(f) + R_0^2\delta(f)] \\ &= \underbrace{2R_0^2(T_-g + T_+g)}_{\dagger} + \underbrace{T_+^2(g*g)}_{\dagger\dagger} + T_-^2(g*g) + \underbrace{2\,g*g}_{\dagger\dagger\dagger} + R_0^4\delta(f) \,.\end{aligned} \tag{1.46}$$

Hence, restricting to only positive frequencies, the function $S * S(f)$ has a peak at $\hat{f}$ (term † in Eq. (1.46)), scaled by $2R_0^2$, at $2\hat{f}$ (higher harmonics) (††) and at zero frequency († † †). The latter two peaks are proportional to $g * g(f)$ and have therefore increased in width. This means that, compared to the original spectrum S, its self convolution has a peak with an increased width at $f = 0$.

Fig. 1.12 shows this phenomenon for the power spectrum of the box train of an LIF neuron $\bar{S}_b(f) = |\tilde{\mathcal{B}}|^2 S_{x_0}(f) + R_0^2\,\delta(f)$, where $|\tilde{\mathcal{B}}(f)| = \Delta\,\mathrm{sinc}(\Delta\pi f)$ and the power of the single LIF spike train, S_{x_0}, is stated in the appendix (Eq. (A.4)).

The power spectrum of the synchronous output thus exhibits an additional peak around zero frequency and is flattened compared to the power spectrum of the single neuron or of the summed output [7]. If the neuron pair is subject to a common stimulus, the power spectrum of Y_{SO} will have additional terms to Eq. (1.44), which we state in the appendix

[7] The summed population activity of a pair of independent neurons, $A = (b_1 + b_2)/2$, has the power spectrum $S_A = S_b/2$ and thus exhibits the same shape as the power spectrum of the single box train.

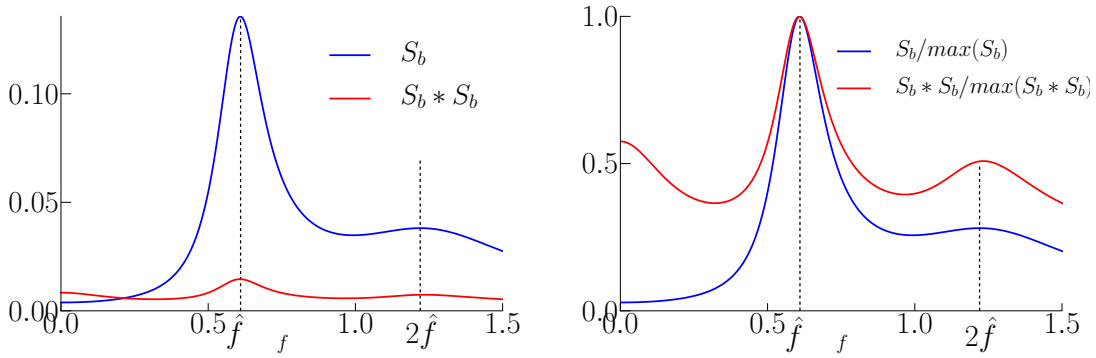

Figure 1.12.: **Self-convolution of single neuron power spectrum leads to additional peak at zero frequency.** The power spectrum of the single LIF box train [blue] is compared to its self-convolution [red]. [a] Absolute value. [b] Functions are rescaled by their maximal value. The convolution $\bar{S}_b * \bar{S}_b$ leads to additional peaks at zero frequency and at twice the frequency $\hat{f}$ there S_b has its global maximum. The peak frequency $\hat{f}$ equals approximately the firing rate r_0 (here: $\hat{f} = 0.61, r_0 = 0.58$). Parameters: $\mu = 1.2, D = 0.01, R_0 = 0.2$.

A.2. The major term in the case of weak stimulation, however, will still be the self convolution of the power spectrum of the single filtered spike train.

The additional peak at zero frequency of the synchro power spectrum leads to a synchro coherence that is reduced at low frequencies (see Fig. 1.13). However, whether there is a 'synchrony code' as described in Fig. 1.11, is also determined by the shape and magnitude of the single neuron cross-spectrum in relation to the single neuron power spectrum, which we demonstrate in the following chapter.

Sharafi et al. (2013) showed that the total synchronous output of populations of arbitrary size also shows a band-pass filtering effect, if the cross-spectrum of the single neuron features a pronounced peak around the firing rate. However, for large populations one cannot speak of a synchrony code, because then the magnitude of the synchro coherence is close to zero. The event that the entire population fires in synchrony is simply so rare that almost no information about the stimulus is encoded by the SO. In Chapter 5 we will show that the biologically more relevant *partially* synchronous output can indeed exhibit a synchrony code.

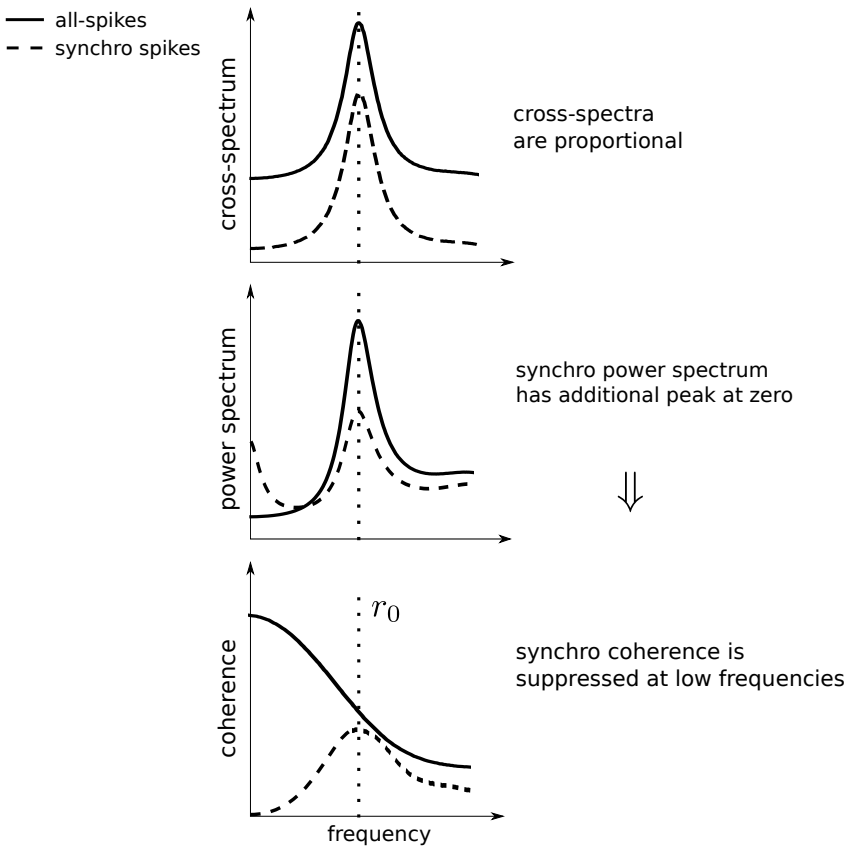

Figure 1.13.: **Mechanism behind a 'synchrony code'.** Sketch of the cross-, power and coherence spectrum of the summed [solid lines] and the synchronous [dashed lines] output of a pair of neurons that feature a synchrony code. The cross-spectra with a weak common stimulus are approximately proportional for both outputs. The power spectrum of the synchronous output has in comparison to the one of the summed output an additional peak at zero frequency. As a consequence, the synchro coherence is suppressed at low frequencies, which may lead to a band-pass filtering effect .

Chapter 2.

The role of leak conductance in information transmission

In Sec. 1.8 we reviewed that P-units and ampullary cells, although being closely related electroreceptor afferents in weakly electric fish, differ in their encoding properties. In contrast to the P-units, the synchronous output of ampullary cells does not encode special features of a stimulus. In this chapter we investigate the question whether these different coding properties are solely a consequence of the different intrinsic noise levels of the two cell types or whether other physiological properties play a role as well. We employ a modified version of the simple LIF neuron model, which is able to reproduce the different spectral statistics of both cell types. We show that in order to obtain a synchrony code, a moderate level of spiking variability is necessary but not sufficient; the neurons also need to feature a noticeable leak current.

Integrate-and-fire-neuron model with variable leak term

The usual LIF model Eq. (1.36) is not capable of mimicking the spectra of the ampullary cells. Choosing a low value of the intrinsic noise and a high mean input current can lead to similar coherence functions of the summed and synchronous output of pairs of neurons observed in ampullary cells, but one major limitation is the shape of the stimulus-response cross-spectrum. The cross-spectrum of the LIF model features a pronounced peak around the firing rate if the noise is weak (Vilela and Lindner, 2009a). Ampullary cells show in general a rather flat, declining cross-spectrum exhibiting only a small peak around the firing rate (see Fig. 1.9 D for an example). Such a cross-spectrum can be derived by reducing the leak current in the LIF model. We do so by introducing a new parameter $\alpha \geq 0$ to the usual LIF voltage dynamics:

$$\dot{v}_k = -\alpha\, v_k + \mu + \sqrt{2D_i}\,\xi_k(t) + s(t)\,, \quad k = 1,2\,, \tag{2.1}$$

complemented by the usual fire-and-reset rule ($v_R = 0, v_T = 1$). Like in the experiments, the common stimulus $s(t)$ is modelled by broad-band Gaussian white noise with cutoff frequency f_c and noise intensity D_s. The parameter α can be regarded as setting the leak conductance of the cell membrane. In the circuit model, Eq. (1.17), $\alpha = g_L/C$ describes the ratio between the effective leak conductance (inverse resistance) and the capacitance of the cell. The conductance g_L is directly connected to the number of open ion channels in the subthreshold (resting) state, whereas the capacitance is proportional to the cell's

surface area. The case $\alpha = 1$ corresponds to the ordinary LIF model. If $\alpha = 0$, Eq. (2.2) generates the spike train of a perfect integrate-and-fire neuron (PIF).

Figure 2.1 shows that we can find parameter values such that the spectra of the simulated model neurons look similar to the ones of the example cells presented in figure 1.9. An ampullary-cell-like behavior is obtained for low intrinsic noise intensity and a small leak term ($D_i = 0.002, \alpha = 0.1 \rightarrow$ CV = 0.06). A dynamics similar to the one observed in P-units is obtained by setting the intrinsic noise and leak to higher values ($D_i = 0.02, \alpha = 1 \rightarrow$ CV = 0.3).

The role of the intrinsic noise is to a great extent clear. A higher value of D_i leads to more irregular spiking (higher CV), and consequently to widened spectra and in general to a reduced stimulus-response coherence. But how does the leak influence the statistics of the single neuron and the population activity? In the next section we investigate this question in detail.

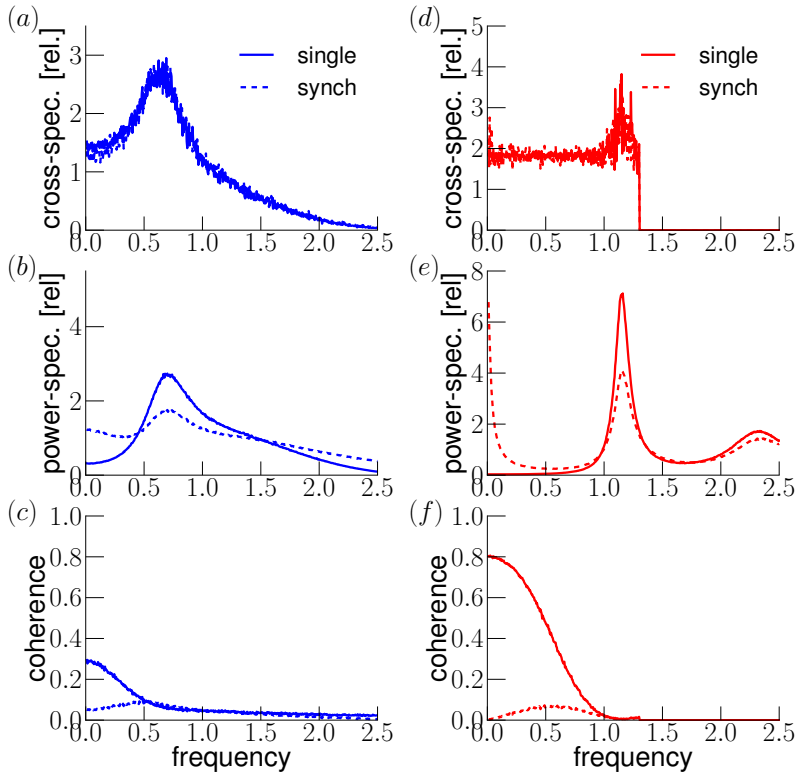

Figure 2.1.: **LIF model with variable leak term can qualitatively reproduce experimental results.** Same analysis as in Fig. 1.9 for simulation results of model Eq. (2.1). Left column: $\alpha = 1.0, D_i = 0.02, f_c = 3.0$; Right column: $\alpha = 0.1, D_i = 0.002, f_c = 1.3$. Coinciding parameters: $\mu = 1.2, D_s = 0.01, r_0\Delta = 0.2$.

2.1. Consequences of leak reduction in the LIF model

First, we investigate the baseline statistics of the single neuron, obeying the dynamics

$$\dot{v}(t) = -\alpha\, v(t) + \mu + \sqrt{2D}\, \xi(t)\,. \tag{2.2}$$

In Fig. 2.2 voltage traces are shown for $\alpha = 1$ and for $\alpha = 0.1$, keeping all other parameters fixed.

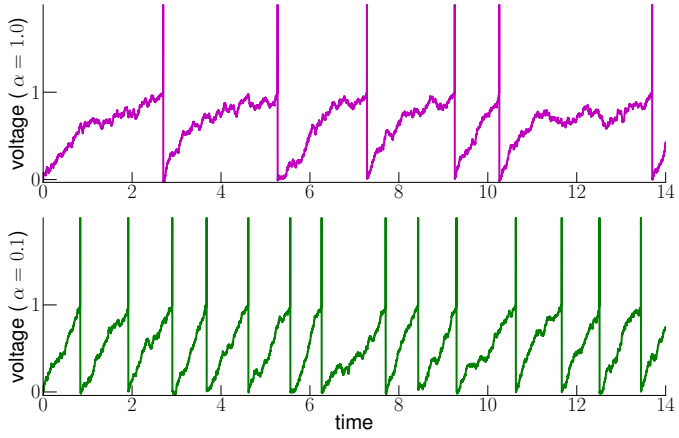

Figure 2.2.: Top row: voltage trace of LIF neuron with high leak term ($\alpha = 1.0$). Bottom row: voltage trace of low-leak neuron ($\alpha = 0.1$). Spikes at threshold crossings at $v_T = 1$ are added for the purpose of illustration. Remaining parameters: $\mu = 1.2, D = 0.02$.

Equivalent LIF dynamics

Dividing both sides of Eq. (2.2) by α we obtain the Langevin equation for the equivalent ordinary LIF dynamics:

$$\begin{aligned} \frac{d}{\alpha dt}\, v(t) &= -v(t) + \frac{\mu}{\alpha} + \frac{\sqrt{2D}}{\alpha}\, \xi(t) \\ \leftrightarrow \frac{d}{d\hat{t}}\, v\left(\frac{\hat{t}}{\alpha}\right) &= -v\left(\frac{\hat{t}}{\alpha}\right) + \frac{\mu}{\alpha} + \frac{\sqrt{2D}}{\alpha}\, \xi\left(\frac{\hat{t}}{\alpha}\right)\,, \end{aligned} \tag{2.3}$$

where we introduced a new time scale $\hat{t} = \alpha t$. If we further use that $\xi(\hat{t}/\alpha) = \sqrt{\alpha}\, \xi(\hat{t})$, because by definition

$$\left\langle \xi\left(\frac{\hat{t}}{\alpha}\right) \xi\left(\frac{\hat{t}'}{\alpha}\right) \right\rangle = \delta\left(\frac{\hat{t}}{\alpha} - \frac{\hat{t}'}{\alpha}\right) = \alpha\, \delta(\hat{t} - \hat{t}') = \alpha \langle \xi(\hat{t}) \xi(\hat{t}') \rangle\,,$$

Eq. (2.3) reads

$$\dot{v} = -v + \frac{\mu}{\alpha} + \sqrt{2\frac{D}{\alpha}}\,\xi(\hat{t})\,. \tag{2.4}$$

Eq. (2.2) is therefore equivalent to an ordinary LIF neuron with mean current μ/α, intrinsic noise strength D/α and rescaled time αt ($\leftrightarrow$ rescaled frequency f/α).

Hence, one can apply the analytical formulas for the firing rate $r_0[\mu, D]$, power spectrum $S_x(f)[\mu, D]$ and susceptibility $\chi(f)[\mu, D]$ of the LIF, stated in appendix A.1, to Eq. (2.2), by inserting the rescaled parameter values. The corresponding functions for the α-model are then in the original time scale given by

$$r_0^{(\alpha)} = \alpha \cdot r_0[\mu/\alpha, D/\alpha] \tag{2.5}$$

$$S_x^{(\alpha)}(f) = \alpha \cdot S_x(f)[\mu/\alpha, D/\alpha] \tag{2.6}$$

$$\chi^{(\alpha)}(f) = \chi(f/\alpha)[\mu/\alpha, D/\alpha]\,. \tag{2.7}$$

Note that quantities having the units of a frequency, like the firing rate and power spectrum, need to be multiplied by α in order to retain the original time scale.

Reduced leak leads to higher firing rate and more regular spiking

From Eq. (2.4) we see that for a neuron with low leak, i.e. for $\alpha < 1$, the effective mean current and intrinsic noise increases. The higher mean drive leads to an increased firing rate and a more regular output (lower CV), despite of the increased intrinsic noise level. This behavior can be observed Fig. 2.2 and in Fig. 2.3, where we see that the firing rate is a monotonically decreasing function of the leak α, whereas the CV is an increasing function of α. The low variability for small values of α leads to a power spectrum which is sharply peaked and concentrated around the firing rate r_0 (compare green graph for $\alpha = 0.1$ to the broader power spectrum [purple] for $\alpha = 1.1$ in Fig. 2.4).

Potential picture

It is insightful to picture $v(t)$ as the position of an overdamped Brownian particle that diffuses inside an potential $U(v)$ with absorbing boundary at the firing threshold:

$$\dot{v}(t) = -U'(v) + \sqrt{2D}\,\xi(t) \quad \text{with} \quad U(x) = \frac{\alpha}{2}v^2 - \mu v\,. \tag{2.8}$$

This analogy was first introduced by Bulsara et al. (1996) and used to characterise different firing regimes of integrate-and-fire neurons in (Vilela and Lindner, 2009b). As can be seen in Fig. 2.5, the ordinary LIF model [purple] has a distinctive quadratic potential that becomes less steep towards the threshold value v_T [1], i.e. the 'particle' slows down towards the firing threshold. Reducing the leak parameter α [green line in Fig. 2.5] leads

[1] This holds true in the suprathreshold regime where $\mu > v_T$.

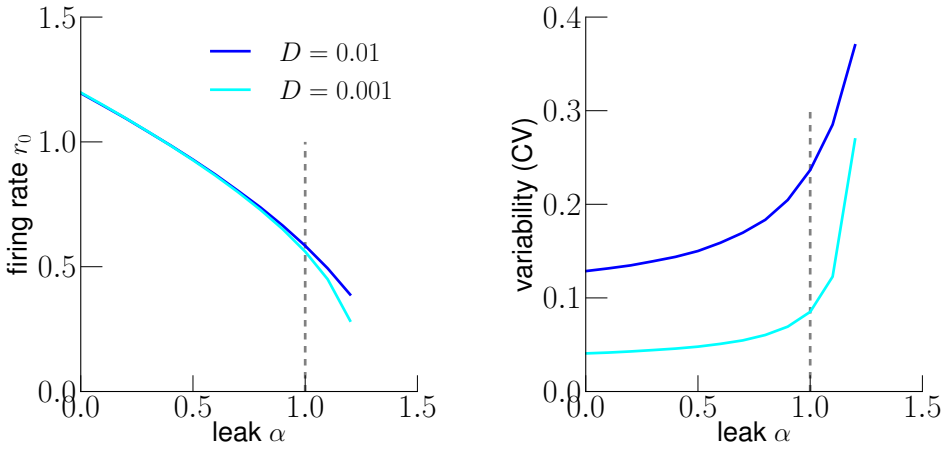

Figure 2.3.: **Leak reduction leads to higher firing rate and more regular spiking.** Firing rate and coefficient of variation for neuron model Eq. (2.2) in dependence on the leak constant α for two different intrinsic noise strengths as indicated. Vertical dashed line marks the ordinary LIF neuron. The case $\alpha = 0$ is equivalent to a PIF neuron. $\mu = 1.2$.

essentially to an almost linear potential with a steeper 'ramp', such that the particle rolls down the potential more quickly ($\rightarrow$ increased firing rate).

The different curvature of the potentials also influence the response to noise. If the derivative of the potential changes with the position of v, noise has a much higher influence on the firing statistics. Noise can push the particle to a region where it stays longer or the opposite: help it to escape slow regions more quickly. This leads to a more variable firing statistics than in the low-leak scenario, where the potential looks essentially the same for all v-values, such that noise does not influence the interspike time interval too strongly ($\rightarrow$ decreased coefficient of variation).

Impact of leak on coding properties

How does the leak influence the response properties of the single neuron and the synchronous output of pairs of neurons to a common stimulus? In Fig. 2.6 the cross-/power and coherence spectra of the summed [solid lines] and synchronous activity [dashed lines] of a pair of LIF neurons with $\alpha = 1$ is compared to the ones of a low-leak pair with $\alpha = 0.1$. The synchrony precision Δ is chosen, such that the mean spiking probability of the single neuron within a Δ-interval, given by $R_0 = r_0\Delta$, is kept constant. This allows a fair comparison. All other parameters are fixed [2].

[2] In Fig. 2.6 we also plot the linear response approximations of the spectra [black solid lines]. The equations are derived in chapter 4 and explicitly stated in the appendix A.2 for the case of pairs of neurons. Deviations from numerical simulation results are due to the high intensity of the stimulus compared to the strength of the intrinsic noise ($D_s = 5D_i$ in Fig. 2.6a).

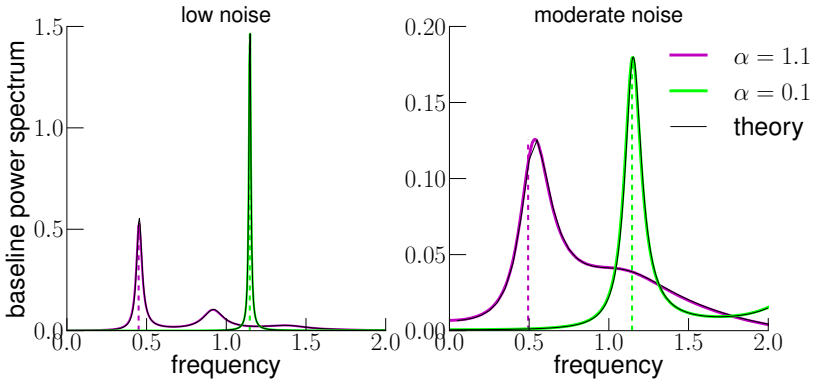

Figure 2.4.: **Reduction in leak leads to a sharper peak in the power spectrum.** Baseline power spectrum of the single neuron for high leak ($\alpha = 1.1$; purple) and low leak ($\alpha = 0.1$; green) for two intrinsic noise strengths (a) $D = 0.001$ and (b) $D = 0.01$. Firing rates are indicated by vertical dashed lines. Black line marks the analytical result Eq. (2.6). Mean input current: $\mu = 1.2$.

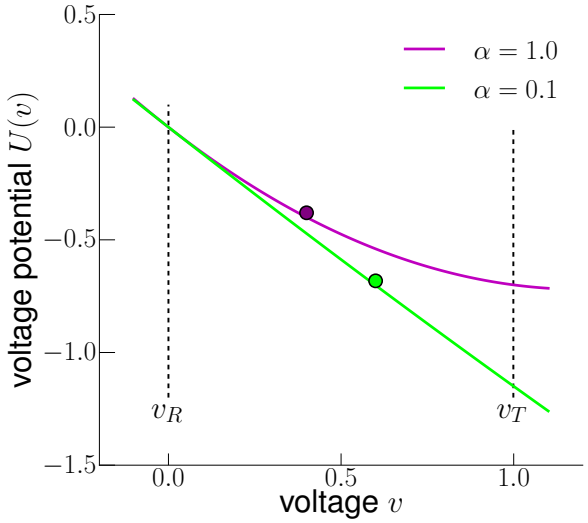

Figure 2.5.: **Potential picture of the voltage dynamics.** The voltage dynamics of an integrate-and-fire neuron can be interpreted as an overdamped particle that moves along a potential $U(v)$ [Eq. (2.8)]. Reducing the leak constant α leads to a steeper and more linear potential [green line] compared to the quadratic potential of the ordinary LIF neuron [purple line]. $\mu = 1.2$.

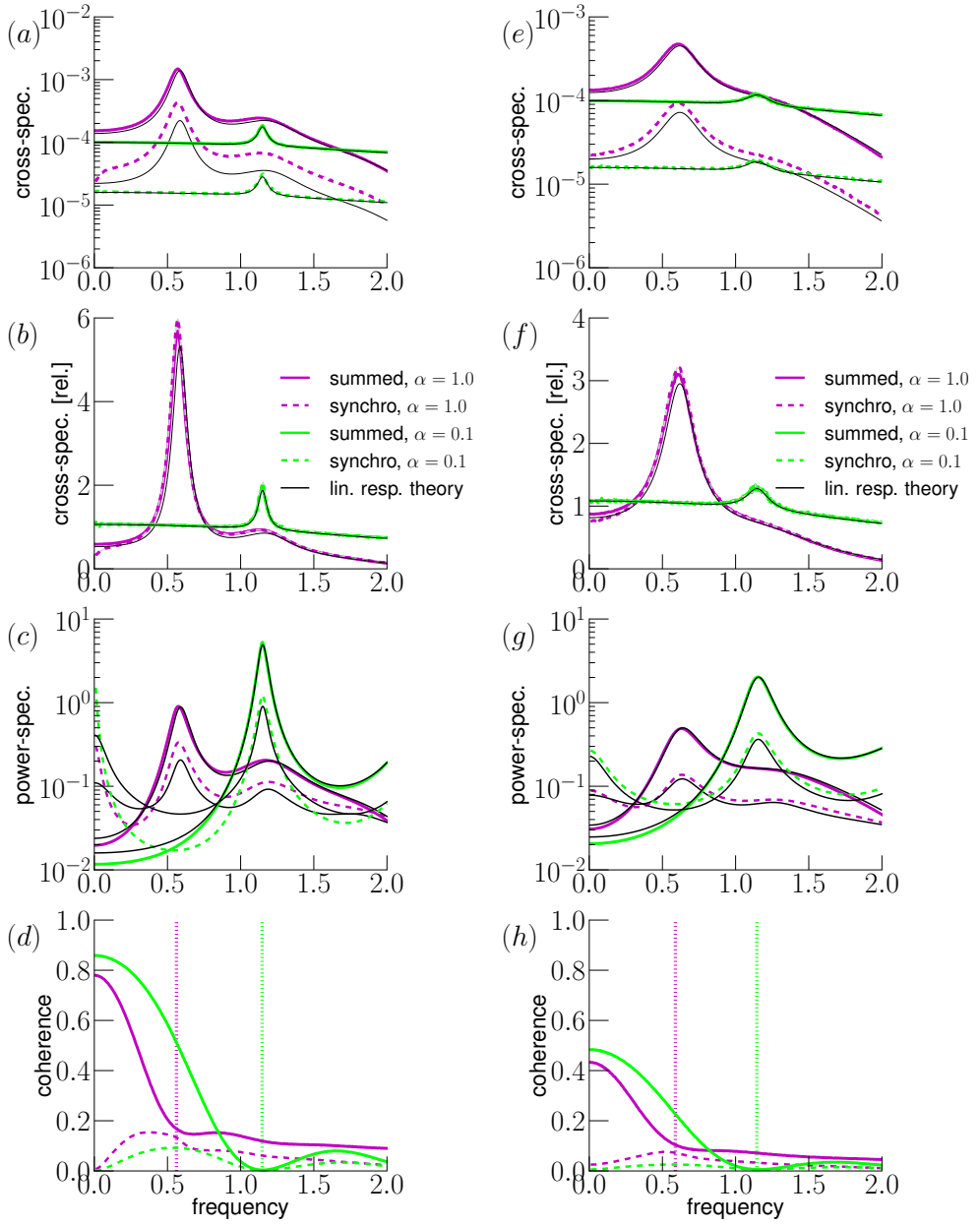

Figure 2.6.: **Change in spectral statistics due to leak reduction.** Spectra for the summed population activity [solid colored lines] and the synchronous output [dashed lines] of neuron model Eq. (2.1) for $\alpha = 1$ [purple] and $\alpha = 0.1$ [green] for two intrinsic noise levels $D_i = 0.001$ [left] and $D_i = 0.01$ [right]. Top row: absolute square of the cross-spectrum between output and common stimulus. Second row: absolute square of the cross-spectrum relative to its mean value. Third row: output power spectrum. Bottom row: coherence function. Vertical dotted lines mark the single neuron firing rate. Black solid lines show analytical results from linear response theory (see appendix A.2). To ease the comparison, the power and cross-spectra are divided by Δ^2 (which occurs in the Fourier transformed box filter $|\tilde{\mathcal{B}}|^2 = \Delta^2 \operatorname{sinc}^2(\Delta\pi f)$). Remaining parameter: $\mu = 1.2, D_s = 0.005, f_c = 4.0, R_0 = 0.2$.

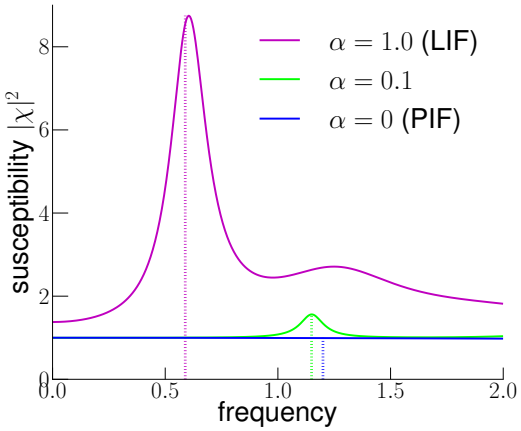

Figure 2.7.: **Leak reduction leads to decreased and flattened susceptibility.** Absolute square of the susceptibility $|\chi(f)|^2$ of neuron model Eq. (2.2) for $\alpha = 1$ (usual LIF neuron), $\alpha = 0.1$ (LIF with reduced leak) and for $\alpha = 0$ (leak-free PIF neuron). Vertical dotted lines mark the respective firing rates. Parameters: $\mu = 1.2, D = 0.01$.

Leak reduction leads to a decreased and flattened susceptibility/cross-spectrum

In the absence of a leak current ($\alpha = 0$), Eq. (2.1) is the voltage dynamics of a PIF neuron, which has a flat or monotonically decreasing susceptibility $|\chi(f)|$ [cf. blue solid line in Fig. 2.7]. The ordinary LIF neuron has in general a susceptibility which is peaked around the firing rate [cf. purple graph in Fig. 2.7]. A neuron with very low leak α has a susceptibility similar to the flat one of the PIF neuron but with a small peak at the firing rate [cf. green line in Fig. 2.7]. One notices that the magnitude of $|\chi(f)|$ decreases with a lower leak value, if one keeps all other parameters unchanged. The potential picture Eq. (2.8) can again supply some intuition for this behavior. For a distinct quadratic potential the response to a signal is dependent on the voltage value, or put differently, on the phase of the particle (whether it is close to the reset value or to the threshold). This results for a high leak neuron to a resonant response, i.e. the susceptibility is increased and peaked around the firing rate and multiples of it. For a linear potential, the signal acts the same way on the 'particle', independently on the voltage position, such that the susceptibility is a flat function.

The cross-spectrum between the spike train and a weak white stimulus reads $|S_{x,s}(f)| = 2D_s|\chi(f)|$ (see Eq. (1.22)) , such that the stated properties of the susceptibility hold true for the cross-spectrum of the single spike train and summed activity as well [3]. Accordingly, the cross-spectrum of the low-leak neuron is decreased and less peaked (compare green and purple solid lines in the top two rows of Fig. 2.6 and Fig. 2.9).

[3]The cross-spectrum of the summed activity, $A = (b_1 + b_2)/2$, includes the box-filter: $|S_{A,s}(f)| = 2D_s|\tilde{B}(f)\chi(f)|$ with $|\tilde{\mathcal{B}}(f)| = \Delta\ \mathrm{sinc}(\Delta\pi f)$.

For low leak, the coherence of the summed and synchronous activity is close to zero at the firing rate

The coherence function of the summed activity of a low-leak neuron is close to zero at the firing rate (see green solid line in bottom row of Fig. 2.6 and Fig. 2.9). This is because a flat cross-spectrum is divided by a power spectrum that has a sharp peak at the firing rate. Because the synchronous spikes carry less information about the stimulus than the summed spikes, the synchro coherence is always smaller than the coherence of the summed activity. Consequently, the coherence of the synchronous output is likewise close to zero at the firing rate (see green dashed line in bottom row of Fig. 2.6 and Fig. 2.9).

Reduction of leak leads to less synchronous spiking and to a reduced synchro coherence

One main experimental observation in (Grewe et al., 2017) was that the coherence between the synchronous output and the stimulus is much smaller for ampullary cells than for the P-units. For the α-model we notice that a leak reduction leads to a reduced synchro coherence (compare dashed green lines to dashed purple lines in Fig. 2.6 d,h). In Fig. 2.8b we compare the lower bound of the mutual information rate, R_{info}, of the summed activity to the one of the synchronous output for various stimulus intensities. While R_{info} of the summed activity of the low-leak neuron [solid green] is above the one of the LIF neuron [solid purple], the opposite holds true for the synchronous output [dashed lines]. There is less information encoded in the synchronous spikes if the leak is reduced. How can this behavior be explained?

In Fig. 2.8a one sees that the probability of a synchronous event, which equals the mean synchronous output, $\langle Y_{SO} \rangle$, decreases for smaller values of α. This can be a simple explanation for the reduction in the synchro coherence: fewer synchronous spikes carry less information. But why does the mean SO decrease although we fix the single cell spiking probability R_0 within a Δ-bin? This is a consequence of the reduced susceptibility of a low-leak neuron: If the single neuron is less susceptible to a stimulus, a population will be less synchronized by a common signal. This can be directly seen in mathematical terms if we look at the linear-response approximation of the mean SO (using Eq. (1.28)):

$$\begin{aligned} \langle Y_{SO} \rangle &= \langle b_1 \cdot b_2 \rangle = \langle \langle b_1 \rangle_{\xi_1} \langle b_2 \rangle_{\xi_2} \rangle_s \\ &\approx \langle (R_0^2 + \hat{s}\,)^2 \rangle_s = R_0^2 + \langle \hat{s}^2 \rangle \,, \end{aligned} \tag{2.9}$$

where $\langle \hat{s}^2 \rangle = 2D_s\Delta^2 \int_{-\infty}^{\infty} \mathrm{sinc}^2(\Delta\pi f)|\chi(f)|^2 \, df$ is the variance of the effective stimulus. Here, the mean synchronous output depends on the integral over the absolute value of the susceptibility (which we have shown to decrease with vanishing leak term). In addition, the bin width Δ also decreases for smaller values of α, because the firing rate r_0 increases, while the product $r_0\Delta = R_0$ is kept constant. In conclusion, approximation Eq. (2.9) predicts a decreased synchronous output for a low-leak neuron.

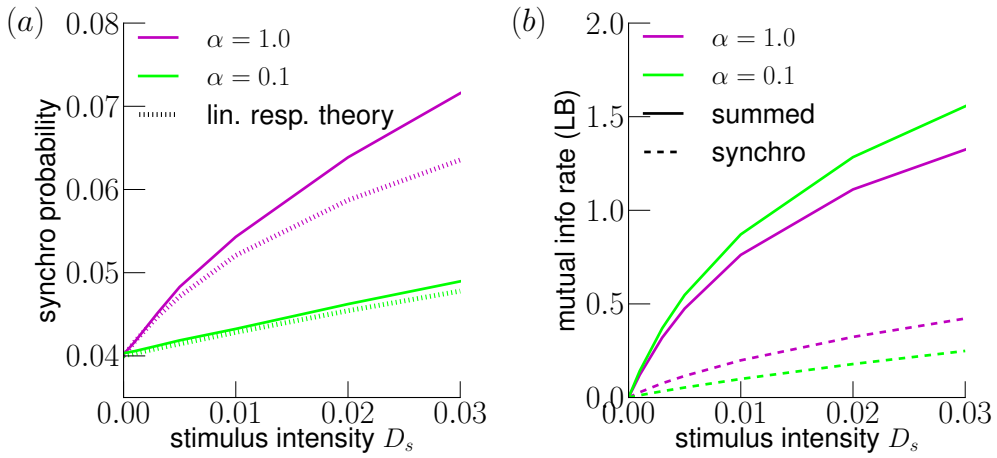

Figure 2.8.: **Leak reduction leads to less synchronous firing and to diminished information transmission of the synchronous output.** [a] Mean synchronous output $\langle Y_{SO} \rangle$ (probability of having a synchronous event within a Δ-time bin) vs noise intensity of the common stimulus for low [green] and high [purple] leakage current. Black lines show the theoretical approximation from linear response theory, Eq. (2.9). [b] Lower bound of the mutual information rate R_{info} for the summed [solid] and synchronous activity [dashed]. Remaining parameters: $\mu = 1.2, D_i = 0.01$.

As can be seen in Fig. 2.8a the simple approximation Eq. (2.9) [dashed lines] underestimates the measured mean SO, but it qualitatively captures the decrease of $\langle Y_{SO} \rangle$ with decreasing α.

At the first glance, this result seems to be in contradiction to Fig. 1.10C. There, the rate of synchronous spikes, $r_{synch} = \langle Y_{SO} \rangle / \Delta$, relative to the mean single neuron firing rate, r_0, is plotted against the response modulation σ_r (standard deviation of the instantaneous firing rate). The graphs overlap for P-units and ampullary cells [4]. However, using our notation, Fig. 1.10C shows $\langle Y_{SO} \rangle / (r_0 \Delta)$ versus $\sqrt{\langle \hat{s}^2 \rangle} / \Delta = \sigma_r$. Hence, in this plot the mean synchronous output is already arranged in order of the effective susceptibility $\sqrt{\langle \hat{s}^2 \rangle}$, such that it is no surprise that the data points of both cell types overlap. In fact, this is a confirmation of our theory that the mean synchronous output is most notably determined by the response modulation of the single cell, which corresponds in the linear response regime to the effective susceptibility.

In table 2.1 we summarize the influence of the leak current on the baseline and response statistics of the single neuron and the summed and synchronous population activity.

[4] In the experiments, the synchrony bin width Δ was the same for all cells.

single neuron/summed activity	synchronous output
• firing rate increases • CV decreases ⇒ power spectrum is sharply peaked and concentrated around the firing rate	
⇒ coherence function is high at low frequencies and approx. zero at firing rate	⇒ synchro coherence function is approx. zero at the firing rate
• reduced and flattened susceptibility	⇒ probability of a synchronous event decreases
⇒ cross-spectrum of all-spikes is rather flat	⇒ overall reduced synchro coherence

Table 2.1.: Overview of the consequences of reducing the leak current in the LIF model (decrease of constant α in Eq. (2.1)).

High-leak neuron can imitate coding properties of low-leak neuron but not the other way around

We have seen that a leak reduction in the LIF model leads to an increase in the firing rate and to a decrease in the variability. Are the different coding properties of high- and low-leak neurons simply a consequence of these two single-neuron statistics? To investigate this question we adjust the mean current input μ and the intrinsic noise strength D_i first of the ordinary LIF neuron ($\alpha = 1$) to match the firing rate and CV of the low-leak neuron ($\alpha = 0.1$).

In Fig. 2.9a IV we see that the coherence function of the summed and synchronous spikes of a low-leak neuron can be obtained by a usual LIF neuron, if the latter is subject to the same intrinsic noise and stimulus, but is driven by a high mean current μ, such that the mean firing rate and CV are matched. The low ISI-variabilty of this strongly driven LIF neuron leads to a power spectrum that matches the one from the low-leak neuron [5], i.e. it is sharply peaked around the firing rate and is strongly decreased at low frequencies (see Fig. 2.9a III). As a consequence, the all-spikes coherence is high at low frequencies and close to zero at the firing rate, regardless of the shape of the cross-spectrum, which is still very different in both cases (see Fig. 2.9a I and II). Also, the mean synchronous output still differs slightly for both cells ($\langle Y_{SO} \rangle_{\alpha=1} = 0.05$ and $\langle Y_{SO} \rangle_{\alpha=0.1} = 0.04$), which is a consequence of the weaker susceptibility of the low-leak neuron (cross-spectrum for $\alpha = 0.1$ is smaller than the one for $\alpha = 1$).

In conclusion, the information filtering of a low-leak neuron can be mimicked by a high-leak neuron that is driven by a strong mean input current. Or phrased differently: A high-leak neuron becomes a low-leak neuron for strong input currents, because then the leak term is simply negligible in Eq. (2.1). Here, it is the low variability (small CV) that determines the filtering properties and the drop of the synchro coherence.

[5] This is in accordance with Vilela and Lindner (2009b), where the authors show that the power spectra of the LIF and PIF model under white-noise stimulation are often very similar if the mean firing rate and CV are matched.

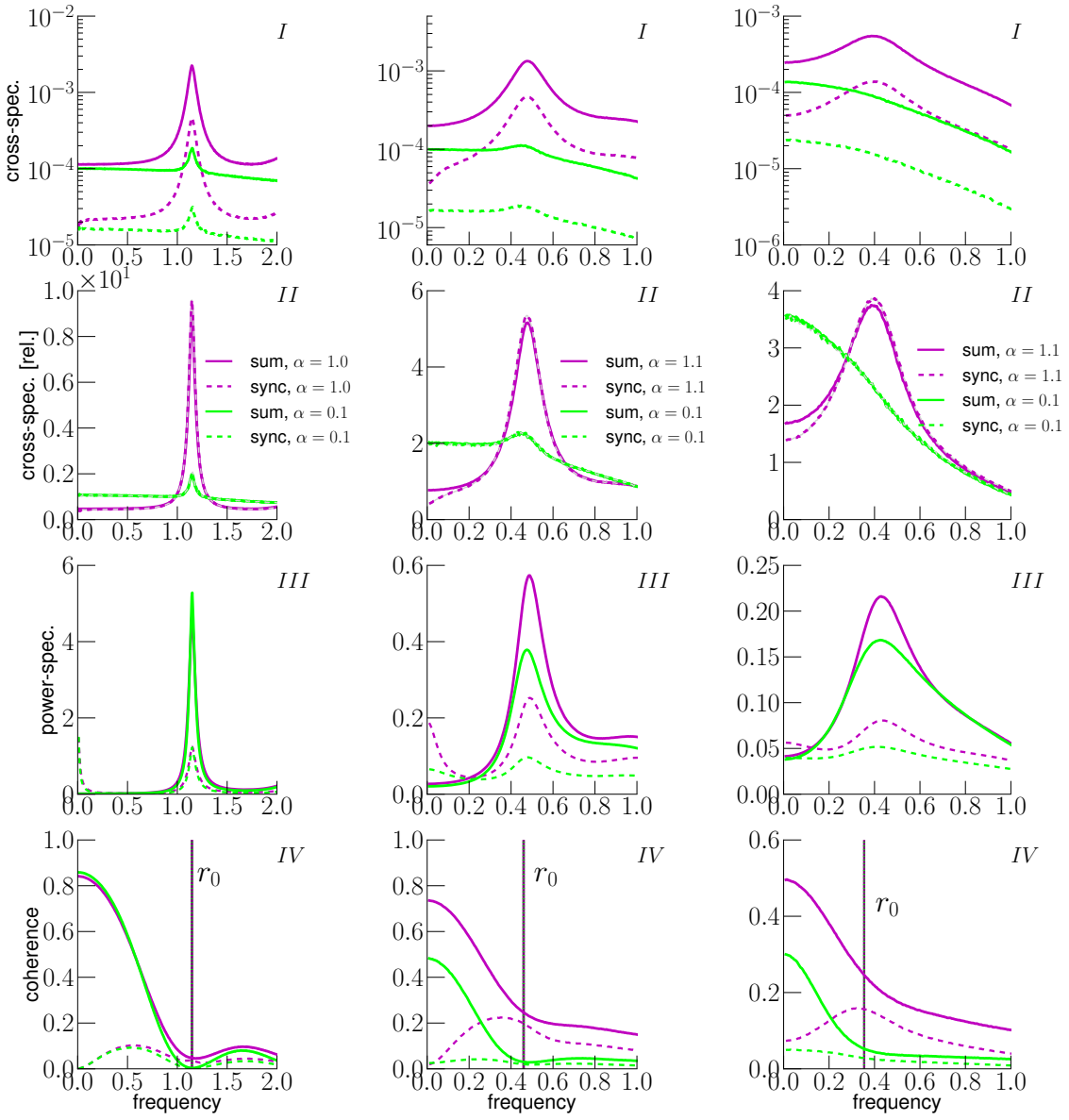

(a) $CV = 0.1$ (b) $CV = 0.25$ (c) $CV = 0.42$

Figure 2.9.: **LIF can mimic low-leak neuron but not the other way around. Moderate noise and high leak are necessary for a synchrony code.** Mean input current μ and intrinsic noise strength D_i have been adjusted, such that the firing rate r_0 and the CV of the high- and low-leak neuron match ([a] $r_0 = 1.15, CV = 0.1$, [b] $r_0 = 0.46, CV = 0.25$, [c] $r_0 = 0.35, CV = 0.42$). Same spectral statistics as in Fig. 2.6 for parameters: [a] green: $\alpha = 0.1, \mu = 1.2, D_i = 0.001$, magenta: $\alpha = 1.0, \mu = 1.72, D_i = 0.001$, [b] green: $\alpha = 0.1, \mu = 0.51, D_i = 0.01$, magenta: $\alpha = 1.1, \mu = 1.2, D_i = 0.001$, [c] green: $\alpha = 0.1, \mu = 0.4, D_i = 0.027$, magenta: $\alpha = 1.1, \mu = 1.09, D_i = 0.007$. In all graphs: $R_0 = 0.2, D_s = 0.005, f_c = 4$.

However, it does not work the other way around: the information filtering properties of a high-leak neuron can not be mimicked by a low-leak neuron, even if the mean current and intrinsic noise strength are adjusted such that the firing rate and CV are matched. (Please note, that the strength of the common signal and the time scale stay unchanged.[6]) In the middle and right column of Fig. 2.9 we plot the spectra for the low-leak ($\alpha = 0.1$, green) and the high-leak model ($\alpha = 1.1$, magenta), respectively, for a moderate CV of 0.25 (Fig. 2.9b) and a high CV of 0.42 (Fig. 2.9c). Even though the CV and firing rate are matched, the coherence functions of the summed and synchronous spikes are qualitatively very different for high CV values. For low leak, the coherence of both, the summed and the synchronous output, is generally smaller and especially low around the firing rate compared to the high-leak model (Fig. 2.9b and c IV). In contrast, the synchronous output of the high-leak pairs show a pronounced bandpass filtering effect (see dashed magenta line in Fig. 2.9b and c IV).

Here, the shape of the cross-spectrum does indeed matter. Also in this case, the cross-spectrum of the high-leak neuron is larger in magnitude and shows a more pronounced peak around the firing rate. A a consequence, the coherence of the summed and synchronous output is comparatively high around the firing rate. In contrast, the flat and low-magnitude cross-spectrum of the low-leak neuron leads to a coherence of the summed output that is small around the firing rate, such that the synchro-coherence is very low in all frequency bands; no information filtering effect is established (see green dashed line in Fig. 2.9b and c IV). In conclusion, a synchrony code, by means of a bandpass-filtering effect can only be obtained by a high-leak neuron.

2.2. Summary

Motivated by the different coding properties of P-units and ampullary cells in weakly electric fish, we investigated the simple leaky-integrate-and-fire neuron model with a variable amount of leak current. Real neurons are of course more complex than this model, but from our findings it can be concluded, that the effective leak conductance could indeed account for the different coding properties of the two cell types.

The LIF model with high leak and moderate intrinsic noise can mimic the coding properties of a P-unit: the synchronous output of pairs of neurons exhibits a bandpass filtering effect; the synchro coherence is strongly reduced at low frequencies but close to the all-spikes coherence around the firing rate.

Reducing the leak in the model leads to more regular firing and a flattened and reduced susceptibility. The regular firing (sharply peaked power spectrum) induces a higher all-spikes coherence, that is however small around the firing rate. The reduction in the stimulus response leads to less synchronization of a population by a common stimulus, such that the mean synchronous output is reduced resulting in a lower synchro coherence. All these properties were observed in ampullary cells. It is therefore

[6] By Eq. (2.4), adjusting the parameters to $\hat{\mu} = \alpha\mu, \hat{D}_i = \alpha D_i, \hat{D}_s = \alpha D_s$ and the time scale to $\hat{t} = t/\alpha$, transforms the usual LIF neuron to a neuron with a formal leak conductance α. Here, however, we want to compare cells on the same time scale.

plausible to hypothesize that ampullary cells have effectively a much lower leak conductance than P-units do. We have demonstrated that in order to obtain a synchrony code, moderate noise is a necessary but not a sufficient condition. The neuron has to exhibit a considerable leak conductance as well.

Chapter 3.

Distribution of the summed population activity

In the last chapter we have looked at the coding properties of pairs of neurons. In general there can be hundreds of neurons that process a common signal. In this chapter we examine the summed output of a population of arbitrary size. The statistics of the summed activity of a neuronal population receiving a common external signal has been in the focus of several studies. Expressions of the activity distribution have been derived by Amari et al. (2003) for simple Dichotomized Gaussian (DG) neurons in the limit of infinite large populations. Recently, Leen and Shea-Brown (2015) showed that when matching the mean firing rate and correlation between two neurons, the DG-model gives a good estimation of the activity distribution of populations of the more complicated exponential integrate-and-fire neuron model. These results, however, require computational fitting of model parameters. Here, we present analytical approximations (where no fitting of parameters is needed) of the distribution of the summed activity of a general homogeneous population which is driven by a weak common noise stimulus. This distribution will be a crucial ingredient for calculations of the synchronous population output.

3.1. Definition of the summed population activity

We define the time-dependent *summed population activity* $A(t)$ as the fraction of a spiking population which has been active within the small time interval $[t-\Delta, t]$. It can be formally written as a sum of integrals over the N spike trains

$$A(t) = \frac{1}{N} \sum_{k=1}^{N} \int_{t-\Delta}^{t} x_k(t')dt' \,. \tag{3.1}$$

Because the spike trains $x_k(t)$ are mathematically represented by δ-peaks, the integral of them over a given time window gives the number of spikes within that window. Hence, Eq. (3.1) is the normalized population spike count and differs from the standard definition of a rate (Gerstner et al., 2014). Here, the summed activity is a dimensionless discrete variable, $A \in \{0, 1/N, 2/N, ..., 1\}$. If $A(t) = 0$, then there was no spike within $[t-\Delta, t]$, whereas $A(t) = 1$ corresponds to the case where all neurons fired simultaneously (assuming a sufficiently small bin width Δ, such that the probability that a single neuron fires twice in one bin can be neglected).

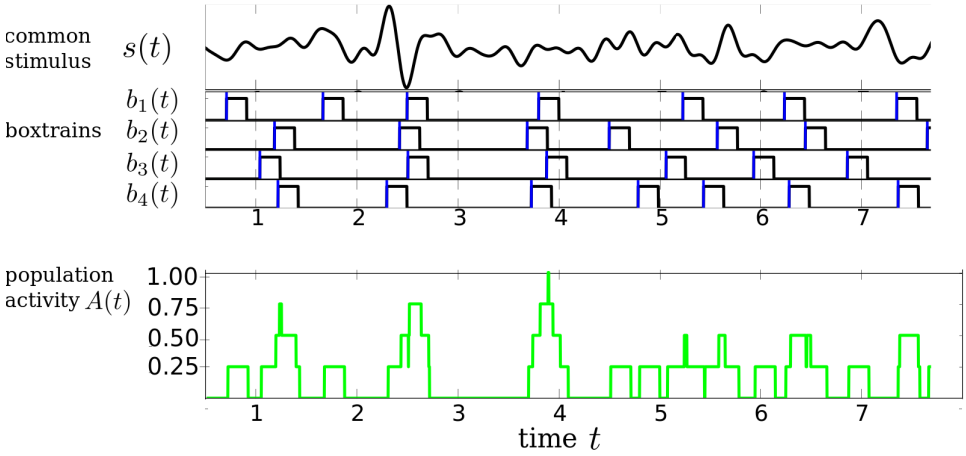

Figure 3.1.: **Definition of the summed population activity.** A population of four neurons is driven by a common stimulus (upper panel). Middle panel: Each spike train (blue) is convolved with a box of width Δ, resulting in a box train (black). The summed activity (lower panel) is given by the sum of all box trains divided by the population size N.

By using the definition of the box train, Eq. (1.15), we can write the summed activity as a sum over the single box trains

$$A(t) = \frac{1}{N} \sum_{k=1}^{N} b_k(t) \,. \tag{3.2}$$

Because $b(t) \in \{0, 1\}$ for small Δ, representation Eq. (3.2) has the advantage of seeing immediately that A is a sum of binary stochastic processes, i.e. Bernoulli processes. Fig. 3.1 shows an example of a raster plot and the corresponding population activity.

3.1.1. Summed activity in dependence on input correlations

Our aim is to find the distribution p_A of the summed activity for the model described in section 1.7. In Fig. 3.2a we show simulation results for the distribution of A for a moderately sized population of $N = 30$ LIF neurons and different values of input correlation c. With increasing correlation, the density changes from a narrow unimodal to a bimodal distribution. The shift of probability towards the extremes can be regarded as the synchronizing effect of the common noise, resulting in common firing ($A \approx 1$) and common silence ($A \approx 0$). The mean value of the population activity is however independent of the input correlation:

$$\langle A \rangle = \frac{1}{N} \sum_{k=1}^{N} \langle b_k \rangle = R_0 \,, \tag{3.3}$$

where we used Eq. (1.16). Hence, the average activity is given by the probability $R_0 = r_0 \Delta$ that a single neuron spikes within a Δ-bin.

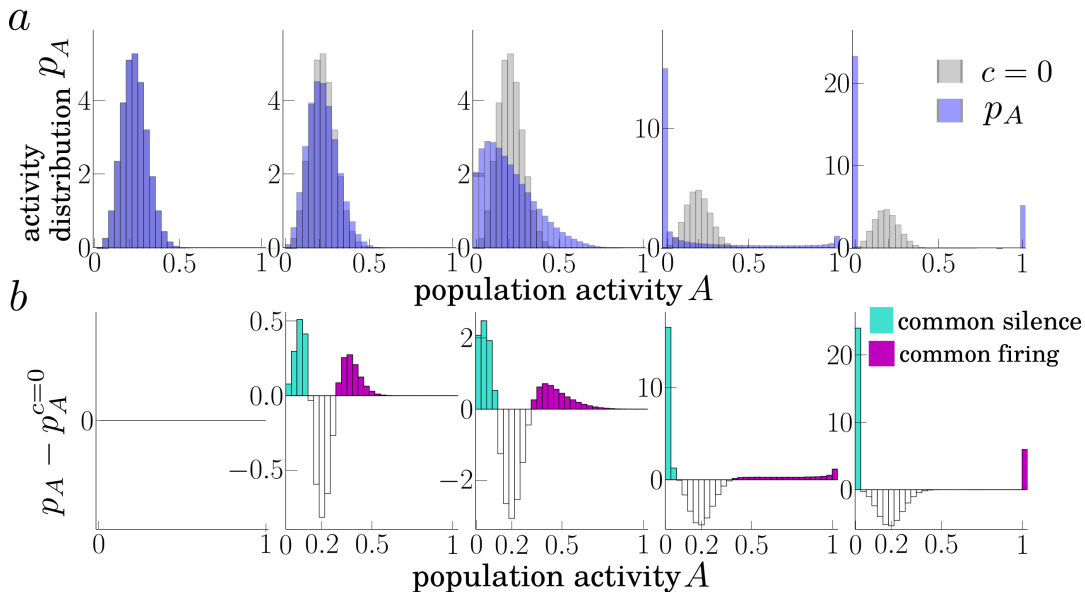

Figure 3.2.: **Synchronizing effect of common noise.** [a] Activity distribution for different values of the input correlation c (from left to right: $c = 0.0, 0.05, 0.4, 0.99, 1.0$). For comparison, the density p_A for totally independent input ($c = 0$) is plotted in gray. [b] Respective difference between the activity distribution for positive c and the one for the uncorrelated case reveals the synchronization of the population that is solely induced by the common external noise. Positive weight close to zero corresponds to a common 'silence' of the population, whereas positive weight close to one, depicts enhanced common firing. Parameters: $N = 30, \mu = 1.2, D = 0.2, \Delta = 0.25$.

It is important to bring to mind, that even in the case of no input correlation, neurons fire simultaneously by chance. In fact, $R_0 \cdot N$ neurons fire on average simultaneously inside a Δ-interval. To extract the synchrony which is solely induced by the common noise, it is revealing to subtract from the activity distribution the independent baseline activity (see Fig. 3.2b). For our analytical calculations, we focus on the weak correlation regime ($c \ll 1$), in which linear response theory can be applied.

General theoretical considerations

We consider the bin width Δ to be substantially smaller than the mean interspike interval $1/r_0$, i.e. $R_0 \ll 1$, such that the probability for one neuron to spike more than once inside a bin is negligible. Hence, the individual neuron either spikes with some probability R and it does not spike with probability $1 - R$. For a fixed realization s of the common stimulus every neuron of the homogeneous population spikes with the same probability $R[s]$. Here, $R[s] = R[s(t'), t' \leq t]$ is a functional of a single realization s up to time t due to causality. Because the spiking probability is the same for each neuron and the neurons are statistically independent of each other for a fixed stimulus realization, the number of active neurons inside $[t - \Delta, t]$ obeys a binomial distribution. To obtain the

distribution of $A(t)$, this conditional firing probability needs to be averaged over all possible realizations of the stimulus. The total probability that exactly $m \in \{0, 1, ..., N\}$ out of N neurons are active is given by

$$\mathbb{P}\left(A = \frac{m}{N}\right) = \left\langle \binom{N}{m} (R[s])^m (1 - R[s])^{(N-m)} \right\rangle_s . \tag{3.4}$$

This equation has already been used for specific neuron models by Amari et al. (2003); Leen and Shea-Brown (2015). In order to get a probability density p_A for A, such that $\mathbb{P}(A) = p_A(A)\,\Delta A$ with $\Delta A = 1/N$, Eq. (3.4) must be multiplied by $1/\Delta A = N$

$$p_A(A) = N\binom{N}{AN} \left\langle \left((R[s])^A (1 - R[s])^{(1-A)}\right)^N \right\rangle_s . \tag{3.5}$$

How to perform the average over all stimulus realizations is a nontrivial problem because one must specify $R[s]$. We approximate $R[s]$ for a weak stimulus in sec. 3.1.2. Alternatively, one can incorporate the stochasticity of s into R directly: R can be interpreted as a random variable with probability density p_R. If this density is known, we can express the probability density Eq. (3.5) by

$$p_A(A) = N\binom{N}{AN} \int_0^1 \left(R^A (1 - R)^{(1-A)}\right)^N p_R(R)\, dR . \tag{3.6}$$

This means, that one only needs to know the distribution of the single neuron spiking probability/firing rate within a time bin. Then, using Eq. (3.6), one can analytically compute the distribution of the population activity.

It is instructive to consider the limit cases concerning the input correlation. In the absence of correlation ($c = 0$), the firing rate is not modulated by a common stimulus, such that there is only one firing probability, given by the mean firing rate. Hence,

$$p_R^{c=0}(R) = \delta(R - R_0) . \tag{3.7}$$

For full correlation ($c = 1$), i.e. in the absence of independent noise, the system is completely deterministic for a frozen stimulus. The probability to spike at a given time is then either one or zero, such that

$$p_R^{c=1}(R) = R_0\, \delta(R - 1) + (1 - R_0)\delta(R) . \tag{3.8}$$

The transition between these extremes of p_R for different input correlation is sketched in Fig. 3.3a with the corresponding activity distributions in Fig. 3.3b.

An important connection between p_R and p_A is

$$p_R = \lim_{N\to\infty} p_A . \tag{3.9}$$

This relation is obtained from Eq. (3.6), using that the binomial distribution converges to

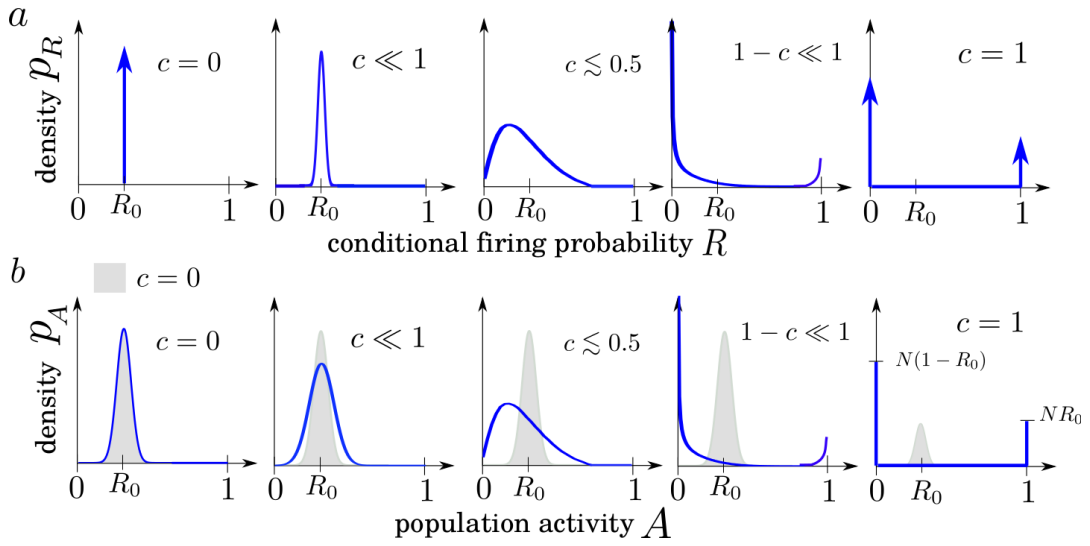

Figure 3.3.: **Sketch of the qualitative change in the distributions of p_R and p_A for varying input correlation c.** [a] Probability density of the stimulus-conditioned windowed firing rate. [b] Corresponding population activity distributions. For comparison, p_A of the stimulus-free case ($c = 0$) is shown in shaded gray.

a normal distribution, which in turn approaches a δ function in the limit of infinite N:

$$N\binom{N}{AN}\left(R^A(1-R)^{(1-A)}\right)^N \approx \sqrt{\frac{N}{2\pi R(1-R)}}\exp\left[\frac{N(A-R)^2}{2R(1-R)}\right] \xrightarrow[N\to\infty]{} \delta(A-R)\,. \tag{3.10}$$

An intuitive way of deriving Eq. (3.9) is to think about how one would measure p_R. If we fix a stimulus realization s and simulate the response of a single neuron in n trials, we can perform an average over the intrinsic noise. For a chosen time bin $[t-\Delta, t]$ we then obtain the firing probability $R[s]$ by adding up the spikes of all n trials within this interval and divide it by n. This value is indeed nothing but the activity of a homogeneous population of size $N = n$ driven by s. Hence, in order to numerically estimate the distribution of R, one simply measures the distribution (average over many realizations s) of the activity A for a very large value of N.

In the following two sections we present analytical approximations for p_R and p_A for the case of weak common stimuli.

3.1.2. Approximation of the firing probability distribution

The probability for a single neuron to fire within a time interval $[t-\Delta, t]$ can be formally derived by integrating the instantaneous firing rate $r(t)$ over this interval

$$R(t) = \int_{t-\Delta}^{t} r(t')dt' = \mathcal{B} * r(t)\,, \tag{3.11}$$

where again $\mathcal{B}(t) = \theta(t) - \theta(t - \Delta)$ is the boxcar filter. For a fixed stimulus realization s, the instantaneous firing rate is the spike train averaged over the intrinsic noise, i.e. $r(t) = \langle x(t) \rangle_\xi$. The time-dependent spiking probability $R(t)$ can be regarded as the instantaneous *windowed firing rate* and is the box train, $b(t) = \mathcal{B} * x(t)$, averaged over the intrinsic noise:

$$R[s](t) = \langle b(t) \rangle_\xi \, . \tag{3.12}$$

For a weak stimulus $s(t)$, we can use the linear response approximation Eq. (1.28):

$$\langle b(t) \rangle_\xi = R_0 + \hat{s}(t) \, ,$$

where the firing probability is modulated by the time-dependent effective stimulus $\hat{s}(t) = \mathcal{B} * K * s(t)$. As elaborated in Sec. 1.6, $\hat{s}(t)$ is a Gaussian process centered around zero with variance

$$\langle \hat{s}^2 \rangle = \Delta^2 \int_{-\infty}^{\infty} \mathrm{sinc}^2(\Delta \pi f) |\chi(f)|^2 S_s(f) \, df \, .$$

In conclusion, if one assumes a linear response of the instantaneous firing rate, the conditional spiking probability R is like the effective stimulus $\hat{s}$ normally distributed with variance $\langle \hat{s}^2 \rangle$, such that

$$\boxed{\hat{p}_R(R) = \mathcal{N}(R_0, \langle \hat{s}^2 \rangle) = \frac{1}{\sqrt{2\pi \langle \hat{s}^2 \rangle}} \exp\left[\frac{-(R_0 - R)^2}{2 \langle \hat{s}^2 \rangle} \right] \, .} \tag{3.13}$$

Eq. (3.13) has to be regarded as a coarse approximation of the true distribution p_R. It has one clear limitation: as a probability, R is supposed to take values only on $[0, 1]$, whereas the density $\hat{p}_R$ is formally distributed (and normalized) on $\mathbb{R}$. However, if $\hat{s}$ is small enough and Δ is not chosen too small (such that R_0 is not too close to zero), the main support of $\hat{p}_R$ will be on $[0, 1]$.

In Fig. 3.4 we compare the linear response approximation Eq. (3.13) with the numerically measured distribution for various parameter settings. For weak common noise ($c = 0.01$), the normal distribution Eq. (3.13) provides an adequate description both in the suprathreshold regime as well as in the subthreshold regime [see left column in Fig. 3.4a and b]. For higher input correlations c, the distribution of R differs from a Gaussian. In particular, the density becomes significantly skewed and looks like a log-normal distribution, which is a plausible behavior: a larger value of c means a larger variance of the effective stimulus, leading to a broadening of the distribution p_R. As a probability, R can only take positive values, such that its density needs to become skewed to the right, because the mean value R_0, is unaffected by c (see Fig. 3.5). This observation is in agreement with the finding by Koulakov et al. (2009), where a log-normal distribution of firing rates has been recorded for a network of neurons receiving highly correlated input.

In Fig. 3.5 we compare the first three moments of the density p_R from numerical simulations to the linear response prediction $\hat{p}_R$ (Eq. (3.13)). While the mean value remains R_0

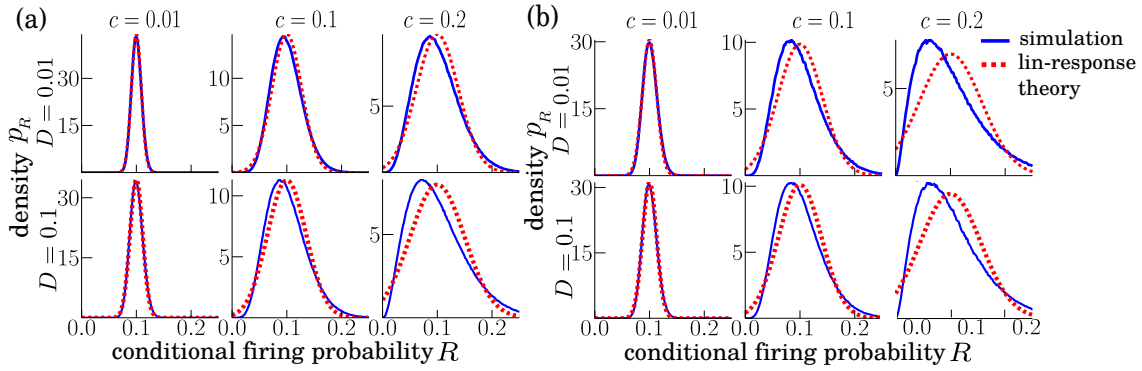

Figure 3.4.: **Probability distribution of the stimulus-conditioned firing probability.** Simulation results [blue solid lines] are compared to the linear response approach Eq. (3.13) [red dashed lines] in [a] the suprathreshold regime with $\mu = 1.2$ and [b] in the subthreshold regime with $\mu = 0.9$ for different values of the input correlation c [from left column to right: $c = 0.001, 0.1, 0.2$] for total noise intensity $D = 0.01$ [top row] and $D = 0.1$ [bottom row], respectively. In all graphs the mean firing probability was fixed to $R_0 = r_0\Delta = 0.1$.

(Fig. 3.5a), the variance first increases in a linear fashion with the input correlation c (just like the approximation) but shows a stronger growth for larger c (Fig. 3.5b). The skewness of the density increases (Fig. 3.5c) in a non-linear fashion, whereas the Gaussian approximation is unskewed.

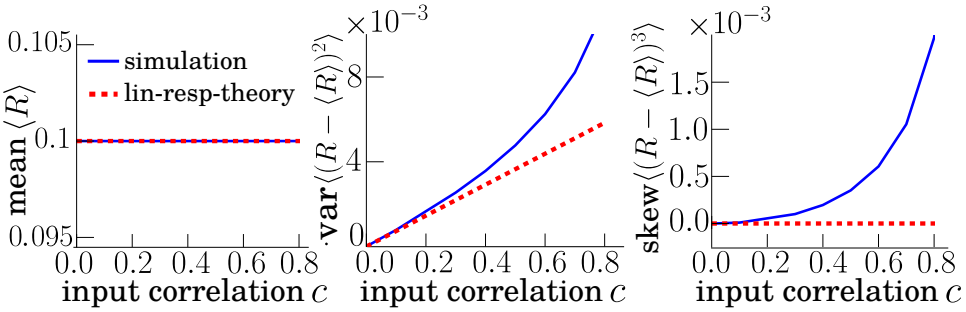

Figure 3.5.: **First three central moments of the stimulus-conditioned rate vs input correlation.** Simulation results [blue solid] are compared to the linear response approximation [red dashed]. Parameters: $D = 0.01, \mu = 1.2$ (corresponding to Fig. 3.4a upper row).

3.2. Approximations of the summed activity distribution

Combining the general result for the activity distribution with the linear response result from the previous section, yields an integral expression for p_A. In the following, we also derive a simpler Gaussian approximation of this distribution, which is based on a central-limit argument. Both expressions are compared to numerical simulations of the

LIF model in different dynamical regimes.

3.2.1. Integral approximation

By inserting approximation Eq. (3.13) into Eq. (3.6) we obtain an integral expression of the activity distribution, which should be valid for weak input correlation ($c \ll 1$) and arbitrary population sizes

$$\hat{p}_A(A) = N\binom{N}{AN}\int_0^1 \left(R^A(1-R)^{(1-A)}\right)^N \hat{p}_R(R)\, dR\,. \tag{3.14}$$

Result Eq. (3.14) requires the numerical evaluation of an integral over $\hat{p}_R$. Next, we derive an integral-free approximation for the activity distribution.

3.2.2. Gaussian approximation

As shown in the introduction of this chapter, the population activity can be written as a sum of the single box-trains

$$A = \frac{1}{N}\sum_{k=1}^{N} b_k\,. \tag{3.15}$$

For fixed time t, $A(t)$ is a sum of random variables $\{b_k(t)\}_k$, having identical distributions (because we consider a homogeneous population), which are only weakly correlated due to the common stimulus.

The *central limit theorem* states that the sum of independent and identically distributed random variables $\{X_k\}_{k=1,\ldots,N}$,

$$Z_N = \frac{1}{N}\sum_{k=1}^{N} X_k\,, \tag{3.16}$$

converges with increasing N to a Gaussian random variable with mean $\langle X_1\rangle$ and variance $\sigma^2_{X_1}/N$. The obvious constraint that impedes a rigorous application of the central limit theorem to Eq. (3.15) is the non-zero global correlation between the box trains due to the common stimulus. However, because we only consider weak correlations, it is still plausible to approximate A by a Gaussian process for large N, which is fully described by the mean and variance of A.

By Eq. (3.3) $\langle A\rangle = R_0$. The second moment of A reads

$$\begin{aligned}\langle A^2\rangle &= \frac{1}{N^2}\sum_{k=1}^{N}\sum_{k'=1}^{N}\langle b_k b_{k'}\rangle \\ &= \frac{1}{N^2}\left(N\langle b_k^2\rangle + N(N-1)\langle b_k b_{k'}\rangle\right),\ k\neq k'\end{aligned}$$

Because ξ_k and $\xi_{k'}$ are independent for $k \neq k'$

$$\langle b_k b_{k'} \rangle = \langle \langle b_k \rangle_{\xi_k} \langle b'_k \rangle_{\xi'_k} \rangle_s = \langle R[s]^2 \rangle_s \,,$$

where we applied again Eq. (3.12). Using furthermore that $b_k^2 = b_k$, because $b_k \in \{0, 1\}$ we obtain

$$\langle A^2 \rangle = \frac{1}{N} \left(\langle R[s] \rangle_s + (N-1) \langle R[s]^2 \rangle_s \right). \tag{3.17}$$

This relation for the second moment holds true for arbitrary correlation strength. Using once more the linear response ansatz, $\hat{R}[s] = R_0 + \hat{s}$, such that $\langle R[s]^2 \rangle_s \approx R_0^2 + \langle \hat{s}^2 \rangle$, we can further approximate Eq. (3.17) by

$$\langle A^2 \rangle \approx R_0^2 + \langle \hat{s}^2 \rangle \left(1 - \frac{1}{N} \right) + \frac{R_0(1-R_0)}{N} \,. \tag{3.18}$$

Hence, if we assume in the case of large N and weak input correlation a normal distribution, $\mathcal{N}(\langle A \rangle, \sigma_A^2)$, for the population activity, its density can be approximated by

$$\boxed{p_A^G = \mathcal{N} \left(R_0 \,, \langle \hat{s}^2 \rangle \left(1 - \frac{1}{N} \right) + \frac{R_0(1-R_0)}{N} \right) \,,} \tag{3.19}$$

where the 'G' stands for 'Gaussian approximation'.

By Eq. (3.9), we know that $\lim_{N\to\infty} p_A = p_R$. Consistently, both approximations, $\hat{p}_A$ and p_A^G, approach $\hat{p}_R$, i.e. a normal distribution centered at R_0 with variance $\langle \hat{s}^2 \rangle$.

3.2.3. Comparison to simulation results

In Fig. 3.6 both approximations, $\hat{p}_A$ and p_A^G, of the activity distribution are compared to simulation results of populations of LIF neurons in the supra- and subthreshold regime and various combinations of population size and correlation strength.

For weak input correlation [see Fig. 3.6a/b, top row; $c = 0.01$] the simulation results are well approximated by the linear response approach, Eq. (3.14), for all values of the system size. The simple Gaussian approximation, Eq. (3.19), works well at larger system size. Surprisingly, the Gaussian is a reasonable description of the histogram already for $N = 30$.

For larger input correlations, $c = 0.1$ and $c = 0.2$ [Fig. 3.6 middle and bottom rows] we find in the suprathreshold regime small deviations between the linear response theory and the simulation results. The deviations are larger in the subthreshold regime. As anticipated by Eq. (3.9), both approximations converge for large N and show therefore the same discrepancy to the skewed true distribution [e.g. for $N = 500$ in Fig. 3.6a/b right column]. The main character of the distribution is nevertheless still captured by the linear response theory, which in particular performs nicely for small populations even in the case of strong input correlation [see $N = 10$, left column of Fig. 3.6a/b].

Why does the approximation $\hat{p}_A$ work so well for small populations? For small values

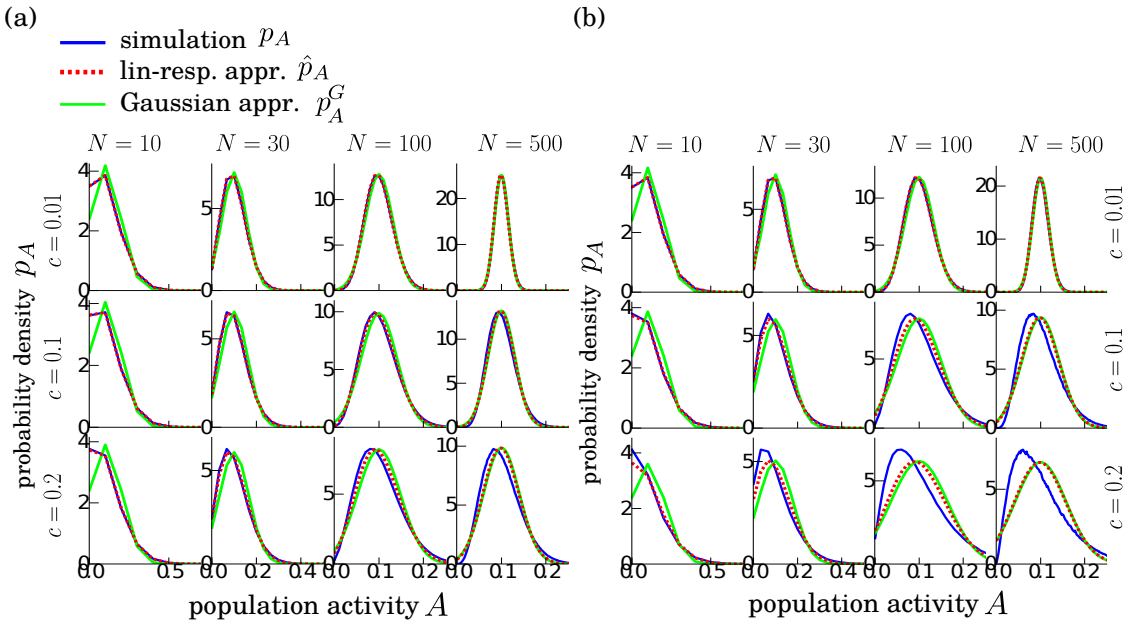

Figure 3.6.: Comparison of simulation results of the activity distribution [blue lines] with the linear response approximation Eq. (3.14) [red dashed lines] and the Gaussian approximation Eq. (3.19) [green lines] for [a] the suprathreshold ($\mu = 1.2$) and [b] the subthreshold regime ($\mu = 0.9$) of the LIF model for different values of the population size N [from left column to right: $N = 10, 30, 100, 500$] and input correlation c [from top row to bottom: $c = 0.01, 0.1, 0.2$]. Remaining parameters: $D = 0.01, R_0 = 0.1$.

of N, the first two moments of the distribution of R matter the most for the activity distribution. For example, for $N = 2$, only the mean and variance of R appear in Eq. (3.5)

$$p_A\left(A = \frac{m}{2}\right) = 2\binom{2}{m}\left\langle (R)^m (1-R)^{2-m}\right\rangle;\ m \in \{0,1,2\}. \tag{3.20}$$

The mean, $\langle R\rangle$, equals R_0 (cf. Fig. 3.5a) and the variance is well described by the linear response theory up to $c = 0.2$ (cf. Fig. 3.5b). Hence, p_A is expected to be well described for $N = 2$. For larger N, also higher central moments and by that also higher cumulants will enter Eq. (3.5) which are not captured by the Gaussian description of p_R. However, their values are much smaller compared to the first two cumulants (see e.g. the skewness in Fig. 3.5c). Only when higher-order cumulants make up many terms in Eq. (3.5), as for larger N, these will notably contribute.

We can quantify the deviations between theory and simulations more systematically. To this end, we use the normalized Jensen-Shannon (JS)-divergence (Lin, 1991; Leen and Shea-Brown, 2015) between the approximation $\hat{p}_A$ and the measured distribution p_A,

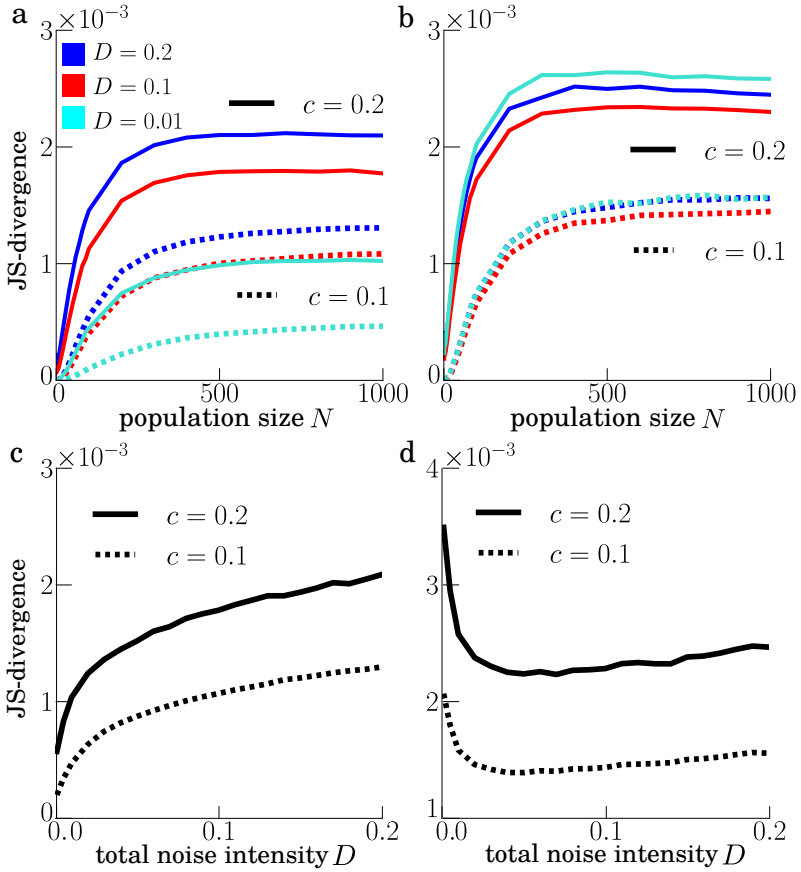

Figure 3.7.: **Jensen-Shannon divergence between theory and simulation vs population size and total noise intensity.** [a,b] JS-divergence, Eq. (3.21), between the simulated population activity distribution p_A and its linear response approximation $\hat{p}_A$ vs population size for two different input correlations c as indicated. [c,d] JS-divergence vs the total noise intensity D for a population of $N = 1000$ neurons. Remaining parameters: $R_0 = 0.1$, $\mu = 1.2$ in [a,c], and $\mu = 0.9$ in [b,d].

which is given by

$$\text{JS-div} = \frac{D_{KL}(p_A||M) + D_{KL}(\hat{p}_A||M)}{2\ln(N)}\,, \tag{3.21}$$

where $M = (p_A + \hat{p}_A)/2$ and

$$D_{KL}(P||Q) = \frac{1}{N}\sum_{k=0}^{N} P(k)\ln\left(\frac{P(k)}{Q(k)}\right) \tag{3.22}$$

is the Kullback-Leibler divergence. The JS-divergence quantifies the discrepancy between two probability densities. In Fig. 3.7 we see that even for moderate input correlations c, the approximation $\hat{p}_A$ is very similar to the real distribution if the population is

small. As N increases the deviation grows and reaches a plateau, which corresponds to the difference between p_R and $\hat{p}_R$. For stronger input correlation, the plateau is reached for smaller N.

Finally, we discuss how the range of validity of the approximation depends on the total noise intensity [see Fig. 3.7c,d]. This dependence differs for the suprathreshold and subthreshold firing regimes of the LIF model. Increasing the total noise intensity D has three effects on the single neuron dynamics: i) the mean firing rate increases (Vilela and Lindner, 2009b); ii) the intrinsic noise becomes stronger, leading to a linearization of the neuron model (Brunel et al., 2001); iii) the signal intensity is increased (for fixed c), which potentially leads to nonlinear rectification effects in the modulation of the firing rate. Rectification means that very strong negative inputs suppress firing and contribute to the event $A = 0$. This effect results in pronounced non-Gaussian features of the activity distribution and leads in the suprathreshold regime to a growth of the JS-divergence with increasing noise (cf. Fig. 3.7c). In the subthreshold regime we observe however a minimum of the divergence at a non-vanishing value of the noise intensity. If the fluctuations are very low, the mean firing rate of single neuron is almost zero, such that only positive values of the stimulus will lead to a notable change in the instantaneous firing rate. Hence, for very small D the response of the firing rate is highly non-linear in the subthreshold regime. Large values of D lead to the same effects as stated for the suprathreshold case. This implies that our linear response theory works best for an intermediate total noise level in the fluctuation driven regime.

3.3. Summary

In this chapter we investigated the distribution of the summed activity of a homogeneous population which is driven by a common noisy stimulus. First, we demonstrated how the distribution depends on the input correlation. A strong input correlation results in vigorously synchronized spiking of the population, such that the activity distribution is bimodal with weights around the extremes zero (total silence) and one (all neurons fire). Our main focus was to find an analytical approximation of the summed activity density p_A for weak input correlation (weak stimulus). To this end, we applied linear response theory to first, approximate the probability R that a single neuron spikes within a small time bin (windowed firing rate), conditioned on a Gaussian stimulus. This approach leads naturally to a normal distribution p_R.

We showed that the distribution of the summed population activity A is uniquely determined by p_R via an integral transformation (Eq. (3.6)), such that the linear response approximation of p_R yields directly an approximation for p_A. We tested its validity for different parameter settings, which works especially well for small populations. Furthermore, we derived a second, simpler approximation of p_A that assumes the activity to be a Gaussian process which is shown to be valid for large population sizes and weak input correlation. Both approximations coincide for large system size.

Next, we will investigate the statistics of the synchronous population activity, which we will show is a nonlinear transformation of the summed activity. In order to derive analytical expressions for large populations, we will employ the Gaussian approximation

of p_A, such that we can utilize the pleasant features of a Gaussian process.

Chapter 4.

The partially synchronous output (PSO) of a neuronal population

We have seen in chapter 2 that the synchronous output of pairs of neurons can extract information about high frequency components of a common stimulus. In this chapter we examine the properties of the synchronous activity of an arbitrarily sized population, where the demand on synchrony can be freely chosen. We first define the partially synchronous output in mathematical terms and then derive analytical approximations of important statistics, like its mean value, its cross-correlation/spectrum with the common stimulus and its autocorrelation/power spectrum. These measures are necessary ingredients of the coherence function, which reveals further coding properties of the synchronous output. We will in particular elaborate the role of the synchrony demand, i.e. the minimal fraction of the population which needs to fire simultaneously. The theory is tested against numerical simulations of the LIF model, using white and colored noise as a common stimulus.

4.1. Definition and mathematical representation of the PSO

We define for a population of N neurons the *partially synchronous output (PSO)* with *synchrony threshold* γ in the following way:

$$Y_\gamma(t) := \begin{cases} 1, & \text{if at least } \gamma N \text{ neurons} \\ & \text{spike within } [t-\Delta, t] \\ 0, & \text{else} \end{cases} . \tag{4.1}$$

Here again, Δ is to be chosen small, such that Y_γ can be truly regarded as a measure of synchrony. The partially synchronous output is a two-state process and can be interpreted as a coarse representation of a postsynaptic cell which is activated (having the value one) if at least γN out of N presynaptic neurons fired together in a time window of width Δ (see again Fig. 1.7 for illustration). In this interpretation, Δ corresponds to the time over which the postsynaptic neuron integrates incoming inputs. Because we choose Δ to be small, this postsynaptic cell can be regarded as a coincidence detector.

The choice of γ determines the strictness of synchrony that one wants to measure. If γ is close to one, then Y_γ will be one only at very few times, because it is very unlikely that almost the entire population fires together, especially for large populations (see purple

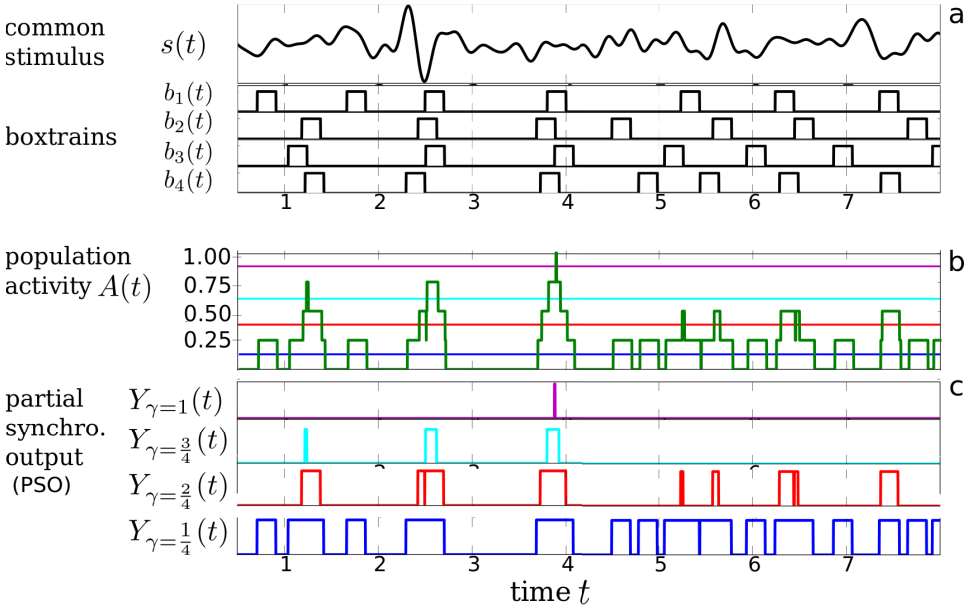

Figure 4.1.: **The PSO is a threshold function of the summed population activity.** Illustration of the measurement of the partially synchronous output $Y_\gamma(t)$, given by Eq. (4.2) for different synchrony thresholds γ for a population of $N = 4$ neurons. [a] Common stimulus and single box trains. [b] Summed population activity [green line]. [c] PSO for different synchrony thresholds $\gamma \in \{1, 0.75, 0.5, 0.25\}$ (corresponding thresholds are marked as horizontal lines in [b]). LIF-parameters: $\mu = 1.2, D = 0.01; \to r_0 = 0.58, R_0 = 0.2$ (corresponding to the box width $\Delta = 0.35$).

line in bottom subplot in Fig. 4.1). On the other hand, if γ is set close to zero, then the demand on synchronous firing is very low, such that Y_γ is most of the times one and only at rare occasions zero. Here, the PSO measures rather the events where the population is simultaneously silent (see blue line in bottom subplot of Fig. 4.1 and Fig. 4.2). Another interesting scenario is $\gamma = R_0$, i.e. if the synchrony threshold is set to the mean value of the summed population activity. If the distribution of the activity is symmetric around its mean, then the synchronous output Y_{R_0} is half of the time zero, half of the time one, and can be seen as a two-state version of the summed activity (see red line in bottom subplot of Fig. 4.2). For this case, the naming 'synchronous output' might be misleading, because on average $R_0 N$ neurons of the population fire simultaneously, such that the value of Y_{R_0} does not tell us anything about above-average synchronous behavior.

We define by Eq. (4.1) a simple measure of dynamic synchrony that allows us to apply analytical tools. Other ways of quantifying synchrony among neurons are summarized in Kreuz et al. (2009).

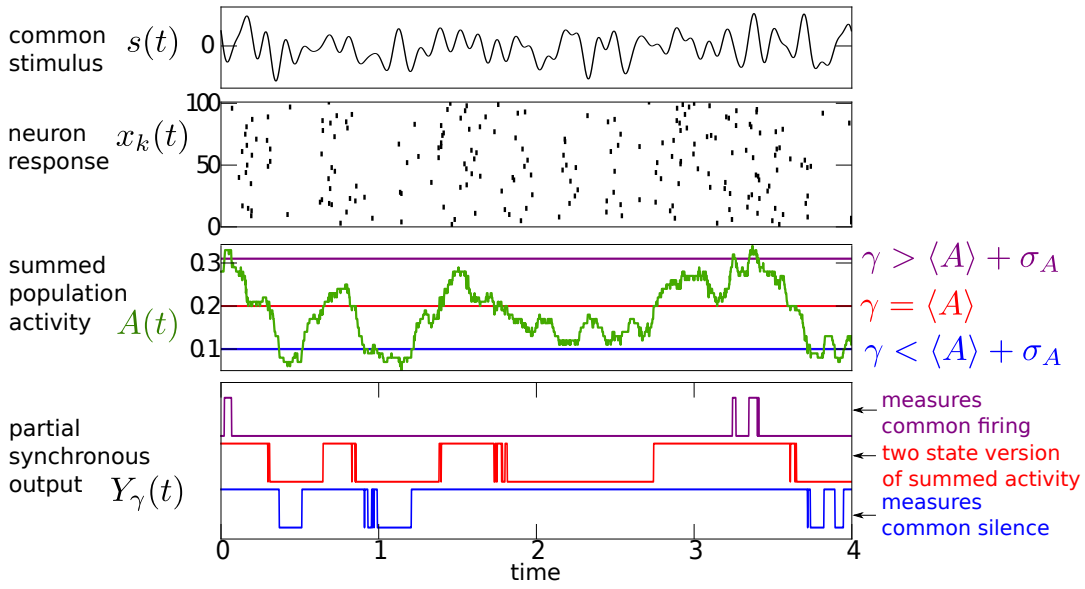

Figure 4.2.: **The PSO can measure common firing or common silence.** Top: Raster plot of a population of 100 LIF neurons, driven by a common stimulus. Middle: Corresponding summed activity [green line]. Bottom: PSO for different synchrony thresholds $\gamma \in \{0.3, 0.2, 0.1\}$ (top to bottom; also marked as horizontal lines in plot above). Parameters: $\mu = 1.2, D = 0.01, c = 0.3, R_0 = 0.2, N = 100$.

Mathematical representations of the PSO

We now introduce two distinct but completely equivalent ways of representing Y_γ in mathematical terms. The first approach represents the PSO as a threshold function of the summed activity, while the second one uses products of the individual box trains.

4.1.1. Activity based representation of the PSO

If we know the summed population activity $A(t)$, i.e. the fraction of the population which is active within $[t - \Delta, t]$, a synchronous event with synchrony threshold γ at time t is simply given if $A(t) \geq \gamma$. The PSO can be therefore written as

$$\boxed{Y_\gamma(t) = \theta\left(A(t) - \gamma + \frac{1}{2N}\right)}, \tag{4.2}$$

where θ is the Heaviside step function. The term $1/(2N)$ assures that Y_γ does not depend on the exact definition of the theta function at zero, in addition it is necessary if we want to approximate the activity by a continuous process taking values on $\mathbb{R}$. Fig. 4.1 and 4.2 illustrate this activity-based representation of the PSO for a population of four and a hundred neurons, respectively.

4.1.2. Combinatorial product representation of the PSO

The Heaviside function in Eq. (4.2) is a strongly nonlinear transformation of A, such that analytical derivations of important statistics of Y_γ are incomprehensible, unless one can assume the summed activity to be a Gaussian process. We can, however, avoid the Heaviside function by generalizing an ansatz introduced in Sharafi et al. (2013).

Not only the sum of the box-trains, but also their products contain information about the population's synchrony. If there are for example exactly n neurons (lets say the first n of the population) that fired within $[t-\Delta, t]$, then the product of their box trains, $\prod_{k=1}^{n} b_k = b_1 \cdot b_2 \cdot ... \cdot b_n$, is one at time t, whereas all higher order products are zero. In order to check if at least j neurons fired, one must look at all combinations of products of j neurons:

$$\kappa_j := \sum_{\substack{\text{over all} \binom{N}{j} \\ \text{combinations } \pi}} \prod_{k=1}^{j} b_{\pi_k} \,. \tag{4.3}$$

The term $\kappa_j(t)$ is non-zero if at least j neurons fired within $[t-\Delta, t]$. However if more than j fired, lets say n, then $\kappa_j = \binom{n}{j}$, because there are $\binom{n}{j}$ combinations that contribute with a one in Eq. (4.3). In order to derive again a two-state process for the synchronous output, one must take into account all higher order products:

$$Y_\gamma(t) = \sum_{j=\gamma N}^{N} q_j \kappa_j(t) \,. \tag{4.4}$$

where q_j are normalizing constants that we can derive in the following way.

Let $n = N \cdot A(t)$ be again the actual number of simultaneously spiking neurons at time t. Then, $\kappa_j(t) = \binom{n}{j}$ if $n \geq j$ and it is zero otherwise. If $n < \gamma N$, then $Y_\gamma(t) = 0$ (as it should be) because by definition $\kappa_j(t) = 0$ for $n < j$. If $n \geq \gamma N$ terms with $j > n$ do not contribute to the sum and we obtain

$$Y_\gamma(t) = \sum_{j=\gamma N}^{n} q_j \binom{n}{j} \,. \tag{4.5}$$

In order for $Y_\gamma(t)$ to have the value one for any n with $N \geq n \geq \gamma N$, the following recursive formula must hold

$$q_n = 1 - \sum_{j=\gamma N}^{n-1} q_j \binom{n}{j} \,, \tag{4.6}$$

which can be translated to the explicit form

$$q_j = (-1)^{j-\gamma N} \binom{j-1}{j-\gamma N} \,. \tag{4.7}$$

The partially synchronous output can thus be represented by

$$\boxed{Y_\gamma(t) = \sum_{j=\gamma N}^{N} (-1)^{j-\gamma N} \binom{j-1}{j-\gamma N} \sum_{\substack{\text{over all} \binom{N}{j} \\ \text{combinations } \pi}} \prod_{k=1}^{j} b_{\pi_k}(t)} \,. \tag{4.8}$$

Eq. (4.8) gives the same output as the activity based representation Eq. (4.2), but it is certainly not as compact as the latter one. However, its advantage is that we can analytically calculate statistics of the PSO without assuming Gaussianity of the summed population activity. Whenever we use this representation of the PSO we refer to it as the *combinatorial product approach*.

4.2. Mean synchronous output

How often does a synchronous event occur and how does this depend on the synchrony threshold? This question can be addressed by looking at the expectation value of the PSO. If we use the activity-based definition, Eq. (4.2), the mean value of the synchronous output reads

$$\langle Y_\gamma \rangle = \left\langle \theta\left(A - \gamma + \frac{1}{2N}\right) \right\rangle \,, \tag{4.9}$$

where $\langle \cdot \rangle$ denotes the average over all independent intrinsic noise sources $\xi = \{\xi_1, \xi_2, ..., \xi_N\}$ and the common stochastic signal s. Eq. (4.9) is in a simple way related to the cumulative probability of the summed activity:

$$\langle Y_\gamma \rangle = \int_{\gamma - \frac{1}{2N}}^{1} p_A(A)\, dA = \mathbb{P}(A \geq \gamma - 1/(2N)) \,. \tag{4.10}$$

For finite population sizes, A is a discrete variable, such that

$$\langle Y_\gamma \rangle = \sum_{j=\gamma N}^{N} \mathbb{P}\left(A = \frac{j}{N}\right) = \mathbb{P}(A \geq \gamma) \,. \tag{4.11}$$

The mean synchronous output is therefore the probability that the activity is equal to or above γ. Because $\mathbb{P}(A \geq \gamma) = \mathbb{P}(Y_\gamma = 1)$, the mean value $\langle Y_\gamma \rangle$ is the probability of having a partially synchronous event.
To give an overview over the possible limit cases, Fig. 4.3 shows how the mean synchronous output depends on the input correlation c. If the driving noise is identical for all neurons ($c = 1$), they all act asymptotically as one neuron, such that the activity can only take two values, zero or one with $\mathbb{P}(A = 1) = R_0$ and $\mathbb{P}(A = 0) = 1 - R_0$. By Eq. (4.11), the mean value of the synchronous output is consequently R_0 for any $\gamma > 0$ [purple circles in Fig. 4.3]. The other extreme is the case where all neurons are completely independent of each other ($c = 0$). For the limit of an infinitely large population the activity becomes a deterministic process, because the sum averages out the independent

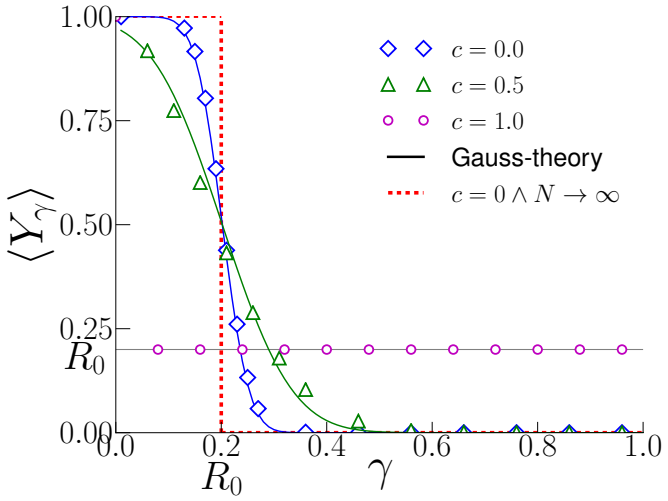

Figure 4.3.: **Sensitivity of the mean synchronous output depends on the input correlation.** Probability of having a partially synchronous event ($\langle Y_\gamma \rangle = \mathbb{P}(Y_\gamma = 1)$) vs synchrony threshold γ for different input correlations c as indicated. Symbols mark simulation results. Solid lines show the Gaussian approximation Eq. (4.14) for the cases $c \in \{0, 0.5\}$. For an infinite large population and without any correlation [red dashed line], the mean PSO is either one for $\gamma \leq R_0$ or zero for $\gamma > R_0$. For full correlation ($c = 1$) [purple circles] the mean synchronous output equals the mean activity R_0 for any $\gamma > 0$ (and is one for $\gamma = 0$). LIF-parameters: $\mu = 1.2, D = 0.01, R_0 = 0.2, N = 100$.

noise:

$$\lim_{N\to\infty} A(t) = \lim_{N\to\infty} \frac{1}{N} \sum_{k=1}^{N} b_k(t) \overset{c=0}{=} \langle b \rangle = R_0 \,. \tag{4.12}$$

Hence, the probability of having a synchronous event for $c = 0$ is therefore either one for $\gamma \leq R_0$ or zero for $\gamma > R_0$ [see red dashed line]. For a finite population this step function is smoothed, resulting in a sigmoid function [see blue diamonds], because the activity can take different values around R_0. As c is increased, $\langle Y_\gamma \rangle$ undergoes a transformation from this sigmoid to the constant case for $c = 1$. We now show how the mean PSO can be calculated for small input correlations c.

Gaussian approach to the mean PSO

If we use the Gaussian approximation of the probability density of the summed activity, Eq. (3.19), we can approximate Eq. (4.10) by

$$\langle Y_\gamma \rangle^G = \int_{\gamma - \frac{1}{2N}}^{\infty} p_A^G(A)\, \mathrm{d}A \,, \tag{4.13}$$

leading to the complementary error function

$$\boxed{\langle Y_\gamma \rangle^G = \frac{1}{2}\,\mathrm{erfc}\left(\frac{\gamma - R_0 - 1/(2N)}{\sqrt{2}\,\sigma_A}\right)}\,, \tag{4.14}$$

where the activity's variance is approximated by $\sigma_A^2 = \langle \hat{s}^2 \rangle [1 - 1/N] + R_0(1 - R_0)/N$. For increasing population size the mean synchronous output approaches

$$\lim_{N\to\infty} \langle Y_\gamma \rangle^G = \frac{1}{2}\,\mathrm{erfc}\left(\frac{\gamma - R_0}{\sqrt{2\langle \hat{s}^2 \rangle}}\right)\,. \tag{4.15}$$

Combinatorial approach to the mean PSO

If we use the combinatorial product representation of Y_γ, Eq. (4.8), we can directly compute the average of the synchronous output:

$$\begin{aligned}\langle Y_\gamma \rangle &= \sum_{j=\gamma N}^{N} q_j \sum_{\substack{\text{over all} \binom{N}{j} \\ \text{combinations } \pi}} \langle \langle \prod_{k=1}^{j} b_{\pi_k} \rangle_\xi \rangle_s \\ \langle \hat{Y}_\gamma \rangle &= \sum_{j=\gamma N}^{N} q_j \binom{N}{j} \langle \langle b \rangle_\xi^j \rangle_s\,, \end{aligned} \tag{4.16}$$

where we used the independence of the intrinsic noise sources ξ_k of different neurons. Applying again the linear response ansatz, Eq. (1.28), we can approximate Eq. (4.16) by

$$\langle \hat{Y}_\gamma \rangle = \sum_{j=\gamma N}^{N} q_j \binom{N}{j} \langle (R_0 + \hat{s})^j \rangle_s\,. \tag{4.17}$$

By the binomial theorem we can further evaluate

$$\langle (R_0 + \hat{s})^j \rangle_s = \sum_{k=0}^{j} \binom{j}{k} R_0^{j-k} \langle \hat{s}^k \rangle\,. \tag{4.18}$$

Considering only orders up to the variance of the effective stimulus, we get the following combinatorial approximation of the mean synchronous output

$$\boxed{\langle \hat{Y}_\gamma \rangle = \sum_{j=\gamma N}^{N} q_j \binom{N}{j} R_0^{\,j} \left[1 + \frac{j(j-1)}{2}\,\frac{\langle \hat{s}^2 \rangle}{R_0^2}\right].} \tag{4.19}$$

In Fig. 4.4 both approximations of the mean PSO are compared to numerical simulations of LIF populations for a weak common stimulus ($c = 0.1$). Fig. 4.4a shows the mean synchronous output for comparatively small populations, while in Fig. 4.4b the large population limit is explored. As can be seen in Fig. 4.4a the combinatorial approximation, Eq. (4.19), [dashed lines] is in excellent agreement with the numerical simula-

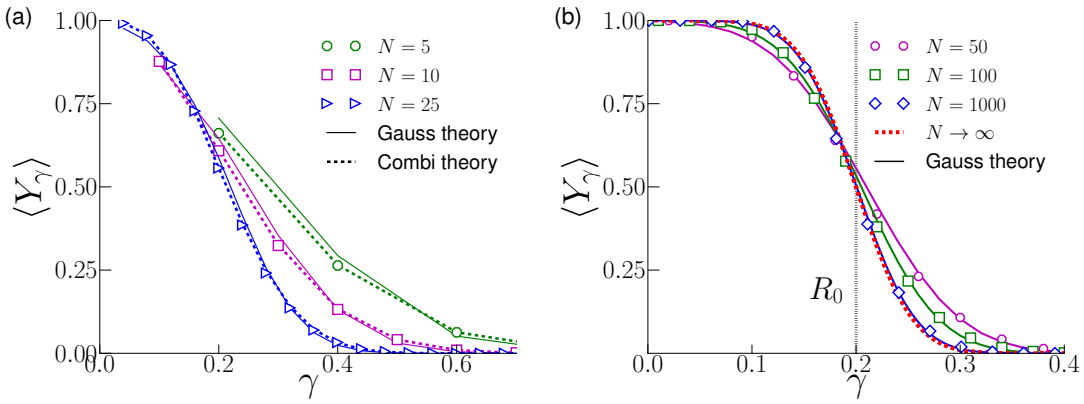

Figure 4.4.: **The probability of having a synchronous event is a sigmoid function of the synchrony threshold.** Mean PSO in dependence of the synchrony threshold γ for LIF populations of various sizes N as indicated. [a] For small populations, simulation results [symbols] are compared to the Gaussian approximation, Eq. (4.14) [solid lines] and to the combinatorial theory, Eq. (4.19) [dashed lines]. [b] For large populations simulations are compared to the Gaussian theory only. The red dashed line in b marks the limit case for an infinite large population given by Eq. (4.15). The vertical line marks the mean population activity R_0. Parameters: $\mu = 1.2, D = 0.01, c = 0.1, R_0 = 0.2$.

tions [symbols]. One limitation of its applicability, however, is the numerically expensive evaluation of the combinatorial factors in Eq. (4.19), which becomes intractable for large values of N. For this reason we apply the combinatorial approach only to small or moderately sized populations ($N < 50$). The Gaussian approach, Eq. (4.14), [solid lines] gives a reasonable approximation of the mean synchronous output, even though we consider only small populations in Fig. 4.4a. In Fig. 4.4b we see that for large population sizes, the Gaussian approximation gives an adequate description of $\langle Y_\gamma \rangle$.

Discussion of the mean PSO for weak stimuli

If the input correlation is small, the probability of having a synchronous event is a sigmoidal function of the synchrony threshold γ. When γ is set notably below the mean population activity R_0, the probability that the activity is above γ is close to one. In this case the population fires almost always 'in synchrony'. In the other extreme, when γ is set exceedingly above R_0, i.e. when we demand a very large fraction of the population to fire simultaneously, the probability that the activity exceeds the value γ is close to zero. In this scenario there is hardly ever a synchronous event. Both extremes are therefore unfavorable to encode a weak time-dependent signal. The common signal is encoded in the change of the instantaneous population activity $A(t)$. In fact, for large populations, the activity is approximately given by $A(t) = \langle b \rangle_\xi = R_0 + \hat{s}(t)$ (see Eq. (1.28)). If γ is set too far away from the mean activity R_0, then this small change of A will not influence the synchronous output. Hence, we can expect that the cross-correlation between the

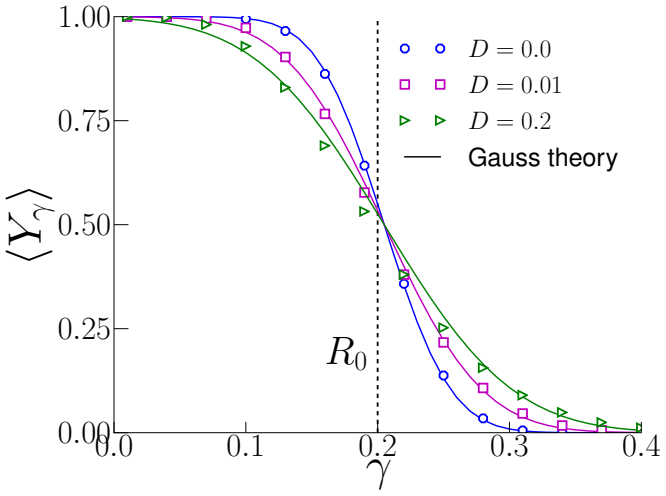

Figure 4.5.: Mean synchronous output for fixed input correlation $c = 0.1$ and for different total noise intensities $D \in \{0, 0.01, 0.2\}$ leading to the mean firing rates $r_0 \in \{0.56, 0.58, 0.80\}$. Simulation results [symbols] are compared to the Gaussian approximation, Eq. (4.14) [solid lines]. Remaining parameters: $\mu = 1.2, R_0 = 0.2, N = 100$.

synchronous output Y_γ and the common signal s is maximal for $\gamma = R_0$.

Fig. 4.5 shows the mean synchronous output for different values of the total noise intensity D for a fixed input correlation $c = 0.1$. An increase in the total noise results in an increase of the variance of the stimulus and with it to a larger value of the variance of A (see Eq. (3.19)). As a consequence, the integral over the distribution p_A, Eq. (4.13), i.e. $\langle Y_\gamma \rangle$, displays a slower decay in γ. Also for the deterministic case ($D = 0$), $\langle Y_\gamma \rangle$ is a sigmoid function if we assume an asynchronous initial state (random initial voltage values of the single neurons), resulting in a normally distributed activity.

4.3. Cross-spectrum between synchronous output and common stimulus

An important statistics telling us how each frequency component of the common stimulus influences the synchronous output, is the cross-spectrum between these two processes.

4.3.1. Gaussian approach to the cross-spectrum

If we assume the population activity to be a Gaussian process, we can apply the Bussgang theorem (Bussgang, 1952). It states that for any two stationary Gaussian processes, the cross-correlation function taken after one of them has undergone a nonlinear transformation is identical to the cross-correlation of the two original processes up to a factor.

Bussgang theorem

Let X and Z be stationary Gaussian processes with $\langle Z\rangle = 0$ and variances σ_X^2 and σ_Z^2, having the cross-covariance $C_{XZ}(\tau) = \langle X(0)Z(\tau)\rangle$. Then, for any distortion $V : \mathbb{R} \mapsto \mathbb{R}$, the cross-covariance between the distorted process $V(X)$ and the original signal Z is given by

$$C_{V(X),Z}(\tau) = a\, C_{X,Z}(\tau) \tag{4.20}$$

with the proportionality factor

$$a = \frac{1}{\sigma_X^2}\int_{-\infty}^{\infty} V(x)(x - \langle X\rangle)p_X(x)dx\,. \tag{4.21}$$

In the original version of the Bussgang theorem, both processes, X and Z, have a mean value of zero and a variance of one. We show the proof of the version we use in the Appendix A.3. Because

$$\langle V(x)\rangle = \int_{-\infty}^{\infty} V(x)\frac{1}{\sqrt{2\pi\sigma_X^2}}\exp\left[-\frac{(x-\langle X\rangle)^2}{2\sigma_X^2}\right]dx$$

we can rewrite Eq. (A.11) by:

$$a = \left.\frac{d}{d\langle X\rangle}\langle V(X)\rangle\right|_{\sigma_X=\text{const}}\,. \tag{4.22}$$

If we apply this theorem to the Gaussian approximation of the population activity $A(t)$ [$\leftrightarrow X(t)$] and to the distortion $V(A) = \theta(A - \gamma + 1/(2N)) = Y_\gamma$ we obtain the following relation for the cross-covariance between the synchronous output and the common stimulus $s(t)$ [$\leftrightarrow Z(t)$]:

$$\boxed{C_{Y_\gamma,s}(\tau) = a_\gamma C_{A,s}(\tau) = a_\gamma C_{b,s}(\tau)\,.} \tag{4.23}$$

The last equality holds true because all box trains are equally distributed, such that $\langle A(0)s(\tau)\rangle = \langle N^{-1}\sum_{k=1}^{N} b_k(0)s(\tau)\rangle = \langle b(0)s(\tau)\rangle$. According to Eq. (4.22) the proportionality factor a_γ is obtained by taking the derivative of Eq. (4.14) with respect to the mean activity R_0

$$\begin{aligned} a_\gamma &= \left.\frac{d}{dR_0}\langle Y_\gamma\rangle^G\right|_{\sigma_A=\text{const}} = p_A^G\left(\gamma - \frac{1}{2N}\right) \\ &= \frac{1}{\sqrt{2\pi\sigma_A^2}}\exp\left[-\frac{\beta_\gamma^2}{2}\right]\,. \end{aligned} \tag{4.24}$$

In the last line we have expressed the dependence on γ by the important parameter

$$\beta_\gamma := \frac{\gamma - R_0 - 1/(2N)}{\sigma_A}\,. \tag{4.25}$$

The proportionality factor a_γ is thus a Gaussian function in γ, centered around $R_0 + 1/2N$. For a large population we obtain

$$\lim_{N\to\infty} a_\gamma = \frac{1}{\sqrt{2\pi\langle\hat{s}^2\rangle}} \exp\left[\frac{-(\gamma - R_0)^2}{2\langle\hat{s}^2\rangle}\right] . \tag{4.26}$$

Turning now to the Fourier domain, by virtue of Eq. (1.6) and Eq. (4.23), the cross-spectrum between PSO and common stimulus has the same frequency dependence as the cross-spectrum between the summed activity with the stimulus (which is proportional to the cross-spectrum between the single box train and the stimulus)

$$S^G_{s,Y_\gamma}(f) = a_\gamma \, S_{A,b}(f) = a_\gamma \, S_{s,b}(f) . \tag{4.27}$$

Because $\langle s\rangle = 0$ and because the intrinsic noise is independent of the stimulus

$$C_{b,s}(\tau) = \langle b(0)s(\tau)\rangle = \langle\langle b(0)\rangle_\xi \, s(\tau)\rangle_s \tag{4.28}$$

$$= \langle R(0)s(\tau)\rangle_s \approx \langle\hat{s}(0)s(\tau)\rangle , \tag{4.29}$$

where we used the linear response ansatz for the conditioned firing probability $\hat{R}(t) = R_0 + \hat{s}(t)$ (Eq. (1.28)). The single box-train cross-spectrum is consequently given by

$$\hat{S}_{s,b}(f) = \tilde{B}\chi S_s(f) \tag{4.30}$$

with absolute value (using Eq. (1.33))

$$|\hat{S}_{s,b}(f)| = \Delta \, \mathrm{sinc}(\Delta\pi f)|\chi(f)|S_s(f) . \tag{4.31}$$

For the cross-spectrum between the synchronous output and the common stimulus we therefore obtain in the Gaussian approximation

$$\boxed{|S^G_{s,Y_\gamma}(f)| = \frac{e^{-\beta_\gamma^2/2}}{\sqrt{2\pi\sigma_A^2}} \Delta \, \mathrm{sinc}(\Delta\pi f)|\chi(f)|S_s(f) .} \tag{4.32}$$

From the derived formulas we can deduce interesting properties of the PSO-stimulus cross-spectrum.

4.3.2. Properties of the PSO cross-spectrum that can be deduced from the Gaussian approach

i) Cross-spectrum between PSO and stimulus shares the same relative frequency dependence with the cross-spectrum between the summed activity and stimulus

Eq. (4.27) predicts that for all values of γ the cross-spectrum between the synchronous output and the stimulus is proportional to the cross-spectrum between the summed activity and the stimulus. (The activity cross-spectrum $S_{A,s}(f)$ equals in turn the single box-train cross-spectrum $S_{b,s}(f)$, because we assume a homogeneous population.)

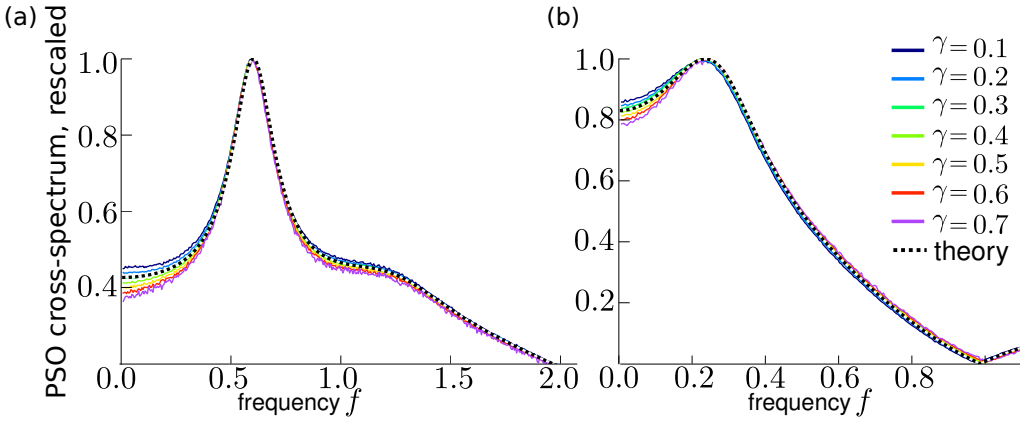

Figure 4.6.: **Cross-spectrum between partially synchronous output and common noise is proportional to the one of the single box train** Absolute value of the cross-spectrum, $|S_{s,Y_\gamma}(f)|$, rescaled by its maximal value for various synchrony thresholds γ. Simulation results (colored solid lines) are compared to the theoretical prediction, Eq. (4.32), normalized by the maximum (black dashed line). Parameters: $D = 0.01, c = 0.1, R_0 = 0.2, N = 10$, (a): $\mu = 1.2$, (b): $\mu = 0.9$

Fig. 4.6 shows the absolute value of the PSO cross-spectrum for a population of ten simulated LIF neurons, relative to its maximum for different synchrony thresholds γ [colored solid lines] for supra-threshold (a) and subthreshold (b) mean current. One sees that these rescaled spectra almost overlap, i.e. they share indeed approximately the same frequency dependence, which is well described by the single box train cross-spectrum $|S_{s,b}(f)|$ given by Eq. (4.31) [black dashed line]. One observes slight deviations for small frequencies, which are not captured by the linear response approach. In conclusion, the temporal correlations between the synchronous events and the stimulus are similar to those between the single or summed spike trains and the stimulus. This is somewhat surprising because the synchronous output is a strongly non-linear function of the summed activity.

While the relative frequency dependence of the PSO cross-spectrum is roughly the same for all synchrony thresholds, the absolute amplitude of the cross-spectrum depends strongly on γ. The two key parameter β_γ and a_γ are of particular importance to understand the influence of the synchrony threshold.

ii) The cross-spectrum between PSO and stimulus scales with the sensitivity of the PSO

Meaning of the constants β_γ and a_γ

The constant

$$\beta_\gamma = \frac{\gamma - R_0 - \frac{1}{2N}}{\sigma_A}$$

is the distance of the synchrony threshold to the mean population activity relative to the activity's standard deviation. It appears in the proportionality factor

$$a_\gamma = \frac{e^{-\beta_\gamma^2/2}}{\sqrt{2\pi\sigma_A^2}}\,,$$

which is the approximated probability that the summed activity A takes the value $\gamma - 1/(2N)$. The factor a_γ can also be interpreted as the *sensitivity* of the synchronous output. It tells us how much the PSO is influenced by a change in the population activity, which can be quantified by the average of the derivative of the PSO with respect to the activity:

$$\begin{aligned}\left\langle \frac{dY_\gamma}{dA} \right\rangle &= \left\langle \frac{d}{dA}\theta(A-\gamma+1/(2N)) \right\rangle \\ &= \int_0^1 \delta\left(A-\gamma+\frac{1}{2N}\right) p_A^G(A)\,dA \\ &= p_A^G\left(\gamma-\frac{1}{2N}\right) = a_\gamma\,.\end{aligned}$$

Knowing this connection it is quite plausible that the cross-correlation between the PSO and the stimulus should scale with a_γ. The cross-correlation $C_{Y_\gamma,s}$ is related to the amount of information the PSO can linearly carry about the stimulus. Of course, $Y_\gamma(t)$ can only encode information about $s(t)$, if it is able to respond to a change in the input. The stimulus is encoded in the population activity $A(t)$. So only if a change in $A(t)$ leads in average to a change of the PSO, i.e. if $\langle dY_\gamma/dA\rangle \neq 0$, the PSO is capable of encoding information about the stimulus. The overall magnitude of the PSO cross-spectrum scales with the sensitivity a_γ, which is maximal for $\gamma = R_0 + 1/(2N)$ and considerably larger than zero only for $\gamma \in [R_0 - 2\sigma_A, R_0 + 2\sigma_A]$.

It is in particular instructive to consider the *relative sensitivity* of the PSO, which we define by the ratio between a_γ and the maximal possible sensitivity of the PSO:

$$\frac{a_\gamma}{a_{R_0+1/(2N)}} = \frac{e^{-\beta_\gamma^2/2}/\sqrt{2\pi\sigma_A^2}}{1/\sqrt{2\pi\sigma_A^2}} = e^{-\beta_\gamma^2/2}\,. \tag{4.33}$$

Eq. (4.33) shows that the sensitivity of the PSO diminishes exponentially with the squared distance of the synchrony threshold to the mean value of the activity. Note that for any $\gamma \leq R_0$ there is always a $\gamma' > R_0$, namely $\gamma' = 2R_0 + 1/N - \gamma$, such that $\beta_\gamma^2 = \beta_{\gamma'}^2$, leading to the same sensitivity a_γ.

In Fig. 4.7 we compare the Gaussian approximation of the sensitivity a_γ, Eq. (4.24), [solid lines] to the proportionality factor between the numerically simulated PSO cross-spectrum and the cross-spectrum of the single box-train [symbols] for LIF populations of different size. The approximation slightly underestimates the proportionality factor for small population sizes, but gives good results for larger populations (e.g. $N = 100$).

In the following, we derive an alternative approximation of the cross-spectrum by using the combinatorial product representation of the PSO.

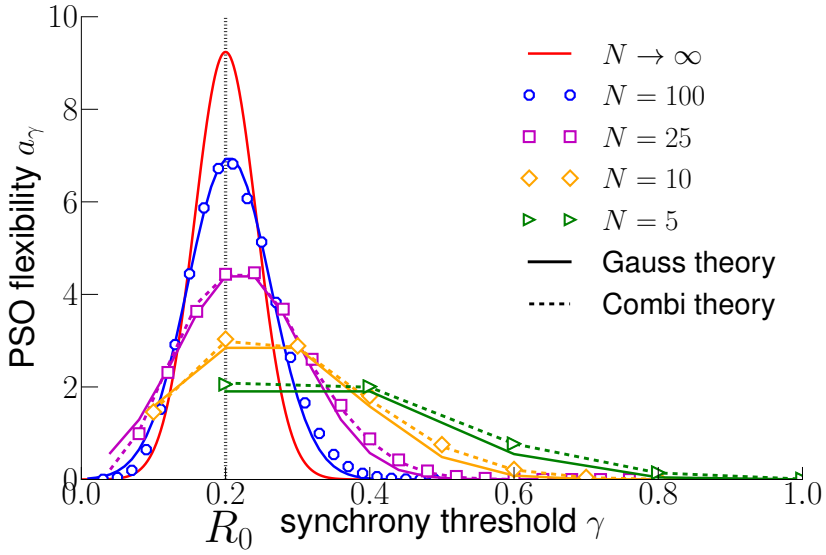

Figure 4.7.: **Absolute value of the cross-spectrum is maximal if the synchrony threshold is set to the mean population activity.** The proportionality constant a_γ quantifies the ratio between the stimulus cross-spectrum of the PSO in comparison to the one of the summed activity $[S_{s,Y_\gamma}(f) = a_\gamma\, S_{s,A}(f)]$. It can be interpreted as the sensitivity of the PSO, $a_\gamma = \langle dY_\gamma/dA\rangle$. The constant a_γ is plotted over the synchrony threshold γ for various population sizes N as indicated. In the simulations [symbols] a_γ was taken as the ratio of the maxima of $S_{Y_\gamma,s}$ and S_{s,b_k}. The simulation results are compared to the Gaussian theory, Eq. (4.24), [solid lines] and the combinatorial approximation, Eq. (4.38), [dashed lines]. The red solid line shows the limit case for infinite large populations, given by Eq. (4.26). The vertical line marks the mean activity value R_0. Parameters: $\mu = 1.2, D = 0.01, c = 0.1, R_0 = 0.2$.

4.3.3. Combinatorial product approach to the cross-spectrum

Using the combinatorial product definition of Y_γ, Eq. (4.8), the cross-covariance between the partially synchronous output and the common stimulus reads

$$\begin{aligned} C_{Y_\gamma,s}(\tau) &= \langle Y_\gamma(0)s(\tau)\rangle \\ &= \sum_{j=\gamma N}^{N} q_j \sum_{\substack{\text{over all}\binom{N}{j}\\ \text{combinations } \pi}} \left\langle \prod_{k=1}^{j} \langle b_{\pi_k}(0)\rangle_{\xi_{\pi_k}} s(\tau) \right\rangle_s \\ &= \sum_{j=\gamma N}^{N} q_j \binom{N}{j} \left\langle \langle b(0)\rangle_\xi^j s(\tau) \right\rangle_s , \end{aligned} \tag{4.34}$$

where we used that the stimulus noise is independent of the intrinsic noise and that all individual box trains, $b_k(t)$, are independent and identically distributed. Using the linear

response ansatz Eq. (1.28), we further evaluate Eq. (4.34) up to the second order of the variance of s :

$$\begin{aligned}\left\langle \langle b(0)\rangle_{\xi}^{j} s(\tau)\right\rangle_{s} &\approx \langle (R_0+\hat{s}(0))^{j} s(\tau)\rangle_{s} \\ &= jR_0^{j-1}\langle \hat{s}(0)s(\tau)\rangle_{s} + \binom{j}{3} R_0^{j-3}\langle \hat{s}^3(0)s(\tau)\rangle_{s}\,, \end{aligned} \tag{4.35}$$

where we used again the binomial formula Eq. (4.18) and that the stimulus s and the effective stimulus $\hat{s}$ are both Gaussian processes with zero mean value, such that $\langle \hat{s}^2(0)s(\tau)\rangle = 0$.
For any Gaussian random variables X_1, X_2, X_3, X_4 with zero mean holds $\langle X_1X_2X_3X_4\rangle = \langle X_1X_2\rangle\langle X_3X_4\rangle + \langle X_1X_3\rangle\langle X_2X_4\rangle + \langle X_1X_4\rangle\langle X_2X_3\rangle$ (Isserlis, 1918), such that

$$\langle \hat{s}^3(0)s(\tau)\rangle_{s} = 3\langle \hat{s}^2\rangle\langle \hat{s}(0)s(\tau)\rangle_{s} = 3\langle \hat{s}^2\rangle C_{\hat{s},s}(\tau)\,. \tag{4.36}$$

Inserting Eq. (4.35) and Eq. (4.36) into Eq. (4.34) yields the following relation of the cross-covariance

$$\hat{C}_{Y_\gamma,s}(\tau) = \hat{a}\, C_{\hat{s},s}(\tau) \tag{4.37}$$

with the proportionality factor

$$\hat{a} = \sum_{j=\gamma N}^{N} q_j \binom{N}{j} jR_0^{j-1}\left(1 + \frac{(j-1)(j-2)}{2}\frac{\langle \hat{s}^2\rangle}{R_0^2}\right). \tag{4.38}$$

Because of Eq. (1.28), $C_{\hat{s},s} = C_{b,s}$ and thus Eq. (4.37) reads in the Fourier domain

$$\boxed{\hat{S}_{s,Y_\gamma}(f) = \hat{a}\, S_{s,b}(f)\,.} \tag{4.39}$$

Using the combinatorial product representation of the PSO leads, like the Gaussian approach, to a cross-spectrum which is proportional to the single box-train cross-spectrum $S_{s,b}(f)$. Note that we did not use the Bussgang theorem to derive this proportionality. Also, using Eq. (4.38) in combination with Eq. (4.19) yields the same relation between the proportionality factor a and the mean PSO as in the Gaussian approach:

$$\hat{a} = \frac{d}{dR_0}\langle \hat{Y_\gamma}\rangle\,. \tag{4.40}$$

This means, that the general relation, Eq. (4.22), holds true in this approximation as well. It is not obvious why this relation should hold. However, if we again think of the proportionality factor as the sensitivity of the PSO, $\langle dY_\gamma/dA\rangle$, and keep in mind that $R_0 = \langle A\rangle$, relation Eq. (4.40) is less surprising.

In Fig. 4.7 the combinatorial approximation of the proportionality factor, Eq. (4.38), is plotted in dashed lines. This approach is in excellent agreement with the simulation results. However, as mentioned before, applying this approach to large populations

yields erroneous results, because of the failing numerical implementation of the huge binomial factors. (That is why we do not show the combinatorial approximation for $N = 100$.)

4.4. Power spectrum of the synchronous output

The common noise does not only affect the cross-correlation but also the autocorrelation of the synchronous activity. However, even if no common stimulus is present, the calculation of the power spectrum of Y_γ is a non-trivial problem. To approximate the power spectrum, $S_{Y_\gamma}(f)$, we will again employ the two different approaches.

4.4.1. Gaussian approach to the power spectrum

If we assume the summed population activity to be Gaussian distributed, we can make use of the Malakov theorem (Malakhov, 1952) which connects the autocorrelation of a Gaussian process with the one of its nonlinear distortion.

Malakov theorem

For any stationary Gaussian process X and any smooth transformation $V(X) = Y$, the autocovariance $C_{YY}(\tau) = \langle Y(0)Y(\tau)\rangle - \langle Y\rangle^2$ of process Y can be expressed by the autocovariance of X via

$$C_{Y,Y}(\tau) = \sum_{n=1}^{\infty} \frac{1}{n!} \left\langle \frac{d^n}{dX^n} V(X) \right\rangle^2 C_{X,X}^n(\tau)\,. \tag{4.41}$$

If we assume the activity A to be normally distributed, we can apply Eq. (4.41) to get an expression for the autocovariance of the PSO, $Y_\gamma = \theta(A - \gamma + 1/(2N))$:

$$C^G_{Y_\gamma,Y_\gamma}(\tau) = \sum_{n=1}^{\infty} \frac{1}{n!} \left\langle \frac{d^n}{dA^n}\, \theta\left(A - \gamma + \frac{1}{2N}\right) \right\rangle^2 C_{A,A}^n(\tau)\,. \tag{4.42}$$

Although the Heaviside step function is not a smooth transformation, we can formally differentiate it, which leads to a δ-distribution. Eq. (4.42) includes only averages of the derivatives of the θ-function. These are integrals over the probability distribution p_A^G and hence, it is clear how this δ-function and its further derivatives need to be evaluated. For $n \geq 1$ we obtain

$$\begin{aligned}
&\left\langle \frac{d^n}{dA^n}\theta(A - \gamma + 1/(2N)) \right\rangle \\
&= (-1)^{n-1} \int_0^1 \delta\left(A - \gamma + \frac{1}{2N}\right) \frac{d^{n-1} p_A^G(A)}{dA^{n-1}} dA \\
&= (-1)^{n-1} \frac{d^{n-1}}{dA^{n-1}}\, p_A^G(A)\Big|_{A=\gamma-\frac{1}{2N}}\,.
\end{aligned} \tag{4.43}$$

The nth derivative of the normal distribution can be expressed in terms of Hermite polynomials (Bronstein et al., 2012) [here, we use the probabilistic version]:

$$He_n(x) := (-1)^n e^{x^2/2} \frac{d^n}{dx^n} e^{-x^2/2} ,$$

such that

$$\begin{aligned} \frac{d^n}{dA^n}\, p_A^G(A)\Big|_{A=\gamma-\frac{1}{2N}} &= \frac{(-1)^n}{\sigma_A^n} He_n(\beta_\gamma) p_A^G\left(\gamma - \frac{1}{2N}\right) \\ &= (-1)^n \frac{a_\gamma}{\sigma_A^n}\, He_n(\beta_\gamma), \end{aligned} \tag{4.44}$$

where β_γ and a_γ are given in Eq. (4.25) and Eq. (4.24).

Plugging Eq. (4.43) and Eq. (4.44) into Eq. (4.42), we obtain

$$C^G_{Y_\gamma Y_\gamma}(\tau) = a_\gamma^2 \sum_{n=0}^{\infty} \frac{He_n^2(\beta_\gamma)}{(n+1)!\,\sigma_A^{2n}}\, C_{AA}{}^{n+1}(\tau) . \tag{4.45}$$

The Fourier transform of this autocovariance function yields an expression for the power spectrum of the PSO

$$S^G_{Y_\gamma}(f) = a_\gamma^2 \left[S_A(f) + \sum_{n=1}^{\infty} \frac{He_n^2(\beta_\gamma)}{(n+1)!}\, \frac{1}{\sigma_A^{2n}} \underset{n}{\ast} S_A\,(f) \right] , \tag{4.46}$$

where by '$\underset{n}{\ast}\ S$' we denote the n-fold convolution of the function $S(f)$ with itself ($\underset{1}{\ast}\ S := S * S$, $\underset{2}{\ast}\ S := S * S * S$, ...). The power of the synchronous output can be thus expressed by a weighted sum of convolutions of the summed activity's power spectrum S_A.
The power spectrum of the population activity is according to Eq. (3.2) given by

$$S_A = \frac{1}{N} S_b + \left(1 - \frac{1}{N}\right) S_{b_k, b_{k'}} . \tag{4.47}$$

Using the linear response ansatz Eq. (1.28), the cross-spectrum between two different box trains equals the power of the effective stimulus (Shea-Brown et al., 2008; Ostojic et al., 2009; Vilela and Lindner, 2009a)

$$\hat{S}_{b_k, b_{k'}}(f) = S_{\hat{s}}(f) \tag{4.48}$$

and the power spectrum of the single box train is given by the product of the Fourier transformed box filter and the power spectrum of the single spike train S_x

$$S_b(f) = |\tilde{\mathcal{B}}(f)|^2 S_x(f) . \tag{4.49}$$

(For an LIF-neuron $S_x(f)$ is given by Eq. (A.4).) Thus, the power spectrum of the activity

can be approximated by

$$\hat{S}_A = \frac{1}{N} S_b + \left(1 - \frac{1}{N}\right) S_{\hat{s}} \,, \tag{4.50}$$

where $S_{\hat{s}}$ is described by Eq. (1.31).

We now have all the ingredients to evaluate Eq. (4.46). However, there is an infinite sum of convolutions that needs to be evaluated numerically and it turns out that the sum cannot be truncated without making a seizable error for most parameter regimes. Nonetheless, we can derive an alternative expression (completely equivalent to Eq. (4.46)) for the power spectrum as follows.

The Hermite polynomials appearing in Eq. (4.45) satisfy the so called Mehler's formula (Watson, 1933):

$$\sum_{n=0}^{\infty} \frac{a^n}{n!} (He_n(x))^2 = \frac{1}{\sqrt{1-a^2}} \exp\left[\frac{x^2}{1+a^{-1}}\right] \,. \tag{4.51}$$

In order to apply this formula we rewrite the terms in Eq. (4.45):

$$\frac{He_n^2(\beta_\gamma)}{(n+1)!}\sigma_A^2 \left(\frac{C_{A,A}(\tau)}{\sigma_A^2}\right)^{n+1} = \sigma_A^2 \int_0^{\rho_A(\tau)} \frac{a^n}{n!} He_n^2(\beta_\gamma)\, da \,, \tag{4.52}$$

where

$$\rho_A(\tau) = \frac{C_{A,A}(\tau)}{\sigma_A^2} = \frac{\mathrm{IFT}(S_A)}{\sigma_A^2} \tag{4.53}$$

is the normalized autocorrelation function of the population activity, which can be derived by taking the inverse Fourier transform (IFT) of Eq. (4.50). With Eq. (4.52) and Eq. (4.51), the infinite sum in Eq. (4.45) can be replaced by an integral, resulting in the desired alternative expression for the autocovariance of the PSO

$$C^G_{Y_\gamma, Y_\gamma}(\tau) = a_\gamma^2 \, I_\gamma(\tau) \tag{4.54}$$

with the time-lag dependent integral

$$I_\gamma(\tau) = \sigma_A^2 \int_0^{\rho_A(\tau)} \frac{1}{\sqrt{1-a^2}} \exp\left[\frac{\beta_\gamma^2}{1+a^{-1}}\right] da \,. \tag{4.55}$$

The power spectrum of the partially synchronous output reads therefore

$$\boxed{S^G_{Y_\gamma}(f) = a_\gamma^2 \, \widetilde{I}_\gamma(f)} \tag{4.56}$$

and explicitly

$$\boxed{S^G_{Y_\gamma}(f) = \frac{e^{-\beta_\gamma^2}}{2\pi}\,\mathrm{FT}\left(\int_0^{\rho_A(\tau)} \frac{1}{\sqrt{1-a^2}}\exp\left[\frac{\beta_\gamma^2}{1+a^{-1}}\right] da\right)\,.} \tag{4.57}$$

where FT stands for the Fourier transform with respect to τ.

4.4.2. Properties of the PSO power spectrum that can be deduced from the Gaussian approach

The evaluation of expression (4.57) involves three integrals, two Fourier transforms (ρ_A is calculated by a FT of S_A) and the integral over a. This is manageable compared to the large number of convolutions that potentially have to be evaluated in Eq. (4.46). Unfortunately, there is no closed analytical solution of the integral Eq. (4.55) for a general value of γ. However, one can deduce a number of qualitative and quantitative properties about the autocorrelation and power spectrum of the PSO from this approximation.

i) If the synchrony threshold is set to the mean activity value, the PSO power spectrum is proportional to the power spectrum of the summed activity

A special case where we can solve the integral Eq. (4.55) is the case $\gamma = R_0$, i.e for $\beta_\gamma \approx 0$. [1] Because $\int_0^x 1/\sqrt{1-a^2}\,da = \arcsin(x)$, we obtain

$$I_{R_0} \approx \sigma_A^2 \arcsin(\rho_A)\,. \tag{4.58}$$

For time lags τ considerably larger than zero the activity autocorrelation has a small amplitude, such that $\arcsin(\rho_A(\tau))\rho_A(\tau)$ (see Fig. 4.8). With this approximation we can further estimate Eq. (4.58)

$$I_{R_0}(\tau)\sigma_A^2\rho_A(\tau) = C_{A,A}(\tau)\,. \tag{4.59}$$

For $\gamma = R_0$ the power spectrum of the PSO, Eq. (4.56), can be consequently approximated by

$$S^G_{Y_{R_0}}(f) \approx \frac{1}{2\pi}\,\mathrm{FT}[\arcsin(\rho_A)] \tag{4.60}$$

$$\frac{1}{2\pi}\,\frac{S_A(f)}{\sigma_A^2} = a_{R_0}^2\,S_A(f)\,. \tag{4.61}$$

Eq. (4.60) describes simulation results indeed very well (see Fig. 4.9), and even the simple approximation Eq. (4.61) gives a rough estimate. In conclusion, if the synchrony threshold is set to the mean population activity, the power spectrum of the PSO is approximately proportional to the power spectrum of the summed activity, i.e. to the power of 'all spikes'.

[1] Formally $\beta_{\hat{\gamma}} = 0$ for $\hat{\gamma} = R_0 + 1/(2N)$. For reasons of clarity we will omit the summand $(2N)^{-1}$ most of the times, which is after all only important for small populations.

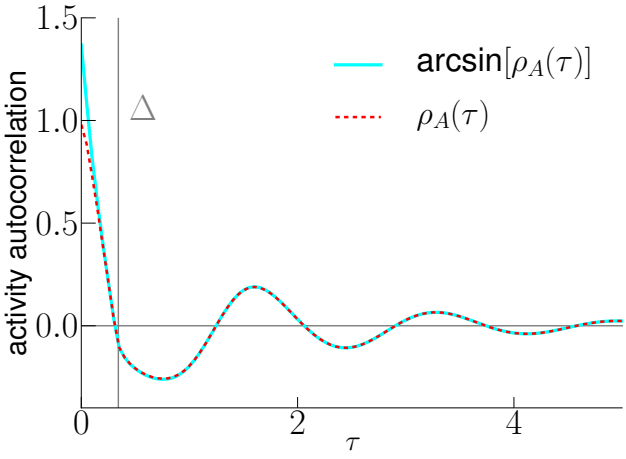

Figure 4.8.: Normalized autocorrelation function of the activity, $\rho_A(\tau)$ [red dashed line], compared to $\arcsin[\rho_A(\tau)]$ [cyan solid line]. Here, $\arcsin[\rho_A(\tau)] \approx \rho_A(\tau)$ for $\tau > 0.16$, which is smaller than the synchrony box width Δ [vertical gray line]. LIF-parameters: $\mu = 1.2, D = 0.01, c = 0.1, N = 100$.

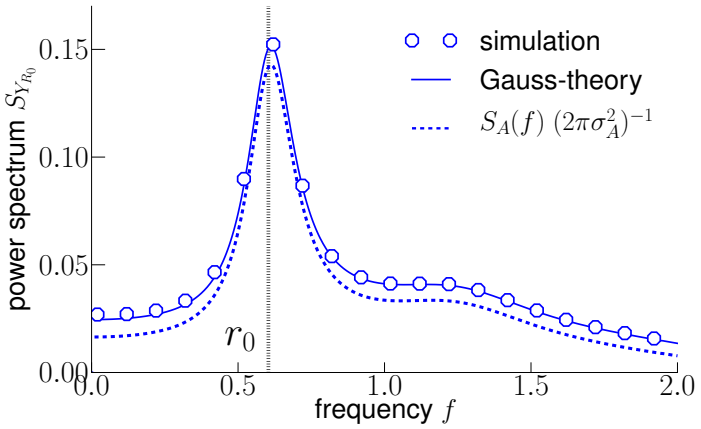

Figure 4.9.: **For $\gamma = \langle A \rangle$ the power spectrum of the PSO is approximately proportional to the power spectrum of the summed population activity.** Power spectrum of the partially synchronous output if the synchrony threshold γ is set to the mean activity $\langle A \rangle = R_0$. Simulation results [circles] are compared to the Gaussian approximation Eq. (4.60) [solid line] and to Eq. (4.61) [dashed line]. The spectra have their maximum at roughly the single neuron firing rate $r_0 = 0.58$ (vertical dotted line). Parameters: $\mu = 1.2, D = 0.01, c = 0.1, R_0 = 0.2, N = 100$.

ii) The PSO power spectrum is symmetric in the synchrony threshold around the mean activity value

Eq. (4.57) illustrates that within the Gaussian approach the power spectrum depends on the synchrony threshold γ only through the key parameter $\beta_\gamma^2 = (\gamma - R_0 - 1/(2N))^2/\sigma_A^2$, i.e. the normalized distance between γ and the expected population activity. In Fig. 4.10 we compare the Gaussian approximation, Eq. (4.57), to simulations of a population of 100 LIF neurons. The theory agrees well with the simulation results. As predicted by the theory, the power spectra corresponding to γ-values with the same β_γ^2-value are very close to each other, especially for larger frequencies. At low frequencies however, the power spectrum for $\gamma < R_0$ is larger than for $\gamma' > R_0$, if $\beta_\gamma^2 = \beta_{\gamma'}^2$ (see inset in Fig. 4.10).

iii) The magnitude of the PSO power spectrum decreases exponentially with β_γ^2

From Eq. (4.46) we see that the overall magnitude of the PSO power spectrum/autocorrelation is scaled by the sensitivity $a_\gamma = e^{-\beta_\gamma^2}/(2\pi\sigma_A^2)$. Hence, the overall synchrony power is maximal for $\gamma = R_0$ and drops exponentially as γ diverges from the mean activity value. Fig. 4.12a illustrates the strong reduction in the magnitude of the PSO power spectrum with increasing β_γ^2.

iv) Autocorrelation of the PSO concentrates around $\tau = 0$ for large $|\beta_\gamma|$, leading to a flat power spectrum.

The relative time dependence of the PSO autocorrelation (Eq. (4.54)) is given by the integral

$$I_\gamma(\tau) = \sigma_A^2 \int_0^{\rho_A(\tau)} \frac{1}{\sqrt{1-a^2}} \exp\left[\frac{\beta_\gamma^2}{1+a^{-1}}\right] da \,.$$

The second factor in the integrand, $\exp[\beta_\gamma^2/(1+a^{-1})]$, amplifies the pole at $a = 1$ of the first term $1/\sqrt{1-a^2}$ by a factor of $e^{\beta_\gamma^2/2}$, which becomes huge for large values of $|\beta_\gamma|$. For small values of $a < 1$, the exponential factor has less and less influence, because $\lim_{a\to 0} \exp[\beta_\gamma^2/(1+a^{-1})] = 1$. For a given time lag τ, only values of a contribute to the integral $I_\gamma(\tau)$ for which hold $|a| \leq |\rho_A(\tau)|$. The pole value $a = 1$ does only appear for $\tau = 0$ (because for $\tau > 0, \rho_A(\tau) < \rho_A(0) = 1$). In conclusion, the ratio between $I_\gamma(0)$ and $I_\gamma(\tau)$ for a time lag $\tau > 0$ increases with β_γ^2. As a consequence, the correlation function is strongly peaked around $\tau = 0$ for large values of β_γ^2. This behavior can be observed in Fig. 4.11b. A strongly peaked autocorrelation leads in the Fourier domain to a flat power spectrum

$$\boxed{S_{Y_\gamma}(f) \approx \text{const} \quad \text{for } \beta_\gamma^2 \gg 1\,,} \tag{4.62}$$

This behavior is intuitively not surprising. For large values of β_γ^2, i.e. if the synchrony threshold is set far away from the expected activity, the PSO is almost always zero for $\gamma > \langle A \rangle$ or almost always one for $\gamma < \langle A \rangle$ (see Sec. 4.2). Deviations from these values,

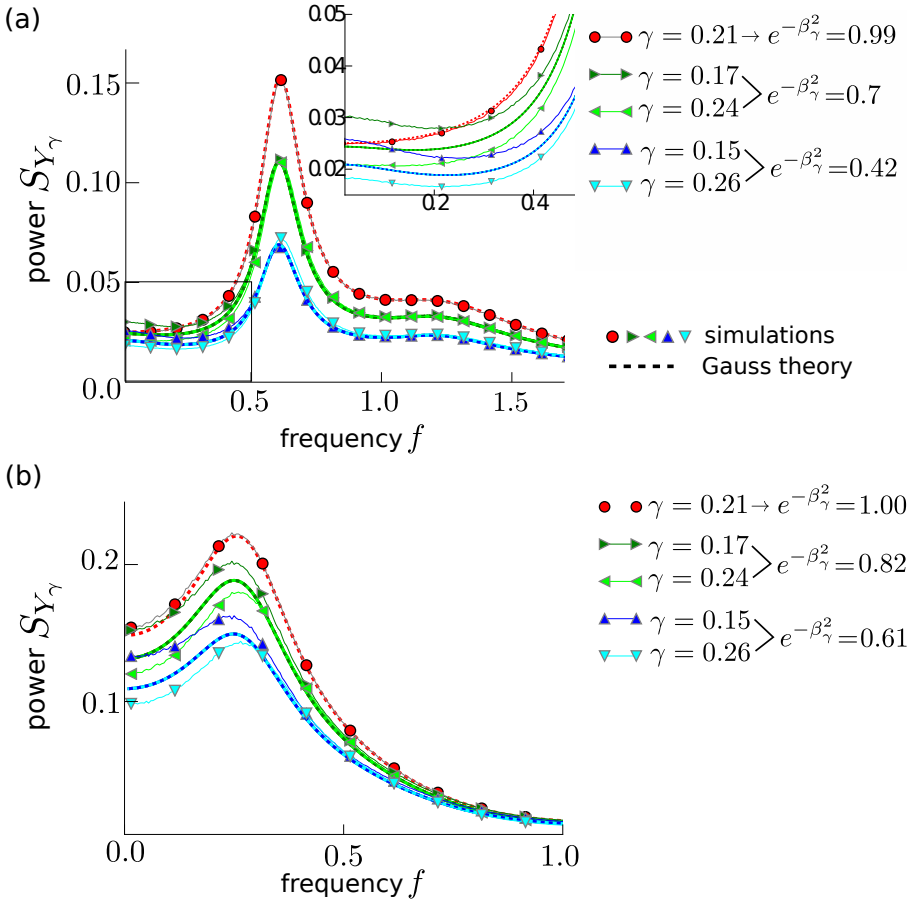

Figure 4.10.: **The distance of the synchrony threshold γ to the mean activity determines the magnitude of the power of the synchronous output.** Power spectrum of the partially synchronous output for a population of $N = 100$ LIF neurons for various synchrony thresholds γ. The Gaussian theory, Eq. (4.57), predicts the identical result for γ-values which lead to the same value of $\beta_\gamma^2 = (\gamma - R_0 - 1/(2N))^2/\sigma_A^2$. The inset in (a) shows the power spectrum for small frequencies. Parameters: $D = 0.01, c = 0.1, R_0 = 0.2$, (a) $\mu = 1.2$, (b) $\mu = 0.9$.

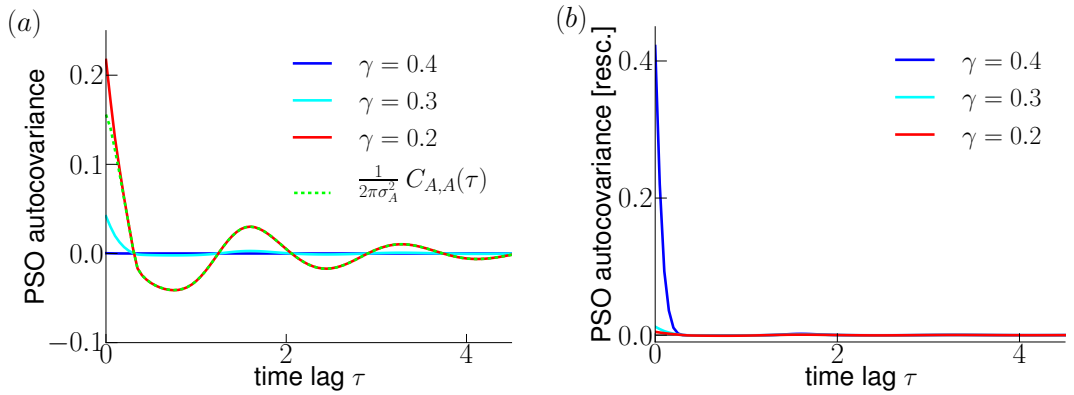

Figure 4.11.: **Autocorrelation function of the PSO is strongly peaked around zero for high synchrony demand.** [a] Autocovariance function of the PSO for different synchrony thresholds $\gamma \in \{0.2, 0.3, 0.4\}$ (corresponding to $\beta_\gamma^2 \in \{0.0, 2.6, 11.0\}$). For comparison, the autocovariance of the summed activity (divided by $2\pi\sigma_A^2$) is plotted in dashed green. [b] Rescaled PSO autocorrelation $I_\gamma(\tau)$, Eq. (4.55). For large values of β_γ^2, the autocovariance function of the PSO is strongly peaked at $\tau = 0$ and diminishes quickly for $\tau > 0$. Parameters: $\mu = 1.2, D = 0.01, c = 0.1, N = 100$.

i.e. synchronous events (common firing for $\beta_\gamma > 0$ or common silence for $\beta_\gamma < 0$) become very rare and statistically independent of each other. This leads to a rare-event (Poissonian) statistics which is characterized by a flat power spectrum.

The limits of extreme γ-values are explored in Fig. 4.12. In panel (b) the power spectra are rescaled by their maximal value in order to compare their frequency dependence. One can observe the flattening of the spectra as $\gamma \to 1$ and $\gamma \to 0$. The power spectrum becomes indeed constant as γ approaches one and is already rather flat for $\gamma \geq 0.6$ in the shown frequency range.

v) Negative correlations get more suppressed than positive ones

From Eq. (4.55) one can easily derive that for all γ_1 and γ_2 with $|\beta_{\gamma_1}| > |\beta_{\gamma_2}|$ holds

$$I_{\gamma_1}(\tau) > I_{\gamma_2}(\tau) \tag{4.63}$$

for all $\tau \geq 0$. If $\rho_A(\tau)$ is positive, i.e. for $0 \leq a \leq 1$, holds true that $\exp\left[\beta_{\gamma_1}^2/(1+a^{-1})\right] \geq \exp\left[\beta_{\gamma_2}^2/(1+a^{-1})\right]$, such that Eq. (4.63) is fulfilled. For negative $\rho_A(\tau)$, i.e. for $-1 < a < 0$, holds $\exp\left[\beta_{\gamma_1}^2/(1+a^{-1})\right] < \exp\left[\beta_{\gamma_2}^2/(1+a^{-1})\right]$. Because both integrals are negative in this case, one finds again that $I_{\gamma_1}(\tau) > I_{\gamma_2}(\tau)$.

From relation Eq. (4.63) we see that for any γ with $|\beta_\gamma| > 0$ holds

$$I_\gamma(\tau) > I_{R_0}(\tau) \approx C_{A,A}(\tau)\,, \tag{4.64}$$

where we used Eq. (4.59) for the last equality. In conclusion, by distorting the popula-

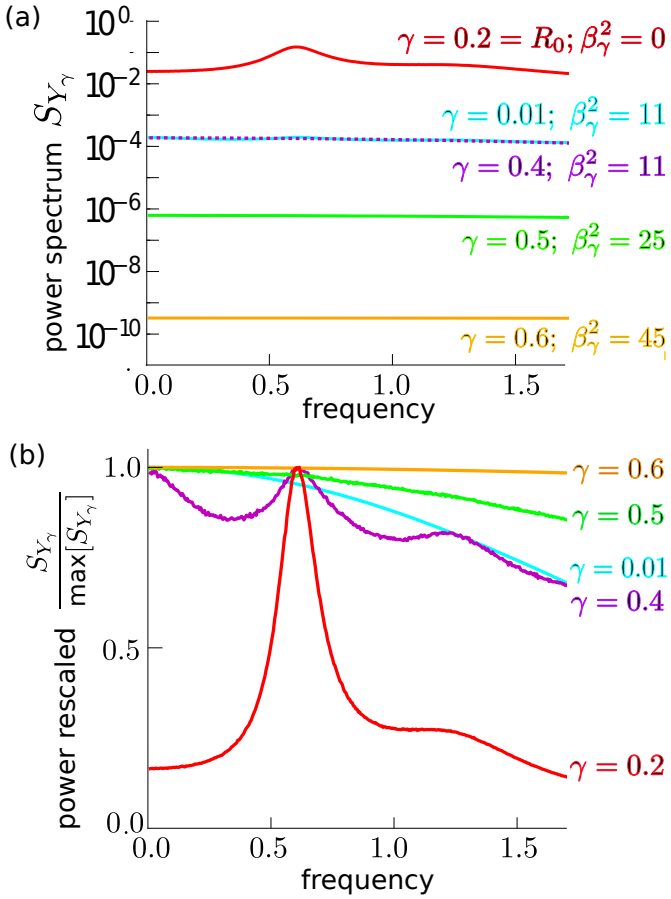

Figure 4.12.: **The power spectrum of the synchronous output converges to a constant as $\gamma \to 1$ or $\gamma \to 0$.** Power spectrum of the partially synchronous output for various synchrony threshold values γ. [a] Total value in log-scale. [b] S_{Y_γ} scaled by its maximal value. The power spectrum is maximal and the most peaked for $\gamma = R_0$ [red line]. As γ approaches one or zero, the power spectrum converges to a flat spectrum as predicted by Eq. (4.62). Parameters: $\mu = 1.2, D = 0.01, c = 0.1, R_0 = 0.2, N = 100$.

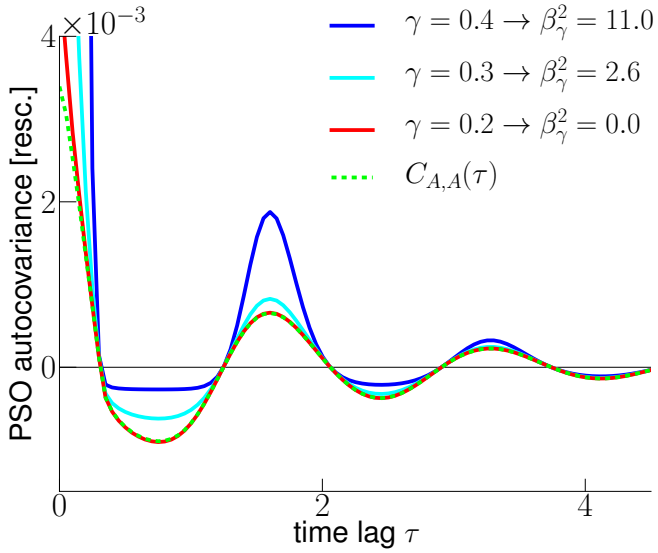

Figure 4.13.: **Negative autocorrelations get more suppressed than positive ones.** Rescaled PSO autocovariance $I_\gamma(\tau)$, Eq. (4.55), for different synchrony thresholds (this is a zoom of Fig. 4.11b). For $\gamma = \langle A \rangle$ [red line] the PSO autocovariance shares approximately the same relative τ-dependence as the autocovariance of the summed activity [dotted green line]. As β_γ^2 increases negative autocorrelations of the summed activity are stronger suppressed than positive ones by the synchrony threshold criterion. Parameters: $\mu = 1.2, D = 0.01, c = 0.1, N = 100$.

tion activity with a threshold function, negative autocorrelations are stronger suppressed than positive ones. In Fig. 4.13 we can see this effect, which becomes more and more pronounced for increasing $|\beta_\gamma|$. (Remember that I_γ is the rescaled autocovariance of the PSO: $I_\gamma = C_{Y_\gamma,Y_\gamma}/a_\gamma^2$.)

This behavior can be understood intuitively. It is a consequence of the lack of sensitivity of the PSO for large values of $|\beta_\gamma|$. The summed activity has negative autocorrelations for times larger than the box width Δ. If there was for example a large activity in one bin, the activity in the following bins necessarily has to be smaller on average, such that the mean value R_0 is preserved (see Fig. 4.8). On the contrary, for large values of $|\beta_\gamma|$, i.e. for vanishing sensitivity a_γ, the PSO is almost constant, such that autocorrelations are mostly positive (if $Y_\gamma(t)$ is almost always one, then it is very likely that the following values $Y_\gamma(t+\tau)$ are one as well).

4.4.3. Combinatorial product approach to the power spectrum

The derivation of the PSO power spectrum in the combinatorial product approach is much more cumbersome than the respective calculation in the Gaussian approach. We will first show the analytical derivation for the stimulus-free case. The derivation of the

power spectrum in the first order of the common stimulus' variance is more tricky and involves a rather unorthodox linear response approach. Both approximations are tested against numerical simulations of small LIF populations and compared to the Gaussian estimation.

Combinatorial approach to the PSO power spectrum in absence of a stimulus

Using the combinatorial representation of the PSO, Eq. (4.8), the autocorrelation function of the partially synchronous output reads

$$\begin{aligned}\langle Y_\gamma(0)Y_\gamma(\tau)\rangle &= C_{Y_\gamma Y_\gamma}(\tau) + \langle Y_\gamma\rangle^2 \\ &= \sum_{j,j'=\gamma N}^{N} q_j q_{j'} \sum_{\substack{\text{over all}\binom{N}{j}\\ \text{combinations } \pi}} \sum_{\substack{\text{over all}\binom{N}{j'}\\ \text{combinations } \pi'}} \langle \mathcal{P}^{j,j'}_{\pi,\pi'}\rangle \,, \end{aligned} \tag{4.65}$$

where

$$\mathcal{P}^{j,j'}_{\pi,\pi'} := \prod_{k=1}^{j} b_{\pi_k}(0) \prod_{k'=1}^{j'} b_{\pi_{k'}}(\tau)\,. \tag{4.66}$$

The mean value of $\mathcal{P}^{j,j'}_{\pi,\pi'}$ depends on the number of matching pairs, $b_k(0)b_k(\tau)$, i.e. when the same neuron index appears twice in Eq. (4.66). If there are exactly m matching pairs we find

$$\langle \mathcal{P}^{j,j'}_{\pi,\pi'}\rangle = \left\langle \langle b(0)b(\tau)\rangle_\xi^m \langle b(0)\rangle_\xi^{j-m} \langle b(\tau)\rangle_\xi^{j'-m} \right\rangle_s \,. \tag{4.67}$$

If we neglect the influence of the weak stimulus $s(t)$, Eq. (4.67) reads

$$\langle \mathcal{P}^{j,j'}_{\pi,\pi'}\rangle = (C_{b,b}(\tau) + R_0^2)^m R_0^{j+j'-2m}\,, \tag{4.68}$$

where $C_{b,b}(\tau) = \langle b(0)b(\tau)\rangle - \langle b(0)\rangle^2$ is the autocovariance of the single box-train. Hence, instead of summing over all combinations π and π' in Eq. (4.65), we only need to sum over the number of matching pairs m, resulting in

$$C_{Y_\gamma Y_\gamma}(\tau) + \langle Y_\gamma\rangle^2 = \sum_{j,j'=\gamma N}^{N} q_j q_{j'}\, R_0^{j+j'} \sum_{m=\max(0,j+j'-N)}^{\min(j,j')} \#_{j,j',m} \left(\frac{C_{b,b}(\tau)+R_0^2}{R_0^2}\right)^m, \tag{4.69}$$

where

$$\#_{j,j',m} = \binom{N}{m}\binom{N-m}{j-m}\binom{N-j}{j'-m} \tag{4.70}$$

is the number of possible combinations of having exactly m matching pairs given a fixed number j of boxtrains at time zero and j' at time τ. Fig. 4.14 illustrates the derivation of this factor.

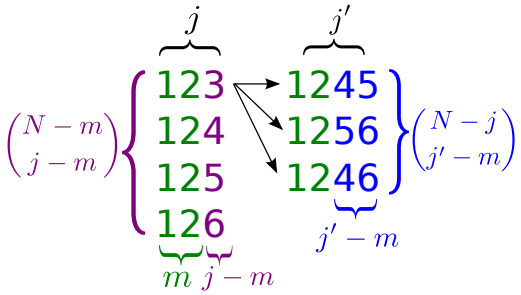

Figure 4.14.: **Illustration of the derivation of the prefactor $\#_{j,j',m}$ in Eq. (4.69)** Example: $N = 6, j = 3, j' = 4, m = 2$. The series of numbers represent the indices of the individual neurons, e.g. the left "123" represents the product $b_1(0)b_2(0)b_3(0)$, and the right "1245" represents $b_1(\tau)b_2(\tau)b_4(\tau)b_5(\tau)$. The first factor $\binom{N}{m}$ in Eq. (4.70) is the number of possibilities to choose m different indices out of N. Once m indices have been fixed (in the example indices 1 and 2), one can still vary the $j - m$ indices that label the possible boxtrains $b_\bullet(0)$ that can be chosen from $N - m$ remaining indices. There are $N - j$ indices to choose from to fill the $j' - m$ indices that label the not matching boxtrains $b_\bullet(\tau)$.

By the convolution theorem we obtain for the power spectrum of Y_γ ($f \neq 0$)

$$\hat{S}^{(0)}_{Y_\gamma}(f) = \sum_{j,j'=\gamma N}^{N} q_j q_{j'} \, R_0^{j+j'} \sum_{m=\max(1,j+j'-N)}^{\min(j,j')} \frac{\#_{j,j',m}}{R_0^{2m}} \underset{m-1}{\ast} \overline{S}_b\,(f) \tag{4.71}$$

with $\overline{S}_b(f) = S_b(f) + R_0^2\,\delta(f)$ being the power spectrum of the single box train including the DC-peak. Taking into account the δ-function in $\overline{S}_b$ is important, because it affects the convolutions. By $\underset{m}{\ast}\,\overline{S}_b$ we again denote the m-fold convolution of $\overline{S}_b$ with itself ($\underset{0}{\ast}\,\overline{S}_b = \overline{S}_b$, $\underset{1}{\ast}\,\overline{S}_b = \overline{S}_b * \overline{S}_b$, ...).

In Fig. 4.15 a,b approximation Eq. (4.71) [solid lines] is compared to simulation results [symbols] of a population of ten uncorrelated ($c = 0$) LIF-neurons. For both, the suprathreshold (a) and subthreshold regime (b), the combinatorial approach predicts well the power spectrum of the synchronous output. As a matter of fact, it performs better than the Gaussian approximation for small populations, which is plotted for comparison in Fig. 4.15c and d.

However, we were originally interested in the response of the PSO to a weak common stimulus. We now derive an approximation of the PSO power spectrum which includes the stimulus, up to the first order of its variance.

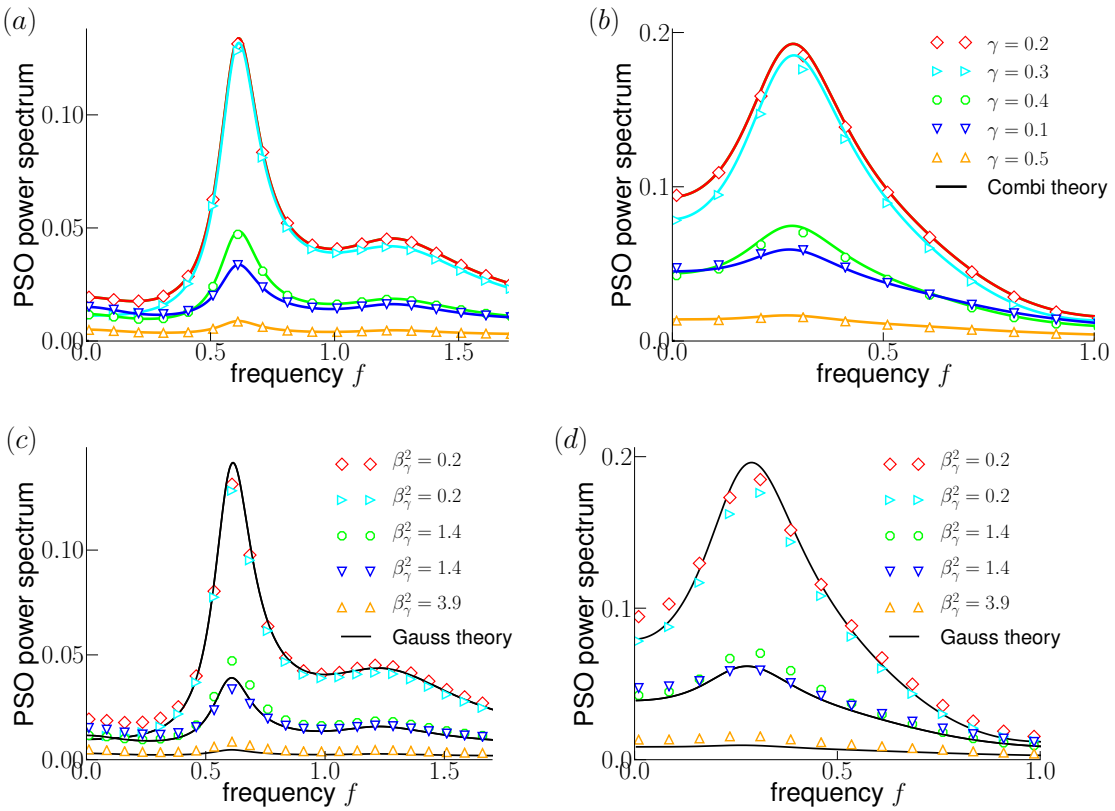

Figure 4.15.: **Combinatorial theory predicts well the spontaneous PSO power spectrum of a small population.** Power spectrum of the partially synchronous output for a population of $N = 10$ independent ($c = 0$) LIF-neurons for various synchrony-thresholds γ. Symbols mark simulation results (same symbols mark the same value of γ in all plots as indicated in the legend in [b]). [a,b] Combinatorial product approximation Eq. (4.76) [colored solid lines]. [c,d] Gaussian approximation Eq. (4.57) [black solid lines] compared to same simulation results as in [a,b]. The Gaussian approximation is identical for γ-values with equal values of β^2_γ [see legend]. Parameters: $\mu = 1.2, D = 0.01, c = 0, R_0 = 0.2, (a,c) : \mu = 1.2, (b,d) : \mu = 0.9$

Combinatorial approach to the PSO power spectrum with weak common stimulus

In order to incorporate the influence of the common stimulus we extend the linear response ansatz for the windowed firing rate, $\langle b(t)\rangle_{\hat{\xi}} \approx R_0 + \hat{s}(t)$, to a formal linear response ansatz for a single realization of the boxtrain:

$$"b(t) \approx b_0(t) + \hat{s}(t)" \,, \tag{4.72}$$

where b_0 is the spontaneous boxtrain, i.e. for the case $c = 0$. This ansatz, introduced in (Lindner et al., 2005), is to be understood as a tool to derive spectral statistics. It has been successfully employed for calculating spectral measures in neural networks (Lindner et al., 2005; Marinazzo et al., 2007; de la Rocha et al., 2007; Shea-Brown et al., 2008; Sharafi et al., 2013). Technically, the process $b(t)$ can only take the values one and zero, whereas $\hat{s}(t)$ can be any real number. The approximation Eq. (4.72) does therefore only make proper sense if ensemble averages are involved.
Using ansatz Eq. (4.72) we can directly evaluate the first term in Eq. (4.67)

$$\begin{aligned}
\langle b(0)b(\tau)\rangle_{\hat{\xi}}^{m} &\approx \langle b_0(0)b_0(\tau) + b_0(0)\hat{s}(\tau) + b_0(\tau)\hat{s}(0) + \hat{s}(0)\hat{s}(\tau)\rangle_{\hat{\xi}}^{m} \\
&= [\overline{C}_{b_0,b_0}(\tau) + R_0\,\hat{s}(\tau) + R_0\,\hat{s}(0) + \hat{s}(0)\hat{s}(\tau)]^{\,m} \\
&= \overline{C}_{b_0,b_0}^{\,m}(\tau) + m\overline{C}_{b_0,b_0}^{\,m-1}(\tau)[\,R_0\,\hat{s}(\tau) + R_0\,\hat{s}(0) + \hat{s}(0)\hat{s}(\tau)\,] \\
&\quad + \binom{m}{2}\overline{C}_{b_0,b_0}^{\,m-2}(\tau)R_0^2\,[\,\hat{s}^2(\tau) + \hat{s}^2(0) + 2\,\hat{s}(0)\hat{s}(\tau)\,]\,,
\end{aligned} \tag{4.73}$$

where we used the binomial formula and considered only terms up to the order of the variance of the common stimulus ($\sim \mathcal{O}(\hat{s}^2)$). $\overline{C}_{b_0,b_0}(\tau) = \langle b_0(0)b_0(\tau)\rangle$ is the autocorrelation function of the spontaneous boxtrain. The second and third term in Eq. (4.67) can be evaluated by using the usual linear response ansatz for the firing rate, Eq. (1.28):

$$\begin{aligned}
\langle b(0)\rangle_{\hat{\xi}}^{j-m} &\approx (R_0 + \hat{s}(0))^{j-m} \\
&\approx R_0^{j-m} + (j-m)R_0^{j-m-1}\hat{s}(0) + \binom{j-m}{2}R_0^{j-m-2}\hat{s}^2(0)\,.
\end{aligned} \tag{4.74}$$

Plugging Eq. (4.73) and Eq. (4.74) into Eq. (4.67) yields

$$\begin{aligned}
\langle \mathcal{P}_{\pi,\pi'}^{j,j'}\rangle = R_0^{j+j'-2m}\,\{ & \\
&\overline{C}_{b_0,b_0}^{\,m}\left(1 + \left[\binom{j'-m}{2} + \binom{j-m}{2}\right]\frac{\langle\hat{s}^2\rangle}{R_0^2} + (j'-m)(j-m)\frac{C_{\hat{s},\hat{s}}}{R_0^2}\right) \\
&\quad + m\,\overline{C}_{b_0,b_0}^{\,m-1}[\,(j'+j-2m)\{\langle\hat{s}^2\rangle + C_{\hat{s},\hat{s}}\} + C_{\hat{s},\hat{s}}\,] \\
&\quad + m(m-1)\,\overline{C}_{b_0,b_0}^{\,m-2}R_0^2[\,\langle\hat{s}^2\rangle + C_{\hat{s},\hat{s}}\,]\,\}\,,
\end{aligned} \tag{4.75}$$

where $C_{\hat{s},\hat{s}}(\tau) = \langle\hat{s}(0)\hat{s}(\tau)\rangle_s$ is the autocorrelation function of the effective stimulus.
By incorporating Eq. (4.75) into Eq. (4.65) and taking the Fourier transform, the power spectrum of the synchronous output up to the first order of the variance of the common

stimulus reads

$$S^{(1)}_{Y_\gamma}(f) = \sum_{j,j'=\gamma N}^{N} q_j q_{j'}\, R_0^{j+j'} \sum_{m=\max(0,j+j'-N)}^{\min(j,j')} \frac{\#_{j,j',m}}{R_0^{2m}}\, \omega_{j,j',m}(f)\,, \tag{4.76}$$

where

$$\begin{aligned}
\omega_{j,j',m} = \Bigg\{ & \left(1 + \left[\binom{j'-m}{2} + \binom{j-m}{2}\right] \frac{\langle \hat{s}^2 \rangle}{R_0^2}\right) \underset{m-1}{*} \overline{S}_b \\
& + R_0^{-2}(j'-m)(j-m) S_{\hat{s}} * \underset{m-1}{*} \overline{S}_b \\
& + m[j+j'-2m] \langle \hat{s}^2 \rangle \underset{m-2}{*} \overline{S}_b \\
& + m[j+j'-2m+1]\, S_{\hat{s}} * \underset{m-2}{*} \overline{S}_b \\
& + R_0^2\, m(m-1) \left[\langle \hat{s}^2 \rangle \underset{m-3}{*} \overline{S}_b + S_{\hat{s}} * \underset{m-3}{*} \overline{S}_b \right] \Bigg\}\,.
\end{aligned}$$

In Fig. 4.16 a,b Eq. (4.76) is compared to simulation results of ten LIF neurons driven by weak common white noise. The approximation gives reasonable results, but deviates from the numerics especially at higher frequencies. The deviations are more pronounced in the subthreshold regime (see Fig. 4.16b). Fig. 4.16 c,d compares the same simulation results to the Gaussian approximation, Eq. (4.57), which performs much worse than the combinatorial approach for this small system size.

4.5. Application to non-white common stimuli

So far, in all simulations, we considered the common noise to be white, which is useful in order to see how the system reacts to an arbitrary frequency component of a common input. However, white noise is certainly not a very natural stimulus. We can in principle apply our results to a Gaussian stimulus of arbitrary temporal correlation as long as it is weak. For instance, we can consider the Ornstein-Uhlenbeck process (OUP)

$$\tau_s\, \dot{s} = -s + \sqrt{2Dc}\, \xi_s(t)\,, \tag{4.77}$$

where ξ_s is Gaussian white noise. The stationary ($t \gg 1$) autocorrelation function of s reads

$$\langle s(t) s(t+\tau) \rangle = \frac{Dc}{\tau_s}\, e^{-\tau/\tau_s}\,.$$

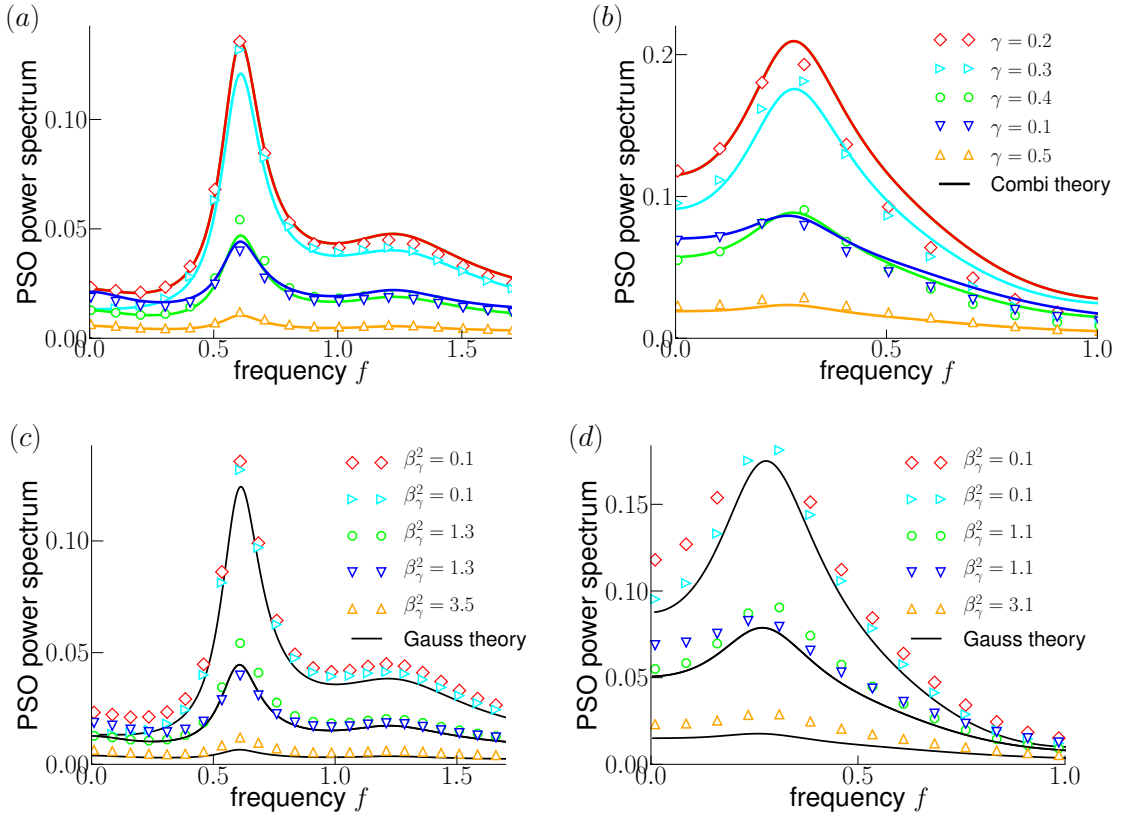

Figure 4.16.: **For small populations, the combinatorial approach works better than the Gaussian one.** PSO power spectrum of a population of $N = 10$ LIF-neurons driven by weak common noise for various synchrony-thresholds γ. Symbols mark simulation results (same symbols mark the same value of γ in all plots as indicated in the legend in [b]). [a,b] Combinatorial product approximation Eq. (4.76) [colored solid lines]. [c,d] Gaussian approximation Eq. (4.57) [black solid lines] compared to same simulation results as in [a,b]. The Gaussian approximation is identical for γ-values with equal values of β^2_γ [see legend]. Parameters: $\mu = 1.2, D = 0.01, c = 0.1, R_0 = 0.2, (a, c) : \mu = 1.2, (b, d) : \mu = 0.9$

Hence, $Dc = \int_0^\infty \langle s(t)s(t+\tau)\rangle d\tau$ is again the intensity of s, but now it has a non-zero (exponential) autocorrelation time τ_s. The power spectrum of process Eq. (4.77) reads

$$S_s(f) = \frac{2Dc}{1 + (2\pi f \tau_s)^2} \,. \tag{4.78}$$

Fig. 4.17 shows the cross- and power spectrum of the synchronous output with synchrony threshold $\gamma = 0.25$ of an LIF population driven by a common OUP for two different autocorrelation times. The power spectrum of the corresponding stimulus is shown in the inset in Fig. 4.17a. We see that the theory agrees well with simulation

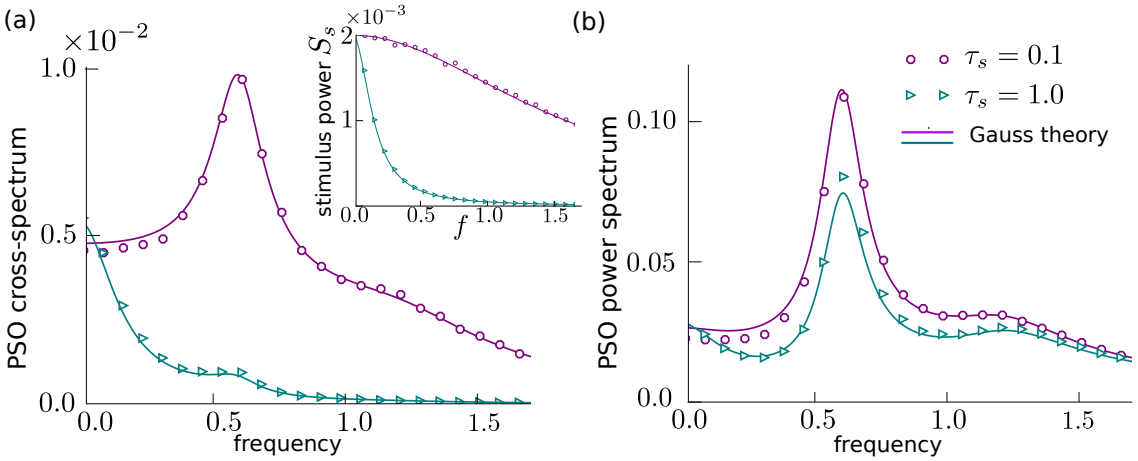

Figure 4.17.: **Theory is also applicable to colored noise.** PSO spectra for an LIF population which is driven by a common Ornstein-Uhlenbeck process, given by Eq. (4.77), with two different autocorrelation times τ_s as indicated. The inset in [a] shows the power spectrum of the OUP. Symbols mark simulation results and the solid lines show the theoretic predictions Eq. (4.32),Eq. (4.78) and Eq. (4.57). Remaining parameters: $\mu = 1.2, D = 0.01, c = 0.1, R_0 = 0.2, N = 100, \gamma = 0.25$.

results, also in the case of colored input.

For small autocorrelation times τ_s [purple circles in Fig. 4.17] we see a similar behavior to the white noise case. For larger values of τ_s [blue triangles in Fig. 4.17] the power of the stimulus (and, consequently that of the effective stimulus) is diminished already at moderate frequencies, such that the cross-spectrum between the synchronous output and the stimulus is concentrated at low frequencies. As a consequence, the ratio between the PSO power at low and high frequencies increases with τ_s [see Fig. 4.17b]. Because we fix the noise intensity, an increase in the autocorrelation time τ_s leads to a decrease in the variance of the stimulus, such that the mean magnitude of the power of the synchronous output is decreased as well.

4.6. Comparison of the Gaussian to the combinatorial product approach

We employed two different approaches to derive analytical approximations of the PSO statistics: the Gaussian and the combinatorial product approach. In both approaches the common stimulus was incorporated by using linear response theory. In the combinatorial approach, the synchronous output is expressed by products of the box-filtered spike trains. As a generalization of the ansatz introduced in Sharafi et al. (2013), this was originally our first attempt to deal with the problem and it yields generally more accurate results of the PSO statistics. In contrast to the Gaussian approach it differentiates between γ-values that have the same distance to the mean activity and it can

quantitatively describe the small differences between these cases. However, the resulting equations are quite cumbersome and do not provide much insight about the roles of parameters. In addition, in practice they can be evaluated only for small populations because of the required numerical effort to compute the combinatorial factors occurring in the formulas.

In the Gaussian approach the PSO is a threshold function of the summed population activity and the activity is assumed to have a Gaussian distribution. Under this assumption, all statistics of the PSO can be expressed in terms of the statistics of the summed activity. The Gaussian approach results in reasonable, sometimes even excellent approximations of the investigated statistics, especially for large populations. The advantage of the Gaussian approach is the simplicity of the formulas, making the role of the synchrony threshold γ more transparent. For instance, it predicts symmetries in γ: the cross- and power spectra are indistinguishable if the synchrony threshold has the same distance to the mean activity R_0, i.e. for values of γ that lead to the same value of $|\beta_\gamma|$. This symmetry reflects the statistical similarity of joint firing and joint silence of the neurons. In numerical simulations this symmetry is found to be valid to a good approximation, especially in large populations.

4.7. Summary

In this chapter we have studied statistical properties of the partially synchronous output of a homogeneous neuronal population which is driven by a common time-dependent stimulus (Gaussian noise). By employing linear response theory, we derived analytical approximations in two different approaches for the PSO mean value, power spectrum, and its cross-spectrum with a weak stimulus. These approximations were tested against numerical simulations of LIF neurons that are driven by common white Gaussian noise or an Ornstein-Uhlenbeck process.

We investigated how the derived statistics depend on the synchrony threshold γ, i.e. the minimal fraction of the population that needs to be simultaneously active such that a synchronous event is recorded. As a key parameter emerged β_γ - the effective distance of the synchrony threshold to the expected value of the population activity. We demonstrated that the related constant $a_\gamma = e^{-\beta_\gamma^2/2}/\sqrt{2\pi\sigma_A^2} \approx p_A(\gamma)$ quantifies the sensitivity of the PSO, i.e. how much the PSO is influenced by a small change in the summed population activity $A(t)$. From the results of the mean value of the PSO (which equals the probability of having a synchronous event) we saw that the PSO is variable only for small distances $|\beta_\gamma|$. For large values of $|\beta_\gamma|$ the PSO is almost constantly one [for $\gamma \to 0$, i.e. for $\beta_\gamma \ll 0$, there is almost always a synchronous firing event] or constantly zero [for $\gamma \to 1$, i.e. for $\beta_\gamma \gg 0$, there is practically never a synchronous firing event]. These different variability regimes impact the auto- and cross-correlation properties of the synchronous output.

We showed that for all values of γ and for any population size, the cross-spectrum of the synchronous output with the common stimulus is approximately proportional to the cross-spectrum between the single neuron (or summed activity) and the stimulus. This

result is in line with Sharafi et al. (2013), where the authors showed this proportionality for the case of $\gamma = 1$. In conclusion, the relative temporal correlations between the synchronous events and the stimulus are similar to those between the single or summed spike trains and the stimulus. This is somewhat surprising because the synchronous output is a strongly non-linear function of the summed activity. The proportionality factor, however, i.e. the overall amplitude of the cross-spectrum between PSO and stimulus is given by the value of the sensitivity a_γ. The amplitude is therefore maximal for $\gamma = \langle A \rangle = R_0$ and decays exponentially with increasing distance $|\beta_\gamma|$ from this value.

The most demanding challenge was the approximation of the autocorrelation or power spectrum of the PSO. For these functions the synchrony threshold does not only influence their magnitude, but also their relative time or frequency dependence. The overall amplitude is again mainly determined by the sensitivity a_γ. In comparison to the process of the summed activity, the synchrony threshold suppresses autocorrelations. We showed that negative autocorrelations get more suppressed than positive ones, which is a consequence of the invariable nature of the PSO for large values of $|\beta_\gamma|$. We saw that for $\gamma = R_0$ the PSO power spectrum is approximately proportional to the power spectrum of the summed activity. This is due to the fact that in this case the synchronous output is a symmetric two-state version of the summed output. In the opposite limits, as γ goes to one or zero, the power spectrum approaches a flat function, revealing the Poisson-like character of rare synchronous firing or silence events if the synchrony threshold is set far away from the mean activity.

We now have all ingredients to obtain the coherence function of the PSO, which reveals the spectral coding properties of the synchronous output. In the following chapter we analyze the PSO coherence in detail.

Chapter 5.

Coherence function of the synchronous output vs summed output

In the introduction we showed that the synchronous output of pairs of neurons can act as a band-pass filter of information and in chapter 2 we discussed requirements of certain cell properties that are necessary to obtain such a 'synchrony code'. The theoretical study by Sharafi et al. (2013) showed that the total synchronous output (all neurons need to fire simultaneously) of arbitrary sized populations can exhibit information filtering as well. However, as discussed in the previous chapter, considering only the times where the entire population is active (corresponding to a synchrony threshold of $\gamma = 1$) is quite inexpedient for the case of large populations, because such events hardly ever happen and are consequently inappropriate to encode a weak time dependent stimulus. In this chapter we look at the information filtering properties of the partially synchronous output. By discussing the spectral coherence function of the PSO, we demonstrate how the synchrony threshold influences the range of frequencies that are preferentially encoded, as well as the amount of information that is transmitted by the synchronous output. Of particular interest is the comparison to the coherence of the summed population activity, i.e. to the encoding capacity of 'all spikes'. Finally, we compare our results with experimental recordings of the weakly electric fish.

5.1. Coherence of the summed population activity

Using Eq. (4.30),(4.50), and (4.49) (and keeping in mind that $S_{A,s} = S_{b,s}$ for a homogeneous population), the coherence of the summed population activity can be approximated by

$$\mathcal{C}_{A,s}(f) = \frac{|S_{A,s}(f)|^2}{S_A(f)S_s(f)} \approx \frac{|\hat{S}_{b,s}|^2}{[S_b/N + (1-1/N)\,S_{\hat{s}}]S_s} \tag{5.1}$$

$$= \frac{|\tilde{\mathcal{B}}\chi|^2 S_s^2}{[\,|\tilde{\mathcal{B}}|^2 S_x/N + (1-1/N)\,|\tilde{\mathcal{B}}\chi|^2 S_s\,]S_s} \tag{5.2}$$

$$= \left(\frac{1}{N2cD}\frac{S_x(f)}{|\chi(f)|^2} + \left(1 - \frac{1}{N}\right)\right)^{-1}, \tag{5.3}$$

where we used that we consider a white noise stimulus (or broadband noise) with $S_s(f) = 2Dc$. The coherence function of the population activity is therefore independent of the

chosen filter $\mathcal{B}$ each spike train is convolved with. The frequency dependence of $\mathcal{C}_{A,s}(f)$ is solely given by the ratio between the power spectrum of the single spike train $S_x(f)$ and the absolute square of the susceptibility of the single neuron firing rate $|\chi(f)|^2$. In fact, we can express the activity's coherence by the coherence of the single spike train, $\mathcal{C}_{x,s} = |\chi|^2 S_s / S_x$:

$$\mathcal{C}_{A,s}(f) = \frac{N\,\mathcal{C}_{x,s}(f)}{1 + (N-1)\mathcal{C}_{x,s}(f)}\,. \tag{5.4}$$

For $N = 1$ it holds consistently $\mathcal{C}_{A,s} = \mathcal{C}_{x,s}$.

For large populations the coherence of the summed activity approaches one

The activity coherence, Eq. (5.4), increases with population size N. A larger number of noisy neurons can encode more features of the stimulus and, in addition, the summing averages out the intrinsic noise. Fig. 5.1 illustrates the elevation of the activity's coherence with growing population size. In the limit of an infinitely large population, Eq. (5.4) converges to one:

$$\lim_{N\to\infty} \mathcal{C}_{A,s}(f) = 1\,. \tag{5.5}$$

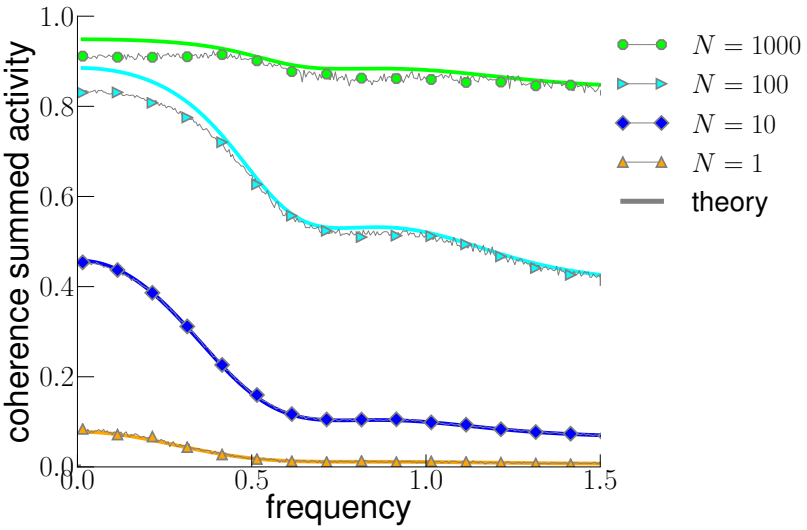

Figure 5.1.: **Coherence of 'all spikes' is low-pass for small populations and converges to one with increasing population size.** Coherence function of the summed population activity, $\mathcal{C}_{A,s}(f)$, for various population sizes N. Simulation results [symbols] are compared to approximation Eq. (5.3) [solid colored lines]. The theory overestimates the coherence for large populations, revealing the limit of the linear response approach. Parameters: $\mu = 1.2, D = 0.01, c = 0.1, R_0 = 0.2$.

This limit is the consequence of the linear response ansatz. As the population size increases to infinity, the activity is in fact equivalent to the single box train, averaged over the intrinsic noise:

$$\lim_{N\to\infty} A(t) = \lim_{N\to\infty} \frac{1}{N}\sum_{k=1}^{N} b_k(t) = \langle b(t)\rangle_\xi \tag{5.6}$$

$$\approx R_0 + \hat{s}(t)\,, \tag{5.7}$$

where the last line is the linear response ansatz introduced in section 1.6. In the linear response approach, $\lim_{N\to\infty} A(t)$ is therefore a deterministic linear distortion of $s(t)$, which results into a coherence of one. This means that the activity of an infinitely large population is a perfect transmitter of information if the stimulus is linearly encoded in the time-dependent firing rate. However, the linear response is only an approximation. In Fig. 5.1 we see that the theoretic activity coherence for a population of 1000 LIF neurons is indeed close to one [green solid line], but although having a similar frequency dependence, the numerical simulations [green circles] exhibit a slightly lower coherence magnitude. This suggests that in fact less information is encoded linearly in the instantaneous firing rate than is anticipated by our ansatz.

Coherence of the summed spike trains has the same extrema as the coherence of the single spike train

The coherence of the summed activity has the same position and kind of extrema as the coherence of the single spike train, which can be deduced by differentiating Eq. (5.4) with respect to the frequency:

$$\mathcal{C}'_{A,s}(f) = \frac{N}{[1+(N-1)\mathcal{C}_{x,s}(f)]^2}\mathcal{C}'_{x,s}(f)\,, \tag{5.8}$$

$$\mathcal{C}''_{A,s}(f) = \frac{-2N(N-1)(\mathcal{C}'_{x,s}(f))^2 + N[1+(N-1)\mathcal{C}_{x,s}(f)]\mathcal{C}''_{x,s}(f)}{[1+(N-1)\mathcal{C}_{x,s}(f)]^3}\,. \tag{5.9}$$

Eq. (5.8) reveals that whenever there is a frequency f_0 with $\mathcal{C}'_{x,s}(f_0) = 0 \Rightarrow \mathcal{C}'_{A,s}(f_0) = 0$ and by Eq. (5.9) $\mathcal{C}''_{A,s}(f_0)$ has the same sign as $\mathcal{C}''_{x,s}(f_0)$. Hence, if $\mathcal{C}_{x,s}$ has a local maximum or minimum at f_0, then so does $\mathcal{C}_{A,s}$.

In conclusion, the coherence of the summed population activity, i.e. of 'all spikes', should show similar information filtering properties as the single spike train. The single integrate-and-fire neuron model (perfect, quadratic and leaky) has been shown to act as a low-pass filter of information (Stein et al., 1972; Vilela and Lindner, 2009b). We therefore expect the summed activity to be always maximal at zero frequency, which we indeed observe (see Fig. 5.1). However, $A(t)$ does not always act as a low-pass filter. For small population size it does indeed preferentially encode slow stimuli, because then the activity coherence is similar to the one of the single neuron (see Eq. (5.4)). However, for large populations, by Eq. (5.5), the summed output becomes close to a perfect transmitter of information in all frequency bands, such that the activity does hardly show any frequency filtering (see green graph for $N = 1000$ in Fig. 5.1).

5.2. Coherence of the partially synchronous output

In chapter 4 we have derived analytical approximations of the PSO power and cross-spectrum, such that we have all ingredients to obtain the coherence function of the synchronous output. We now state qualitative and quantitative properties of the PSO coherence that can be deduced from these approximations (of the 'Gaussian approach') and test them against numerical simulations.

i) PSO coherence is maximal for $\gamma = R_0$ and decreases with increasing $|\beta_\gamma|$

By Eq. (4.27) the cross-spectrum of the synchronous output is approximately proportional to the one of the summed activity

$$S_{Y_\gamma,s} \approx a_\gamma S_{A,s} \,, \tag{5.10}$$

where the proportionality factor is given by the 'sensitivity' $a_\gamma = e^{-\beta_\gamma^2/2}/\sqrt{2\pi\sigma_A^2}$. For the power spectrum of the PSO we obtained in the Gaussian approach

$$S^G_{Y_\gamma}(f) = a_\gamma^2 \widetilde{I}_\gamma(f) \,, \tag{5.11}$$

with the time-lag dependent integral $I_\gamma(\tau)$ given by Eq. (4.55). The coherence between the synchronous output and the common stimulus can thus be approximated by

$$\boxed{\mathcal{C}^G_{Y_\gamma,s}(f) = \frac{|S^G_{Y_\gamma,s}|^2}{S_s S^G_{Y_\gamma}} = \frac{|S_{A,s}(f)|^2}{S_s\, \widetilde{I}_\gamma(f)} \,.} \tag{5.12}$$

In this approximation, only the integral I_γ depends on the synchrony threshold. In section 4.4.2v) we have shown that for all γ_1 and γ_2 with $|\beta_{\gamma_1}| > |\beta_{\gamma_2}|$ holds $I_{\gamma_1}(\tau) > I_{\gamma_2}(\tau)$. Together with Eq. (5.12) this relation leads to

$$\boxed{\mathcal{C}^G_{Y_{\gamma_1},s}(f) < \mathcal{C}^G_{Y_{\gamma_2},s}(f) \quad \text{for} \quad |\beta_{\gamma_1}| > |\beta_{\gamma_2}| \,.} \tag{5.13}$$

The overall magnitude of the coherence function decreases the more the synchrony threshold deviates from the mean population activity. This prediction can be directly observed in Fig. 5.2 [compare red with blue curve].

The same γ-dependence holds true for information measures which involve integrals of the coherence, like the lower bound of the mutual information rate, $R_{info} = -\int_0^\infty df \log_2[1 - \mathcal{C}_{Y_\gamma,s}(f)]$. We plot R_{info} versus γ for a population of 100 LIF neurons in Fig. 5.3a, where we see indeed a maximum for $\beta_\gamma = 0$. The mutual information between the PSO and the stimulus drops with increasing distance between γ and R_0. This behaviour is intuitively plausible. As we have argued in detail in section 4.3.2ii), a large value of $|\beta_\gamma|$ means a low sensitivity of the PSO. This leads to a synchronous output which is not able to encode a weak time dependent stimulus. Put differently, the stricter the synchrony threshold, the more spikes are thrown away that contain information about the stimulus.

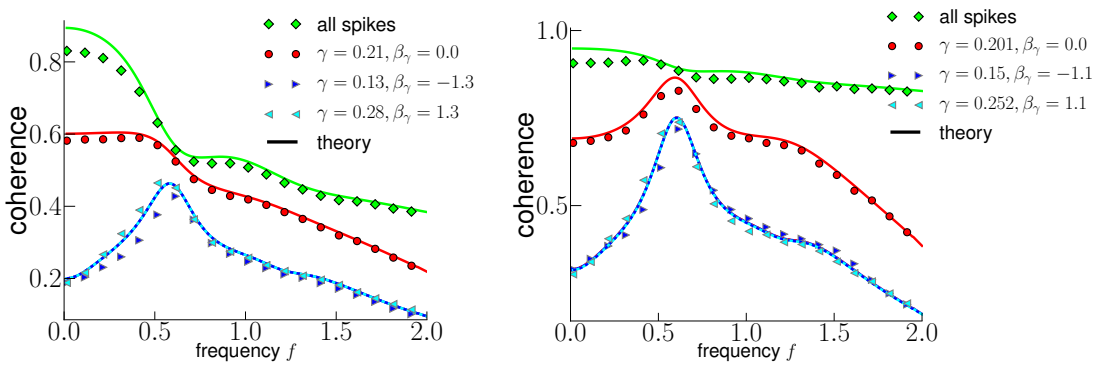

(a) $N = 100$ (b) $N = 1000$

Figure 5.2.: Coherence function of the PSO in comparison to the coherence of the summed activity [green line] for [a] $N = 100$ and [b] $N = 1000$. Simulation results [symbols] are compared to the analytical approximation Eq. (5.12) [solid lines]. Parameters: $\mu = 1.2, D = 0.01, R_0 = 0.2, c = 0.1$.

We now discuss how the relative frequency dependence (i.e. the shape) of the PSO coherence function is influenced by the choice of γ.

ii) For $\gamma \approx R_0$ the PSO acts predominantly as a broadband filter of information

For the special case that the synchrony threshold is set to the value of the mean activity, we showed in Sec. 4.4.2 i) that the power spectrum of the PSO is approximately proportional to the power spectrum of the summed activity (see Eq. (4.61) and Eq. (4.59)), such that

$$\widetilde{I}_{Y_{R_0}}(f) S_A(f) \,. \tag{5.14}$$

Inserting this relation into Eq. (5.12) we obtain a rough estimate of the coherence function for $\gamma = R_0$, i.e. for $\beta_\gamma \approx 0$:

$$\mathcal{C}_{Y_{R_0},s}(f) \frac{|S_{A,s}|^2}{S_A S_s} = \mathcal{C}_{A,s}(f) \,. \tag{5.15}$$

This crude estimate suggests that the PSO coherence for $\gamma = R_0$ is smaller, but close to the coherence function of the summed population activity. As can be seen in Fig. 5.2, $\mathcal{C}_{A,s}(f)$ [green graph] is not really close nor proportional to $\mathcal{C}_{Y_{R_0},s}(f)$ [red graph]. However, for this value of γ the PSO shows the less pronounced bandpass filtering behavior. Hence, if the synchrony threshold is set to the expected activity of the population, the frequency selectivity of the synchronous output is similar to that of the summed activity. From the point of view of a postsynaptic cell, there would be no advantage in selecting this synchrony threshold, because it leads to a more or less equal loss of information in all frequency components of the stimulus compared to an integrator cell that registers

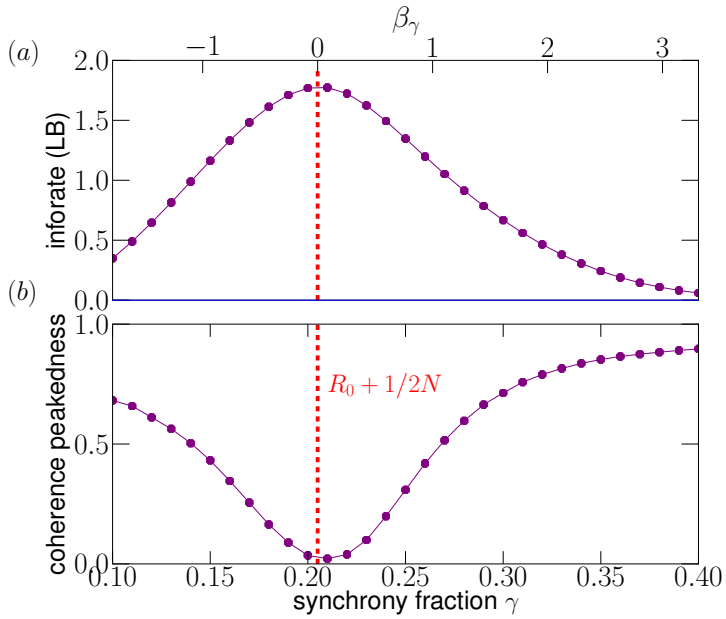

Figure 5.3.: **The better the bandpass filtering effect the less information is transmitted.** [a] Lower bound of the mutual information versus synchrony threshold. Corresponding values of the distance parameter $\beta_\gamma = (\gamma - R_0 - 1/(2N))/\sigma_A$ are shown in the top axis. Most information is transmitted by the PSO if $\beta_\gamma = 0$. [b] The peakedness of the PSO coherence at positive frequency, Eq. (5.17), (as a measure of the band-pass filtering effect) shows the opposite behavior. The band-pass filtering effect is minimal at $\gamma = R_0 - 1/(2N)$ [dashed red line] and increases as γ deviates from this value, i.e. as $|\beta_\gamma|$ increases. Parameters: $\mu = 1.2, D = 0.01, R_0 = 0.2, c = 0.1, N = 100$.

all spikes.

iii) For large $|\beta_\gamma|$ the PSO can act as a bandpass filter of information

In Sec. 4.4.2 iv) we showed that the power spectrum of the PSO becomes flat for large values of $|\beta_\gamma|$. This results in a coherence function that is approximately proportional to the cross-spectrum of the summed activity [1] (see Eq. (5.12)):

$$\boxed{\mathcal{C}_{Y_\gamma,s}(f) \propto |S_{A,s}(f)|^2 = |S_{b,s}(f)|^2 \quad \text{for } |\beta_\gamma| \gg 1.} \tag{5.16}$$

In Fig. 5.4 we see that relation Eq. (5.16) is approximately fulfilled already for $\gamma = 0.4$ (corresponding to $\beta_\gamma = 4.0$ (for $\mu = 1.6$), $\beta_\gamma = 3.0$ (for $\mu = 1.2$) and $\beta_\gamma = 2.0$ (for $\mu = 0.9$) [compare dark blue line for $\gamma = 0.4$ with green/black dashed line for $|S_{b,s}(f)|^2$].

[1] This is true if a white noise (or broad-band) stimulus with a constant power spectrum is presented, which we do in all following applications.

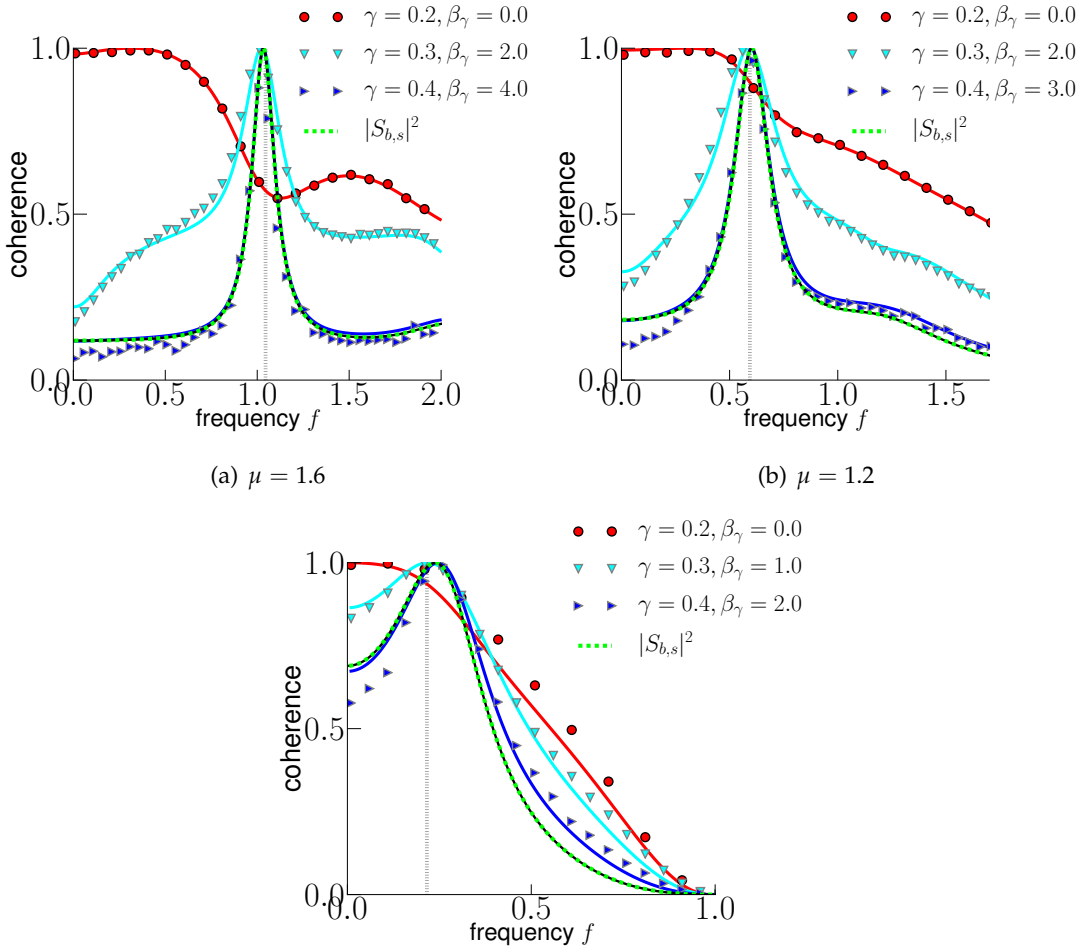

(a) $\mu = 1.6$

(b) $\mu = 1.2$

(c) $\mu = 0.9$

Figure 5.4.: **Synchrony threshold determines information filtering properties.** Coherence function of the PSO, rescaled by the maximal value, for different synchrony thresholds γ as indicated. For $\gamma = R_0$ [red] the PSO acts as a low pass filter. For large values of $|\beta_\gamma|$, the coherence is approximately proportional to the absolute square of the cross-spectrum between the single box-filtered neuron and the stimulus [green-black dashed line]. Vertical gray dashed line indicates the respective firing rate. Parameters: $D = 0.01, c = 0.1, R_0 = 0.2, N = 100$.

As anticipated above, the PSO coherence shows indeed a low-pass/broadband shape for small values of $|\beta_\gamma|$ [see red graph]. Hence, Eq. (5.16) tells us that theoretically, the best bandpass filter the PSO can act as is restricted by the shape of the cross-spectrum between the single-neuron and the stimulus. Only if $|S_{b,s}(f)|^2$ is a peaked function, the coherence of the PSO can be peaked as well for large values of $|\beta_\gamma|$. For instance, we see that the PSO coherence is generally less peaked in the subthreshold case, because the single neuron cross-spectrum has a less pronounced peak (due to a higher coefficient of

variation) compared to the suprathreshold case [compare green dashed lines in Fig. 5.4a ($\mu = 1.6 \rightarrow CV = 0.15$), b ($\mu = 1.2 \rightarrow CV = 0.24$) and c ($\mu = 0.9 \rightarrow CV = 0.55$)].

In the simulation results we see however, that the coherence can be even more suppressed at low frequencies and can thus show a more pronounced peak than the single neuron cross-spectrum has [compare dark blue triangles with green dashed line]. This is due to the fact that the PSO cross-spectrum is only approximately proportional to the single neuron cross-spectrum. For $\gamma > R_0$, the amplitude of the PSO cross-spectrum is slightly decreased at low frequencies compared to the one of the single cross-spectrum (see Fig. 4.6).

In conclusion, depending on the shape of the single-neuron cross-spectrum, the PSO can indeed show a pronounced bandpass filtering effect. We now introduce a simple way to quantify the quality of such a bandpass filter.

5.3. Quality of information filtering

One way of quantifying the bandpass filtering effect is to measure the 'peakedness' of the coherence function which we define by the fraction

$$Q := 1 - \frac{C_{Y_\gamma,s}(0)}{C_{Y_\gamma,s}(\hat{f})}\,, \tag{5.17}$$

where $\hat{f}$ is the frequency at which the PSO coherence has its global maximum [2]. The fraction Q equals zero if the coherence has its maximum at zero frequency, indicating a low-pass filtering behavior of Y_γ. The maximal value of Q is one, which occurs if the coherence vanishes at zero frequency, indicating a pronounced bandpass filtering effect. The factor Q is of course a very simple and rough indicator of a filter, since it only includes two values of the coherence and does not take into account the width of the peak. While Eq. (5.17) is supposed to quantify differences in the shape of the coherence function, it does not take into account the absolute magnitude of the coherence, such that it makes no statement about the amount of information that is transmitted by the output. A high value of Q, however, is worthless if there is practically no mutual information between the PSO and the stimulus. Fig. 5.3 shows that an increase in Q goes in hand with an undesirable decrease in transmitted information.

If one is interested in a pronounced bandpass filtering effect, but without the cost of loosing too much information, the synchrony threshold should be optimized in order to accomplish the best compromise between these two reverse effects. To this end we define a new fraction which quantifies the bandpass filtering quality, but which also takes into account the drop in transmitted information. We do so by multiplying Eq. (5.17) by the

[2] A similar measure was used in (Blankenburg et al., 2015) to quantify the bandpass filtering effect. There, the quality was defined by $Q = C_{Y_\gamma,s}(\hat{f})/C_{Y_\gamma,s}(0)$, which has the disadvantage that it is not bounded if $C_{Y_\gamma,s}(0) \rightarrow 0$.

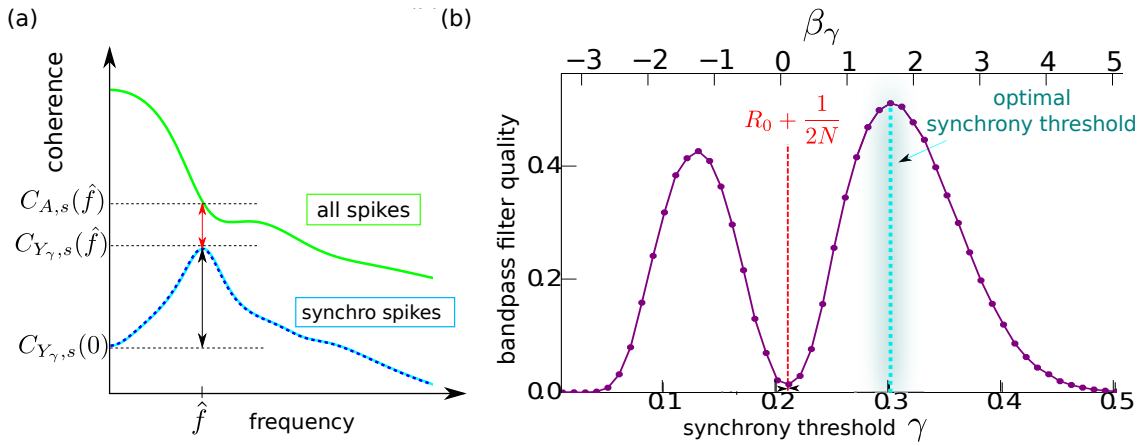

Figure 5.5.: **Optimal quality of the bandpass filtering effect is given by the synchrony threshold which leads to the best compromise between the peakedness of the coherence and its magnitude.** [a] Motivation of definition Eq. (5.18). The PSO acts as a good bandpass filter of information if its coherence function [blue line] is peaked at $\hat{f} > 0$ ($\hat{=}$ large black arrow) and if it has not dropped too much in the optimal frequency band compared to the summed activity [green line] ($\hat{=}$ small red arrow). [b] Bandpass filtering quality of the PSO, Eq. (5.18), vs synchrony threshold for a population of 100 LIF neurons. The top x-axis shows the corresponding values for β_γ. The maximum of Q_{bp} gives an estimate of the optimal synchrony threshold [cyan dashed line] in order to achieve the best bandpass filtering effect. Parameters: $\mu = 1.2, D = 0.01, R_0 = 0.2, c = 0.1, N = 100$.

ratio between the PSO coherence and the all-spikes coherence at the peak position $\hat{f}$:

$$\boxed{Q_{bp} := Q \cdot \frac{C_{Y_\gamma,s}(\hat{f})}{C_{A,s}(\hat{f})} = \frac{C_{Y_\gamma,s}(\hat{f}) - C_{Y_\gamma,s}(0)}{C_{A,s}(\hat{f})}\,.} \tag{5.18}$$

Q_{bp} is again a number between zero and one. If Q_{bp} is close to zero, then either the PSO coherence is maximal at zero frequency (indicating low-pass filtering behavior) or the coherence overall magnitude is so small that the PSO basically does not transmit any information. The factor Q_{bp} equals one, if $C_{Y_\gamma,s}(0) = 0$ and if the maximum of the PSO coherence coincides with the activity coherence evaluated at the peak frequency $\hat{f}$, implying that no coherence is lost in the desired frequency domain (see Fig. 5.5a for illustration). In conclusion, $Q_{bp} = 1$ indicates a desirable bandpass filtering effect.

Fig. 5.5b shows the quality factor Q_{bp} versus the synchrony threshold for a population of 100 LIF neurons. As expected, Q_{bp} tends to zero for large values of $|\beta_\gamma|$, because of the vanishing overall magnitude of the PSO coherence. Q_{bp} is close to zero (shows a local minimum) at $\gamma = R_0 + 1/(2N)$ ($\beta_\gamma = 0$) because for this value the PSO acts approximately as a low-pass filter of information. The best case of $Q_{bp} = 1$ is in general not accomplished. We can however look for the synchrony threshold $\hat{\gamma}$ which maximizes Q_{bp}. In Fig. 5.6a we see that the optimal synchrony threshold $\hat{\gamma}$ [indicated by dashed

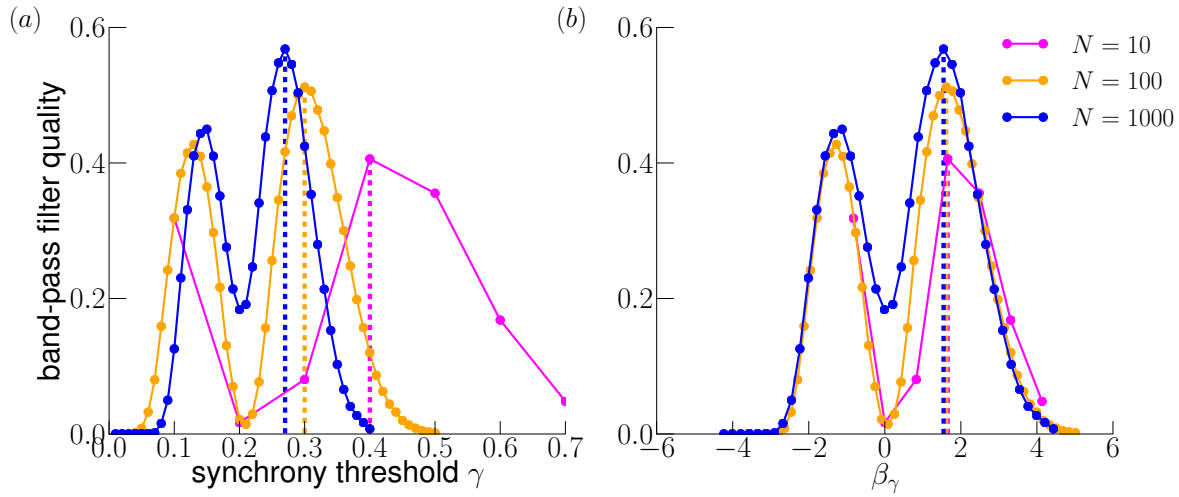

Figure 5.6.: **Optimal synchrony threshold for bandpass filtering depends on the system size.** [a] Bandpass quality factor Q_{bp}, Eq. (5.18), vs synchrony threshold γ for different system sizes N. The synchrony threshold which maximizes Q_{bp} is marked by a dashed line. [b] Bandpass quality Q_{bp} vs 'synchrony demand' β_γ. The value of β_γ which maximizes Q_{bp} (dashed lines) is approximately the same for all population sizes. The optimal filter quality increases with system size. Parameters: $\mu = 1.2, D = 0.01, R_0 = 0.2 - 1/(2N), c = 0.1$.

lines] depends highly on the system size. If we however plot the bandpass quality factor versus the 'synchrony demand' β_γ (Fig. 5.6b), we notice that the different $\hat{\gamma}$ lead to approximately the same value of $\beta_{\hat{\gamma}}$ (dashed lines overlap at $\beta_{\hat{\gamma}} \approx 1.6$). Hence, a synchrony threshold $\gamma \in [R_0 + \sigma_A, R_0 + 2\sigma_A]$ seems to be a good choice in order to accomplish a desired bandpass filtering behavior, since it is far enough from the mean activity, such that it contains different information than the sum of all spikes, but on the other hand it is close enough such that the PSO contains still a noticeable amount of information about the stimulus. In Fig. 5.6 we also see that the quality of the optimal bandpass filter increases with the system size ($Q_{bp} \approx 0.4$ for $N = 10$ and $Q_{bp} \approx 0.6$ for $N = 1000$).

In the following section we show that our predictions on the γ-dependent information filtering behavior of the PSO can be observed in real neurons as well.

5.4. Application to experimental data

Measuring the bandpass quality Q_{bp} from experimental data can be difficult because experimentally measured spectra tend to be very noisy and discontinuous at zero frequency. One way of investigating whether there is a notable change in the shape of the coherence function is to measure the position of its global maximum, as was already discussed in chapter 2 for pairs of neuron. A low-pass filter of information is indicated by a coherence maximum that is close to zero frequency, whereas a bandpass filtering effect is connected to a coherence peak position that is noticeably larger than zero, preferably close to the firing rate.

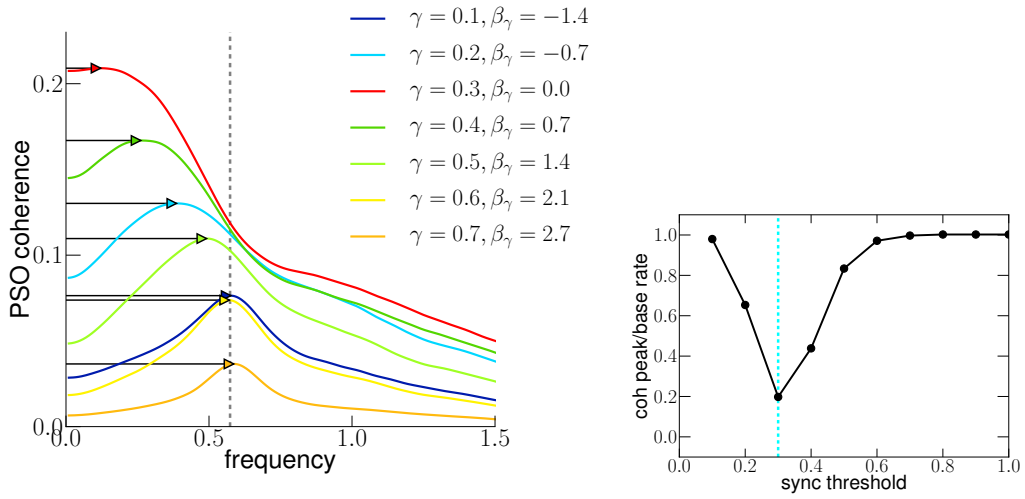

(a) (b)

Figure 5.7.: **Maximum of PSO coherence shifts towards firing rate for increasing $|\beta_\gamma|$.** [a] Coherence function of the PSO for different synchrony thresholds γ as indicated for an LIF population of ten neurons. Gray dashed line indicates the firing rate r_0 of the single neuron. [b] Coherence peak position (marked by arrow in [a]) relative to r_0 vs γ. Parameters: $\mu = 1.2, D = 0.01, R_0 = 0.25, c = 0.1$.

Fig. 5.7a shows the PSO coherence functions for all possible values of $\gamma < 0.8$ for an LIF population of ten neurons. As discussed above, for $\gamma = R_0 + 1/(2N)$ [red graph], the PSO acts as a low-pass filter of information - the coherence is maximal at a frequency close to zero. As predicted by Eq. (5.16), for large $|\beta_\gamma|$ the peak of the coherence function [indicated by arrows in Fig. 5.7a] shifts towards the peak of the cross-spectrum, which is usually located around the firing rate [gray dashed line]. The peak position relative to the firing rate is plotted in Fig. 5.7b.

Experimental data shows similar shift in PSO coherence peak position

Fig. 5.8a shows the coherence peak position of the PSO for ten trials of P-unit recordings (corresponding to a homogeneous population of ten cells) for several cells [black dots]. The solid blue line shows the average peak position relative to the firing rate. Just as the theory predicts, we see a minimum at $\gamma = R_0 + 1/(2N)$ [dashed cyan line]. Here, the peak frequency is not zero, because already the single cell coherence is maximal at small, but positive frequencies (see solid blue line in Fig. 1.9C), which is however still considered as a low-pass filtering behavior. Also, as γ tends to zero or one, the PSO coherence peak position increases, but is still below the firing rate. One reason is that already the cross-spectra of the individual cells have their maximum considerably below the baseline rate (for the example cell in Fig. 1.9A it is at half the firing rate).

Fig. 5.8b shows the peak position of the PSO coherence for the recorded ampullary

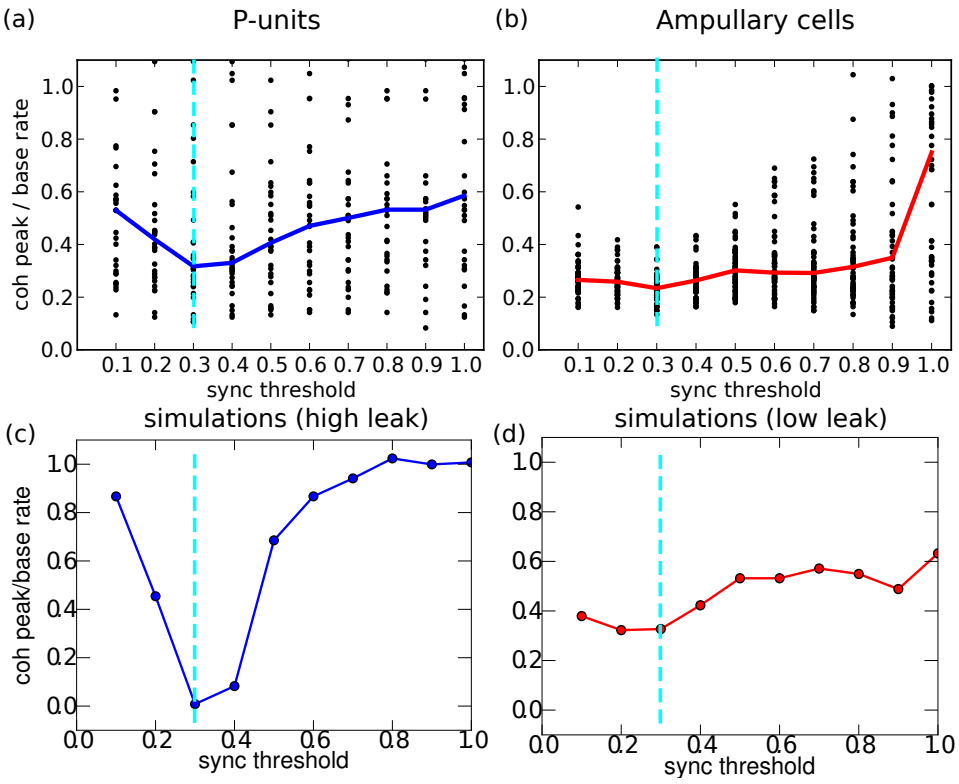

Figure 5.8.: **Comparison to experimental data.** Coherence peak position of the PSO relative to the mean baseline firing rate of a population/trials of ten [a] P-Units and [b] ampullary cells vs the synchrony threshold. Bottom row: simulation results of a high-leak population [c] and a low-leak population [d] (Same parameters were used as in Fig. 1.9). In all plots, $N = 10$ and the box-width Δ was chosen such that the mean activity $R_0 = r_0\Delta = 0.25$. Cyan dashed line marks the theoretically expected minimum at $\gamma = R_0 + 1/(2N)$. Experiments and data evaluation were performed by Jan Grewe, Institute for Neurobiology, Eberhardt Karls Universität Tübingen. Same experimental data was used as in (Grewe et al., 2017). Simulation Parameters of model Eq. (2.1): [c] $\alpha = 1.0, D_i = 0.02, D_s = 0.01, \mu = 1.2$, [b] $\alpha = 0.1, D_i = 0.002, D_s = 0.01, \mu = 1.2$.

cells. Compared to the P-units we see that the peak position is generally lower, which is in agreement with chapter 2. There, we saw that the peak of the coherence of the synchronous output of two ampullary cells does not shift as close to the firing rate as it is the case for P-units. It is therefore plausible that the same holds true for the partially synchronous output as well. As a consequence, there is not a pronounced minimum of the peak position at $\gamma = R_0 + 1/(2N)$ [3].

In Fig. 5.8c and d the PSO coherence peak position is shown for simulations of the

[3]For $\gamma = 1$ the data suggests a strong shift, which is however not to be taken seriously because the PSO coherence is so low and noisy that the determination of the position of its maximum is not easy and quite unreliable. This becomes manifest in a broad distribution of the data points for $\gamma = 1$.

α-model neurons (Eq. (2.1)) with the same parameters used in Fig. 2.1. Despite the fact that the minima are much more pronounced for the model, the synchro-coherence peak position shows for the high-leak population (Fig. 5.8b) just like the P-unit ensemble a pronounced minimum at $\gamma = R_0 + 1/(2N)$ [dashed cyan line]. The coherence peak position of the low-leak model population (Fig. 5.8c) shows like the ampullary cell ensemble a much lower dependence on the synchrony threshold. Here, the peak of the synchro coherence is for all synchrony thresholds far below the firing rate and far above zero. In conclusion, also for larger populations, a minimal leak current is necessary for a synchrony code of the partially synchronous output.

5.5. Summary

In this chapter we have analyzed the information filtering properties of the summed and synchronous output of a homogeneous neuronal population that is driven by weak common noise. The coherence of the summed activity, i.e. of 'all spikes', shows for small population size a frequency dependence similar to the one of the single neuron and thus exhibits a low-pass filtering behavior. For large population size, the independent noise of the single neurons leads to a summed output that is able to encode more features of the stimulus, such that the all-spikes coherence approaches a broadband filter with value one.

The information filtering of the synchronous output depends highly on the choice of the synchrony threshold γ. Most information is transmitted by the PSO if the threshold is set to the mean activity value. However, for this value, the shape of the coherence is close to the one of the summed output. This is in accordance with the previous chapter, where we saw that $Y_{\gamma=\langle A\rangle}(t)$ is simply a two-state version of $A(t)$. Thus, there would be no gain for a postsynaptic cell to operate with this threshold, because it would only mean an overall loss of information without a 'synchrony code'.

The more the synchrony threshold deviates from the mean activity, i.e. for high values of $|\beta_\gamma|$, the PSO coherence approaches approximately the shape of the absolute square of the cross-spectrum between the single box train and the stimulus. This is a consequence of the flattening of the PSO power spectrum for high values of $|\beta_\gamma|$ due to the rareness of synchronous events. If the cross-spectrum is a peaked function, the PSO can thus act as a bandpass filter of information. However, an increase in $|\beta_\gamma|$ goes in hand with a decrease of transmitted information (which we quantified by measuring the lower bound of the mutual information rate between PSO and stimulus). This being the case, we employed a simple measure, Q_{bp}, that is supposed to roughly evaluate the quality of the bandpass filter. This measure takes into account the peakedness of the PSO coherence but also the loss of information in the frequency band that is preferentially encoded by the PSO. We then looked for the 'optimal' synchrony threshold which maximises this quality factor. It turned out that a threshold value $\gamma \in [\langle A\rangle + \sigma_A, \langle A\rangle + 2\sigma_A]$ is the most effective choice because it finds the best compromise between actually measuring more than average synchrony, but still having enough output in order to transmit a reasonable amount of information.

Furthermore, we showed that the optimal filter quality that can be achieved by the

PSO increases with population size. This indicates that it is beneficial if sensory neurons have broadly overlapping receptive fields if their synchronous spikes are used for bandpass filtering. In addition, the postsynaptic target cells should read out a large number of sensory neurons, i.e. coincidence detectors that are supposed to extract high frequencies should have large receptive fields.

Finally, in order to apply our results to experimental data of P-units and ampullary cells of the weakly electric fish, we have measured the peak position of the PSO coherence as an indicator for information filtering. For the P-units (where already the synchronous output of pairs of neurons shows a bandpass filtering behavior) we measure qualitatively the same synchrony threshold dependence of the bandpass filtering effect of the PSO as predicted by the theory. For the ampullary cells (where the synchronous firing of pairs of cells does not exhibit a filtering effect), the PSO does not show a synchrony code regardless of the choice of γ. The same behavior is qualitatively confirmed by the LIF model with variable leak term that we used in Chapter 2 to mimic the spectra of the two cell types. We can thus conclude that also for large populations, a minimal leak conductance is necessary for the existence of a synchrony code.

Chapter 6.

Concluding remarks

Motivated by the individual activation threshold of a postsynaptic coincidence detector we have established a new measure of the dynamic synchronous output of a neuronal population. Using the formalism of stochastic processes and applying linear response theory, we were able to derive analytical expressions of important statistics of the summed and synchronous output of a general spiking population that is driven by a weak common stimulus. At this point, we summarize the main insights we achieved within this work about neuronal coding capacities.

New description of dynamic partial synchrony reveals similarity in common firing and common silence

We extended the two-neuron problem to a population of arbitrary size with arbitrary synchrony demand. We generalized the mathematical analysis of the total synchronous output by Sharafi et al. (2013) to the biologically more relevant partially synchronous output. Furthermore, we found a second approach to analytical calculations that assumes the population activity to be normally distributed, which we showed to be valid for large system size and weak common noise. This Gaussian approach led to more comprehensible and compact expressions that allowed us, for instance, to discern the symmetry in the synchrony threshold around the mean population activity. This formal symmetry unveils that the statistical coding properties of the common firing and common silence of a population are similar. In conclusion, a postsynaptic cell receiving input from a large number of afferents, but exhibiting a low activation threshold, can also act as a bandpass filter of information. Such a cell could be regarded as a coincidence detector of common pauses in presynaptic firing.

Coincidence detection - a tool for extracting high frequency signals

We have shown that, depending on the synchrony threshold, the synchronous output of a population suppresses slow components of a common stimulus and can thus potentially filter out certain frequency bands of a signal. Coincidence detection can therefore be regarded as a mechanism to distinguish between multiple signals that are concurrently present. The cause of this synchrony code is essentially the annihilation of autocorrelations of the population's summed activity by the strong nonlinearity of the synchrony threshold. This leads to a flattened power spectrum and thus to a coherence shape which is similar to the one of the cross-spectrum.

We have further shown that whether a synchrony code is established is not solely determined by the firing variability, but to a substantial degree by the leak conductance of the sensory neuron. The spiking variability was originally the first candidate to account for the different coding performances of P-units and ampullary cells in weakly electric fish observed by Grewe et al. (2017), because it was the most obvious distinction between these two types of electrosensory afferents. Our analysis, however, showed that the sensory cells also need to feature a minimal leak conductance in order to enable a synchrony code. Only then, the cross-spectra with the stimulus are peaked enough, such that a bandpass filter of information can be established. We were thus able to make predictions about experimentally not easily accessible physiological properties of electroreceptor afferents in the weakly electric fish.

Choice of the postsynaptic receptive field size and activation threshold allows to optimize the synchrony code

The shape of the PSO coherence depends strongly on the synchrony threshold, i.e. on the activation threshold of the postsynaptic cell. We defined a coarse but simple quality measure of the bandpass filtering effect of the PSO, which allowed us to estimate an optimal synchrony threshold. This way we were able to make quantitative predictions about the range of synchrony thresholds that leads to the most efficient synchrony code. We saw that this optimal filtering quality increases with the population size. This suggests that a large receptive field (RF) of the postsynaptic coincidence detector is of advantage, if bandpass filtering is desired.

Our results are therefore in line with the study by Middleton et al. (2009), where the authors show that a postsynaptic cell having a large RF and a high activation threshold, requires synchronous presynaptic input and selectively encodes higher frequencies. We showed it the other way around: a postsynaptic cell is best tuned to high frequencies, if it exhibits a large RF and a suitable (high, but not too high) activation threshold.

The topology of the electrosensory system in the weakly electric fish provides further evidence that the synchronous output might be used as a separate information channel. P-units project their output to different types of pyramidal cells. While target cells in the centro-medial segments (CMS) integrate only over a few tens of electroreceptor afferents (small RF) and exhibit low activation thresholds, postsynaptic cells in the lateral segments (LS) integrate over 30 times more afferents (large RF) and display higher activation thresholds (Mehaffey et al., 2008; Maler, 2009). Hence, pyramidal cells in the LS seem to be perfect candidates to extract a synchrony code, and indeed, they are shown to tune for high frequencies (Chacron et al., 2003; Krahe et al., 2008b; Ellis et al., 2007). On the other hand, target cells in the CMS tune to low frequencies, indicating that they read out the summed output of the afferents.

All this implies that the theoretical effect described in this thesis, i.e. the extraction of different information contents of a stimulus by reading out either the summed or the partially synchronous output of the stimulus-encoding units, is actually used in nature. These different processing channels seem to be optimized by a heterogeneity in the receptive field size and activation thresholds of the target cells.

6.1. Outlook

Here, we want to point out certain limitations of our model and propose possible future projects for further research.

Generalization to heterogeneous populations

In this thesis, we look exclusively at homogeneous populations, which is certainly a restriction. It would be interesting to extend the problem to heterogeneous systems where each neuron exhibits an individual baseline current and intrinsic noise level. We hypothesize that our theory can be easily adapted to a heterogeneous population, if the summed activity can still be approximated by a Gaussian process. This should be the case for large populations with weak/moderate heterogeneity level and weak common noise (Beiran, 2016). It can be assumed that the heterogeneity influences the variance of the population activity, but that the derived formulas in the Gaussian approach remain valid. In particular, we believe that the qualitative properties of the PSO remain valid. It would be an interesting future project to test this hypothesis.

Population versus network

We restrict our model to neuronal populations, i.e. the single elements have no lateral connection between each other. As mentioned in the introduction, such a topology of sensory neurons can be found in the olfactory, auditory and electrosensory system. However, there are sensory neurons that do influence each other. One example is the lateral inhibition between photoreceptors in the visual system: activated receptor neurons inhibit activity in neighbors (Yantis, 2013). Also in the visual system, stimulus-evoked synchrony has been recorded (Usrey and Reid, 1999). It is an interesting question how the PSO coding properties presented here, will change in the presence of lateral connections. This would also allow to make statements about recurrent networks of neurons at a later processing stage. The analytical treatment of this challenging problem - if possible at all - would require new tools that go beyond our approach. Most certainly, further insight could be gained by employing numerical simulations.

Appendix A.

Appendix

A.1. Specific equations for the LIF-model

To implement our theory to the special case of the stochastic leaky integrate-and-fire neuron model with the voltage dynamics

$$\dot{v} = -v + \mu + \sqrt{2D}\xi(t) \tag{A.1}$$

with $\langle \xi(t)\xi(t') \rangle = \delta(t-t')$, zero reset value and threshold one, the following expressions are necessary.
The mean firing rate is given by (Ricciardi, 1977)

$$r_0 = \left[\sqrt{\pi} \int_{(\mu-1)/\sqrt{2D}}^{\mu/\sqrt{2D}} e^{y^2} \mathrm{erfc}(y)\, dy \right]^{-1} . \tag{A.2}$$

The susceptibility of the firing rate can be expressed in terms of parabolic cylinder functions $\mathcal{D}_\alpha(z)$ (Lindner and Schimansky-Geier, 2001; Brunel et al., 2001)

$$\chi(f) = \frac{r_0 2\pi i f}{\sqrt{D}(2\pi i f - 1)} \frac{\mathcal{D}_{2\pi i f-1}(\frac{\mu-1}{\sqrt{D}}) - e^{\epsilon}\mathcal{D}_{2\pi i f-1}(\frac{\mu}{\sqrt{D}})}{\mathcal{D}_{2\pi i f}(\frac{\mu-1}{\sqrt{D}}) - e^{\epsilon}\mathcal{D}_{2\pi i f}(\frac{\mu}{\sqrt{D}})} , \tag{A.3}$$

where $\epsilon = (2\mu - 1)/(4D)$. The power spectrum (without DC peak) of the spike train reads (Lindner et al., 2002)

$$S_x(f) = r_0 \frac{|\mathcal{D}_{2\pi i f}(\frac{\mu-1}{\sqrt{D}})|^2 - e^{2\epsilon}|\mathcal{D}_{2\pi i f}(\frac{\mu}{\sqrt{D}})|^2}{|\mathcal{D}_{2\pi i f}(\frac{\mu-1}{\sqrt{D}}) - e^{\epsilon}\mathcal{D}_{2\pi i f}(\frac{\mu}{\sqrt{D}})|^2}. \tag{A.4}$$

A.2. Equations for pairs of neurons

In chapter 4 we have derived analytical approximations for the statistics of the summed population activity and the partially synchronous output for an arbitrarily sized population and synchrony threshold. Here, we explicitly state the analytical expressions for the special case of pairs of neurons, i.e. for $N = 2$ and $\gamma = 1$. In order to apply the results to a concrete neuron model, the single neuron firing rate r_0, its power spectrum $S_x(f)$ and susceptibility $\chi(f)$ must be known. For the α-model, which we introduced in chapter 2, these quantities can be obtained by using the transformations Eq. (2.5)-(2.7), together with appendix A.1.

The power spectrum of the single box train, $b(t) = \mathcal{B} * x(t)$, reads

$$S_b(f) = |\tilde{\mathcal{B}}(f)|^2 S_x(f) \,,$$

where $|\tilde{\mathcal{B}}(f)| = \Delta \, \mathrm{sinc}(\Delta \pi f)$ is the Fourier transformed boxcar filter and Δ is the synchrony bin width. The cross-spectrum between the single box train (or the summed activity A) and a weak stimulus reads

$$|S_{b,s}(f)|^2 = |S_{A,s}(f)|^2 = S_{\hat{s}}(f) \,,$$

where $S_{\hat{s}}(f)$ is the power spectrum of the effective stimulus[1]. For a broadband white noise stimulus with intensity D_s and cutoff frequency f_c holds

$$S_{\hat{s}}(f) = 2D_s |\tilde{\mathcal{B}}\chi(f)|^2 \, \theta(|f_c - f|) \,. \tag{A.5}$$

The power spectrum of the summed population activity is given by (cf. Eq. (4.50))

$$S_A(f) = \frac{1}{2}[S_b(f) + S_{\hat{s}}(f)] \,. \tag{A.6}$$

The mean of the synchronous output, $Y_{SO}(t) = b_1(t) \cdot b_2(t)$, reads in the combinatorial product approximation (cf. Eq. (4.19))

$$\langle Y_{SO} \rangle = R_0^2 + \langle \hat{s}^2 \rangle \,, \tag{A.7}$$

where $R_0 = r_0 \Delta$ is the mean activity and $\langle \hat{s}^2 \rangle = 2D_s \int_{-f_c}^{f_c} |\tilde{\mathcal{B}}(f)\chi(f)|^2 \, df$ is the variance of the effective stimulus. The approximations of the power and cross-spectrum of the synchronous output (cf. Eq. (4.76) and Eq. (4.39)) read

$$S_{Y_{SO}}(f) = S_b * S_b + 2R_0^2 S_b + 2S_b * S_{\hat{s}} + 4R_0^2 S_{\hat{s}} \quad \text{and} \tag{A.8}$$

$$|S_{Y_{SO},s}(f)|^2 = 4R_0^2 |S_{b,s}(f)|^2 \,. \tag{A.9}$$

[1] We defined the 'effective stimulus' by the effective linear modulation of the firing probability within a Δ-time bin: $R(t) = r(t)\Delta \approx r_0\Delta + \hat{s}(t)$.

A.3. Proof of the Bussgang theorem

Here, we want to proof the version of the Bussgang theorem that we use in Sec. 4.3.1, reading

Let X and Z be stationary Gaussian processes with $\langle Z\rangle = 0$ and variances σ_X^2 and σ_Z^2, having the cross-covariance $C_{XZ}(\tau) = \langle X(0)Z(\tau)\rangle$. Then, for any distortion $V : \mathbb{R} \mapsto \mathbb{R}$, the cross-covariance between the distorted process $V(X)$ and the original signal Z is given by

$$C_{V(X),Z}(\tau) = a\, C_{X,Z}(\tau) \tag{A.10}$$

with the proportionality factor

$$a = \frac{1}{\sigma_X^2}\int_{-\infty}^{\infty} V(x)(x - \langle X\rangle)p_X(x)dx\,. \tag{A.11}$$

Proof:

The joint probability density of the Gaussian random variables $x := X(\tau)$ and $z := Z(0)$ (with $\langle z\rangle = 0$ is given by (Bronstein et al., 2012):

$$p(x,z) = \frac{1}{2\pi\sigma_X\sigma_Z\sqrt{1-\rho^2}}\exp\left[-\frac{1}{2(1-\rho^2)}\left(\frac{z^2}{\sigma_Z^2} + \frac{(x-\langle x\rangle)^2}{\sigma_X^2} - \frac{2\rho\, z\,(x-\langle x\rangle)}{\sigma_X\sigma_Z}\right)\right]\,,$$

where

$$\rho = \frac{\langle (x-\langle x\rangle)(z-\langle z\rangle)\rangle}{\sigma_X\sigma_Z} = \frac{\langle x\cdot z\rangle}{\sigma_X\sigma_Z}$$

is the correlation coefficient between x and z (where we used that $\langle z\rangle = 0$). The covariance between the distorted variable $V(x)$ and z is defined by:

$$\begin{aligned}\langle V(x)\, z\rangle &= \int_{-\infty}^{\infty} V(x) z\, p(x,z)\, dxdz \\ &= \frac{1}{2\pi\sigma_X\sigma_Z\sqrt{1-\rho^2}}\int_{-\infty}^{\infty} V(x) z \exp\left[-\frac{1}{2(1-\rho^2)}\left(\frac{z^2}{\sigma_Z^2} + \frac{(x-\langle x\rangle)^2}{\sigma_X^2} - \frac{2\rho\, z\,(x-\langle x\rangle)}{\sigma_X\sigma_Z}\right)\right] dxdz\end{aligned} \tag{A.12}$$

For any $a > 0$ and $b \in \mathbb{R}$ holds true that

$$\int_{-\infty}^{\infty} z\, \exp\left[-\frac{z^2}{a} + bz\right]\, dz = \frac{\sqrt{\pi}}{2} b\sqrt{a}a \exp\left[\frac{ab^2}{4}\right]\,.$$

Using this relation with $a = 2(1-\rho^2)\sigma_Z^2$ and $b = \frac{\rho(x-\langle x\rangle)}{(1-\rho^2)\sigma_X\sigma_Z}$ we can evaluate the integral

over z in Eq. (A.12) by:

$$\begin{aligned}\int_{-\infty}^{\infty} z\, \exp\left[-\frac{1}{2(1-\rho^2)}\left(\frac{z^2}{\sigma_Z^2} - \frac{2\rho\, z\, (x-\langle x\rangle)}{\sigma_X\sigma_Z}\right)\right]\, dz \\ = \sqrt{2\pi}(x-\langle x\rangle)\rho(1-\rho^2)\frac{\sigma_Z^2}{\sigma_X^2}\exp\left[\frac{1}{2}\,\frac{\rho^2}{1-\rho^2}\frac{(x-\langle x\rangle)^2}{\sigma_X^2}\right]\,.\end{aligned}$$

Eq. (A.12) reads therefore

$$\begin{aligned}\langle V(x)\, z\rangle &= \rho\,\frac{\sigma_Z}{\sigma_X}\int_{-\infty}^{\infty} V(x)(x-\langle x\rangle)\frac{1}{\sqrt{2\pi\sigma_X^2}}\exp\left[-\frac{(x-\langle x\rangle)^2}{2\sigma_X^2}\right]dx \\ &= \langle x\cdot z\rangle\,\frac{1}{\sigma_X^2}\int_{-\infty}^{\infty} V(x)(x-\langle x\rangle)p_X(x)dx\,.\end{aligned}$$

This calculation holds true for any $\tau \in \mathbb{R}$, such that the last line is identical with Eq. (A.10).

Bibliography

Allen, C. and Stevens, C. F. An evaluation of causes for unreliability of synaptic transmission. *Proc. Natl. Acad. Sci. USA*, 91(22):10380–10383, 1994.

Amari, S., Nakahara, H., Wu, S., and Sakai, Y. Synchronous firing and higher-order interactions in neuron pool. *Neural Comp.*, 15(1):127–142, 2003.

Bair, W. and Koch, C. Temporal precision of spike trains in extrastriate cortex of the behaving macaque monkey. *Neural Comp.*, 8(6):1185–1202, 1996.

Bal, R. and Oertel, D. Hyperpolarization-activated, mixed-cation current (i h) in octopus cells of the mammalian cochlear nucleus. *J. Neurophysiol.*, 84(2):806–817, 2000.

Bastian, J. Electrolocation. *J. Comp. Physiol.*, 144(4):465–479, 1981.

Beiran, M. A. Effects of neural heterogeneity vs. dynamic noise on population coding of time-dependent stimuli. Master's thesis, Humboldt Universität zu Berlin, 2016.

Benda, J., Grewe, J., and Krahe, R. Neural noise in electrocommunication: From burden to benefits. In Brumm, H., editor, *Animal Communication and Noise*, volume 2 of *Animal Signals and Communication*, pages 331–372. Springer Berlin Heidelberg, 2013.

Berg, H. C. and Purcell, E. M. Physics of chemoreception. *Biophys. J.*, 20(2):193–219, 1977.

Bernardi, D. and Lindner, B. A frequency-resolved mutual information rate and its application to neural systems. *J. Neurophysiol.*, 113(5):1342–1357, 2015.

Bialek, W., Deweese, M., Rieke, F., and Warland, D. Bits and brains - information-flow in the nervous-system. *Physica A.*, 200:581, 1993.

Bialek, W. and Setayeshgar, S. Physical limits to biochemical signaling. *Proc. Natl. Acad. Sci. USA*, 102(29):10040–10045, 2005.

Blankenburg, S., Wu, W., Lindner, B., and Schreiber, S. Information filtering in resonant neurons. *J. Comp. Neurosci.*, 39(3):349–370, 2015.

Borst, A. and Theunissen, F. Information theory and neural coding. *Nat. Neurosci.*, 2:947, 1999.

Bronstein, I. N., Hromkovic, J., Luderer, B., Schwarz, H.-R., Blath, J., Schied, A., Dempe, S., Wanka, G., Gottwald, S., Zeidler, E., et al. Taschenbuch der mathematik. 2012.

Brunel, N., Chance, F. S., Fourcaud, N., and Abbott, L. F. Effects of synaptic noise and filtering on the frequency response of spiking neurons. *Phys. Rev. Lett.*, 86:2186, 2001.

Bullock, T. H. and Heiligenberg, W. *Electroreception*. John Wiley & Sons, 1986.

Bulsara, A., Elston, T. C., Doering, C. R., Lowen, S. B., and Lindenberg, K. Cooperative behavior in periodically driven noisy integrate-and-fire models of neuronal dynamics. *Phys. Rev. E.*, 53:3958, 1996.

Bussgang, J. *Crosscorrelation functions of amplitude-distorted Gaussian signals*. MITRes Lab Elec Tech Rep, 1952.

Chacron, M. J., Doiron, B., Maler, L., Longtin, A., and Bastian, J. Non-classical receptive field mediates switch in a sensory neuron's frequency tuning. *Nature*, 423:77, 2003.

Clarke, S. E., Longtin, A., and Maler, L. Contrast coding in the electrosensory system: parallels with visual computation. *Nat. Rev. Neurosci*, 2015.

Dayan, P. and Abbott, L. F. *Theoretical Neuroscience*. MIT Press, Cambridge MA, 2001.

de la Rocha, J., Doiron, B., Shea-Brown, E., Josic, K., and Reyes, A. Correlation between neural spike trains increases with firing rate. *Nature*, 448:802, 2007.

Destexhe, A. and Rudolph-Lilith, M. *Neuronal noise*, volume 8. Springer Science & Business Media, 2012.

Ellis, L. D., Mehaffey, W. H., Harvey-Girard, E., Turner, R. W., Maler, L., and Dunn, R. J. SK channels provide a novel mechanism for the control of frequency tuning in electrosensory neurons. *J. Neurosci.*, 27(35):9491–9502, 2007.

Engelmann, J., Gertz, S., Goulet, J., Schuh, A., and von der Emde, G. Coding of stimuli by ampullary afferents in gnathonemus petersii. *J. Neurophysiol.*, 104(4):1955–1968, 2010.

Fotowat, H., Harrison, R. R., and Krahe, R. Statistics of the electrosensory input in the freely swimming weakly electric fish apteronotus leptorhynchus. *J. Neurosci.*, 33(34): 13758–13772, 2013.

Fourcaud, N. and Brunel, N. Dynamics of the firing probability of noisy integrate-and-fire neurons. *Neural Comput.*, 14:2057, 2002.

Gabbiani, F. Coding of time-varying signals in spike trains of linear and half-wave rectifying neurons. *Network-Comp. Neural.*, 7:61, 1996.

Gammaitoni, L., Hänggi, P., Jung, P., and Marchesoni, F. Stochastic resonance. *Rev. Mod. Phys.*, 70:223, 1998.

Gardiner, C. W. *Handbook of Stochastic Methods*. Springer-Verlag, Berlin, 1985.

Gerstner, W. and Kistler, W. M. *Spiking Neuron Models*. Cambridge University Press, Cambridge, 2002.

Gerstner, W., Kistler, W. M., Naud, R., and Paninski, L. *Neuronal dynamics: from single neurons to networks and models of cognition*. Cambridge University Press, Cambridge, 2014.

Godfrey, D. A., Kiang, N., and Norris, B. E. Single unit activity in the posteroventral cochlear nucleus of the cat. *J. Comp. Neurol.*, 162(2):247–268, 1975.

Golding, N. L., Robertson, D., and Oertel, D. Recordings from slices indicate that octopus cells of the cochlear nucleus detect coincident firing of auditory nerve fibers with temporal precision. *J. Neurosci.*, 15(4):3138–3153, 1995.

Grewe, J., Kruscha, A., Lindner, B., and Benda, J. Synchronous spikes are necessary but not sufficient for a synchrony code in populations of spiking neurons. *Proc. Natl. Acad. Sci. USA*, 2017.

Henninger, J. *Social interactions in natural populations of weakly electric fish*. PhD thesis, Universität Tübingen, 2015.

Isserlis, L. On a formula for the product-moment coefficient of any order of a normal frequency distribution in any number of variables. *Biometrika*, 12(1/2):134–139, 1918.

Kalmijn, A. J. The detection of electric fields from inanimate and animate sources other than electric organs. In Autrum, H., Jung, R., Loewenstein, W. R., MacKay, D., and Teubner, H., editors, *Handbook of Sensory Physiology*, chapter 5, pages 148 – 200. Springer, 1974.

Kandel, E. R., Schwartz, J. H., and Jessel, T. M. *Principles of Neural Science*. McGraw-Hill Companies, U. S., 2000.

Knight, B. W. Dynamics of encoding in a population of neurons. *J. Gen. Physiol.*, 59(6): 734–766, 1972.

Koch, C. *Biophysics of Computation - Information Processing in Single Neurons*. Oxford University Press, New York, Oxford, 1999.

Koulakov, A. A., Hromádka, T., and Zador, A. M. Correlated connectivity and the distribution of firing rates in the neocortex. *J. Neurosci.*, 29(12):3685–3694, 2009.

Krahe, R. and Gabbiani, F. Burst firing in sensory systems. *Nat. Rev. Neurosci.*, 5:13, 2004.

Krahe, R., Bastian, J., and Chacron, M. J. Temporal processing across multiple topographic maps in the electrosensory system. *J. Neurophysiol.*, 100:852, 2008a.

Krahe, R. and Maler, L. Neural maps in the electrosensory system of weakly electric fish. *Curr. Opin. Neurobiol.*, 24(1):13–21, 2014.

Krahe, R., Bastian, J., and Chacron, M. J. Temporal processing across multiple topographic maps in the electrosensory system. *J. Neurophysiol.*, 100(2):852–867, 2008b.

Kreiman, G., Krahe, R., Metzner, W., Koch, C., and Gabbiani, F. Robustness and variability of neuronal coding by amplitude-sensitive afferents in the weakly electric fish eigenmannia. *J. Neurophysiol.*, 84(1):189–204, 2000.

Kreuz, T., Chicharro, D., Andrzejak, R. G., Haas, J. S., and Abarbanel, H. D. Measuring multiple spike train synchrony. *J. Neurosci. Methods*, 183(2):287–299, 2009.

Kruscha, A. and Lindner, B. Partial synchronous output of a neuronal population under weak common noise: analytical approaches to the correlation statistics. *Phys. Rev. E.*, 94(2):022422, 2016.

Kruscha, A. and Lindner, B. Spike-count distribution in a neuronal population under weak common stimulation. *Phys. Rev. E*, 92:052817, 2015.

Leen, D. A. and Shea-Brown, E. A simple mechanism for beyond-pairwise correlations in integrate-and-fire neurons. *J. Math. Neurosci.*, 5(1):1–13, 2015.

Lillywhite, P. and Laughlin, S. Transducer noise in a photoreceptor. *Nature*, 277(5697): 569–572, 1979.

Lin, J. Divergence measures based on the shannon entropy. *IEEE Trans. Inf. Theory*, 37(1): 145–151, 1991.

Lindner, B. and Schimansky-Geier, L. Transmission of noise coded versus additive signals through a neuronal ensemble. *Phys. Rev. Lett.*, 86:2934, 2001.

Lindner, B., Schimansky-Geier, L., and Longtin, A. Maximizing spike train coherence or incoherence in the leaky integrate-and-fire model. *Phys. Rev. E.*, 66:031916, 2002.

Lindner, B., Doiron, B., and Longtin, A. Theory of oscillatory firing induced by spatially correlated noise and delayed inhibitory feedback. *Phys. Rev. E.*, 72:061919, 2005.

Lindner, B. Mechanisms of information filtering in neural systems. *IEEE Trans. Mol. Biol. Multi-Scale Commun.*, 2016.

Malakhov, A. *Cumulant analysis of stochastic non-gaussian processes and their transformations (in Russian)*. Sov.Radio, Moskva, 1952.

Maler, L. Receptive field organization across multiple electrosensory maps. i. columnar organization and estimation of receptive field size. *J Comp Neurol*, 516(5):376–393, 2009.

Marinazzo, D., Kappen, H. J., and Gielen, S. C. A. M. Input-driven oscillations in networks with excitatory and inhibitory neurons with dynamic synapses. *Neural Comput.*, 19:1739, 2007.

Massot, C., Chacron, M., and Cullen, K. Information transmission and detection thresholds in the vestibular nuclei: Single neurons vs. population encoding. *J. Neurophysiol.*, 105:1798, 2011.

Mehaffey, W. H., Maler, L., and Turner, R. W. Intrinsic frequency tuning in ell pyramidal cells varies across electrosensory maps. *J. Neurophysiol.*, 99(5):2641–2655, 2008.

Meyer, J. H., Leong, M., and Keller, C. H. Hormone-induced and maturational changes in electric organ discharges and electroreceptor tuning in the weakly electric fishapteronotus. *J. Comp. Physiol. A*, 160(3):385–394, 1987.

Middleton, J. W., Longtin, A., Benda, J., and Maler, L. Postsynaptic receptive field size and spike threshold determine encoding of high-frequency information via sensitivity to synchronous presynaptic activity. *J. Neurophysiol.*, 101:1160, 2009.

Neiman, A. B. and Russell, D. F. Sensory coding in oscillatory electroreceptors of paddlefish. *Chaos*, 21(4):047505, 2011.

Nelson, M. E. and MacIver, M. A. Prey capture in the weakly electric fish apteronotus albifrons: sensory acquisition strategies and electrosensory consequences. *J. Exp. Biol.*, 202(Pt 10):1195–1203, 1999.

Olsen, S. R., Bhandawat, V., and Wilson, R. I. Divisive normalization in olfactory population codes. *Neuron*, 66(2):287–299, 2010.

Osen, K. K. The intrinsic organization of the cochlear nuclei in the cat. *Acta otolaryngologica*, 67(2-6):352–359, 1969.

Ostojic, S., Brunel, N., and Hakim, V. How connectivity, background activity, and synaptic properties shape the cross-correlation between spike trains. *J. Neurosci.*, 29:10234, 2009.

Oswald, A.-M. M., Chacron, M. J., Doiron, B., Bastian, J., and Maler, L. Parallel processing of sensory input by bursts and isolated spikes. *J. Neurosci.*, 24:4351, 2004.

Poo, C. and Isaacson, J. S. Odor representations in olfactory cortex:"sparse" coding, global inhibition, and oscillations. *Neuron*, 62(6):850–861, 2009.

Ricciardi, L. M. *Diffusion Processes and Related Topics on Biology*. Springer-Verlag, Berlin, 1977.

Richardson, M. J. E. Firing-rate response of linear and nonlinear integrate-and-fire neurons to modulated current-based and conductance-based synaptic drive. *Phys. Rev. E.*, 76:021919, 2007.

Rieke, F., Bodnar, D., and Bialek, W. Naturalistic stimuli increase the rate and efficiency of information transmission by primary auditory afferents. *Proc. Biol. Sci.*, 262:259, 1995.

Rieke, F., Warland, D., de Ruyter van Steveninck, R., and Bialek, W. *Spikes: Exploring the neural code*. MIT Press, Cambridge, Massachusetts, 1996.

Scheich, H., Bullock, T. H., and Hamstra, R., Jr. Coding properties of two classes of afferent nerve fibers: high-frequency electroreceptors in the electric fish, eigenmannia. *J. Neurophysiol.*, 36(1):39–60, 1973.

Schreiber, S., Fellous, J.-M., Whitmer, D., Tiesinga, P., and Sejnowski, T. J. A new correlation-based measure of spike timing reliability. *Neurocomputing*, 52:925–931, 2003.

Shannon, R. The mathematical theory of communication. *Bell. Syst. Tech. J.*, 27:379, 1948.

Sharafi, N., Benda, J., and Lindner, B. Information filtering by synchronous spikes in a neural population. *J. Comp. Neurosci.*, 34:285, 2013.

Shea-Brown, E., Josić, K., de la Rocha, J., and Doiron, B. Correlation and synchrony transfer in integrate-and-fire neurons: basic properties and consequences for coding. *Phys. Rev. Lett.*, 100:108102, 2008.

Stamper, S. A., Carrera-G, E., Tan, E. W., Fugere, V., Krahe, R., and Fortune, E. S. Species differences in group size and electrosensory interference in weakly electric fishes: implications for electrosensory processing. *Behav. Brain Res.*, 207(2):368–376, 2010.

Stein, R. B. A theoretical analysis of neuronal variability. *Biophys. J.*, 5:173, 1965.

Stein, R. B., French, A. S., and Holden, A. V. The frequency response, coherence, and information capacity of two neuronal models. *Biophys. J.*, 12:295, 1972.

Stocks, N. G. Suprathreshold stochastic resonance in multilevel threshold systems. *Phys. Rev. Lett.*, 84:2310, 2000.

Stocks, N. G. and Mannella, R. Generic noise-enhanced coding in neuronal arrays. *Phys. Rev. E.*, 64:030902, 2001.

Strong, S. P., Koberle, R., van Steveninck, R. R. D., and Bialek, W. Entropy and information in neural spike trains. *Phys. Rev. Lett.*, 80:197, 1998.

Su, C.-Y., Menuz, K., and Carlson, J. R. Olfactory perception: receptors, cells, and circuits. *Cell*, 139(1):45–59, 2009.

Usrey, W. M. and Reid, R. C. Synchronous activity in the visual system. *Annu. Rev. Physiol.*, 61(1):435–456, 1999.

Vilela, R. D. and Lindner, B. Are the input parameters of white-noise-driven integrate & fire neurons uniquely determined by rate and CV? *J. Theor. Biol.*, 257:90, 2009a.

Vilela, R. D. and Lindner, B. A comparative study of three different integrate-and-fire neurons: spontaneous activity, dynamical response, and stimulus-induced correlation. *Phys. Rev. E.*, 80:031909, 2009b.

Vosshall, L. B., Wong, A. M., and Axel, R. An olfactory sensory map in the fly brain. *Cell*, 102(2):147–159, 2000.

Walz, H., Grewe, J., and Benda, J. Static frequency tuning accounts for changes in neural synchrony evoked by transient communication signals. *J. Neurophysiol.*, 112(4):752–765, 2014.

Watson, G. Notes on generating functions of polynomials:(2) hermite polynomials. *J. London Math. Soc.*, 1(3):194–199, 1933.

Wessel, R., Koch, C., and Gabbiani, F. Coding of time varying elcetric field amplitude modulations in a wave-type electric fish. *J. Neurophysiol.*, 75:2280, 1996.

White, J. A., Rubinstein, J. T., and Kay, A. R. Channel noise in neurons. *Trends Neurosci.*, page 131, 2000.

Wilkens, L. A. and Hofmann, M. H. Bahvior of animals with passive, low-frequency electrosensory systems. In Bullock, T., Hopkins, C. D., Popper, A. N., and Fay, R. R., editors, *Electroreception*, chapter 9, pages 229 – 263. Springer, 2005.

Wilson, R. I. and Mainen, Z. F. Early events in olfactory processing. *Annu. Rev. Neurosci.*, 29:163–201, 2006.

Yantis, S. *Sensation and perception*. Palgrave Macmillan, page 77, 2013.

Young, E. D., Spirou, G. A., Rice, J. J., Voigt, H. F., and Rees, A. Neural organization and responses to complex stimuli in the dorsal cochlear nucleus [and discussion]. *Philos. Trans. R. Soc. Lond., B, Biol. Sci.*, 336(1278):407–413, 1992.

Danksagung/ Acknowledgements

Diese Arbeit wäre ohne die Betreuung von Prof. Dr. Benjamin Lindner nicht möglich gewesen. Sein enormes Engagement, sowie seine fachliche und organisatorische Kompetenz und die Gabe wüst erscheinende Sachverhalte klar auf den Punkt zu bringen sind schlicht beeindruckend und mir ein absolutes Vorbild. Dafür und für seine stete Bereitschaft sich Zeit für Diskussionen und Feedback zu nehmen, trotz seiner vielen Verpflichtungen, danke ich ihm sehr. Ebenfalls möchte ich mich bei ihm für das Schreiben des Antrages für Projektmittel der Deutschen Forschungsgemeinschaft bedanken, durch welche diese Arbeit finanziert wurde (DFG Sachbeihilfe LI 1046/2-1).

I thank Prof. Dr. Leonard Maler and Prof. Dr. Martin Nawrot for acting together with Prof. Dr. Benjamin Lindner as referees of this thesis, as well as Prof. Dr. Igor Sokolov and Prof. Dr. Elisa Bernardini for acting as the chairman and member of the doctoral committee.

Dr. Jan Grewe danke ich dafür auf meine nie endenden Extrawünsche in der Datenauswertung der Fischexperimente eingegangen zu sein. Die Diskussionen mit ihm und Prof. Dr. Jan Benda haben mir Einsicht in die Komplexität der experimentellen Datenerhebung, -auswertung und -interpretation ermöglicht. I thank Prof. Dr. Alexander Neiman for fruitful discussions and for giving me valuable hints and references.

Ich bedanke mich bei der gesamten Arbeitsgruppe „Theorie komplexer Systeme und Neurophysik". Besonderen Dank gilt Davide Bernardi für das konstruktive Korrekturlesen von Teilen dieser Dissertation und dafür, dass ich ihn zusammen mit Dr. Felix Droste und Jens Doose stets mit Fragen und Computerproblemen nerven konnte. Ihre Anwesenheit hat eine gemütliche und humorvolle Büroatmosphäre geschaffen.

Ich danke Dr. Kai Dierkes für das Korrekturlesen von Teilen dieser Arbeit. Seine Art in Allem etwas Spannendes und Verstehenswertes zu finden hat mich stets inspiriert. Zudem wäre ich ohne ihn wohl nicht auf unsere Arbeitsgruppe gestoßen.

Nikola Schrenk möchte ich für jegliche Verwaltungsarbeit und ganz besonders für die emotionale Unterstützung und die gemeinsamen Mittagspausen danken.

Ich danke meinen Eltern Ludmilla und Prof. Dr. Johannes Kruscha, die mir ein unbeschwertes Studium ermöglichten. Ein besonderer Dank gilt meinem Schwesterherz Maria Kruscha, dafür, dass sie mich in meinem Leben begleitet und mir stets beteuerte wie schön vorzeigbar eine Schwester mit Physikpromotion ist.

Ich danke Roland Weber und allen meinen Freunden dafür, dass sie da sind und mir Berlin zu einem noch schöneren Ort gemacht haben.

Zu guter Letzt möchte ich unsere Bürocouch preisen, ohne der ich nur halb so produktiv gewesen wäre. Überall sollte eine stehen.

Selbstständigkeitserklärung

Ich erkläre, dass ich die vorliegende Arbeit selbstständig und nur unter Verwendung der angegebenen Literatur und Hilfsmittel angefertigt habe.

Berlin, den 18.02.2017

Alexandra Kruscha